Condition-Based Monitoring System for Diagnostics and Prognostics of Centrifugal Pumps

---

A thesis presented to

the Faculty of the Graduate School

at the University of Missouri-Columbia

In Partial Fulfillment

of the Requirements for the Degree

Master of Science

By

Bilal Kamal Hussain

A. Sherif El-Gizawy, Thesis Supervisor

December 2016

The undersigned, appointed by the dean of the Graduate School, have examined the thesis entitled

Condition-Based Monitoring System for Diagnostics and Prognostics of Centrifugal Pumps

Presented by Bilal Kamal Hussain,

A candidate for the degree of Master of Science,

And hereby certify that, in their opinion, it is worthy of acceptance.

A. Sherif El-Gizawy, Professor, Mechanical and Aerospace Engineering

---

Roger Fales, Professor, Mechanical and Aerospace Engineering

Isabella Zaniletti, PHD, Department of Statistics

Acknowledgments

At first, I would like to thank my professor and godfather in my engineering career, professor Ahmed Sherif El-Gizawy. He believed in me when I was in my undergraduate years, and gave me the support and encouragement to become the engineer and the person I am today. I learned so many valuable things working with him. The humbleness and knowledge professor Ahmed carries have no limits. He taught me to believe in myself and always stay hungry for knowledge and improvement. No matter where my next step will be and how far I travel, his guidance and touch are engraved in my mind and heart. For that I say, thank you very much for shaping my career.

Next, My mother, MD. Bushra Faris. She is the fuel that inflames my heart and soul and keeps me moving forward. She taught me how to be strong and determinant. Her years of staying late, making dinners for me are my favorite memories of being student. You are the sun that shines my world and I will do my best to always make you proud.

My father, engineer Kamal Mohammed Ali. You are the wall that we fall on when we are weak and tired. You inspired me to become an engineer. You showed me how can knowledge and hard work change people's lives. Your smiles and joyful face when I achieve a success are my biggest prize.

My brother, engineer Mohammed Hussain. You been more than a brother, a friend and a colleague. We took classes together, we failed in some but mostly succeeded in some. I never felt alone between the 32,000 students that Mizzou have because I always know you are there for me. I wish you the absolute best in great things you will achieve.

My brother, Karim Hussain and my little sister Afnan. You always keep me moving forward and always encouraged me. Thank you very much and I hope to see you achieving great things in the future.

My wife, Soumaya Necibi. You are my one and only. Your hard work and dedication to achieve your pharmacy doctor degree always made me jealous and inspired me to do my best. Your support and love makes be a better man. I will do everything in my power to make you happy.

My wife's family, Dr. Semi Necibi; Henda Nabil; Saja Necibi; and Malek Necibi. You always showed support and encouragement in my personal and career life. I thank you very much.

My research partner, Amjad Hasan. You encouraged me when I needed it, we were a great teammate. I wish you the best career, and I hope we can work together in the future.

My friends, Akram Faqeeh and Xuewei Ma. You guys were always there for me whenever I need support. The nights and days we spent working on projects, travelling, and having fun will never be forgotten. Thank you and I wish you the absolute best.

Table of Contents

Acknowledgments ii

List of Figures vi

List of Tables ix

Abstract x

1. Introduction 1

2. Literature Review 7

2.1 Centrifugal Pump Problems 7

2.2 Health Monitoring Methods 12

3.Investigation Approach 17

3.1. System Design 21

3.1.1. Hardware 21

3.1.2 Software 25

3.2. Experimental Design and Procedure 30

3.2.1. Full Factorial Design 31

3.2.1. Taguchi Method (Orthogonal Array) 33

3.2.2. Response Surface Methodology 38

3.2.2. Failure Mode Effects Analysis 42

3.3 Vibration Analysis 45

3.4. Control Methods 48

3.4.1. Modeling Speed and Valve angle 48

3.4.2. NARMA-L2 Neural Network 50

3.4.3. Predictive Neural Network 54

3.4.4. Fuzzy Logic Control 57

4. Results and Discussions 64

4.1 Experimental Results 64

4.1.1 Full Factorial Design 64

4.1.2 Orthogonal Array (Taguchi method) 67

4.1.3 Response Surface Methodology 76

4.1.4 FMEA Results 95

4.3 Vibration Analysis Results 99

4.3 Control Results 106

4.3.1 Systems Modeling Results 106

4.3.2 Control Methods Results 110

5. Conclusion 119

6. Future Recommendations 119

References 120

Appendix 124

List of Figures

Figure 1.Global energy consumption from 1980 to 2030 [1] 1
Figure 2. Energy consumption in world's applications [3] 2
Figure 3. Centrifugal pump components [4] 3
Figure 4. Centrifugal pump system components [5] 3
Figure 5. Centrifugal pump system [7] 4
Figure 6. Centrifugal pump life cost [11] 5
Figure 7. NPSH vs flowrate [12] 8
Figure 8. Biological (left) and artificial (right) neural networks [45] 16
Figure 9. Timeline of the operational life of a part [30] 17
Figure 10. Experimental rig used in this research [62]. 21
Figure 11. Inside the main tank 21
Figure 12. Electrical setup 23
Figure 13. DAQ Assistance NI PXIe-1078 24
Figure 14. Signals modules 24
Figure 15. LabVIEW interface 26
Figure 16. DAQmx Create Channel 27
Figure 17. DAQmx Create Channel - Digital Input/Output 27
Figure 18. CO Pulse Frequency 28
Figure 19. Analog Input Channel 28
Figure 20. Sample Clock 28
Figure 21. Case Structure 29
Figure 22. Single Tone Extraction 29
Figure 23. Components of Design of Experiments 30
Figure 24. Types of CCD methods [70] 40
Figure 25. Failure Rate Curve [72] 42
Figure 26. Risk Ranking Matrix [72] 43
Figure 27. Periodic function 45
Figure 28. Simple mass-spring system 46
Figure 29. Time domain data 47
Figure 30. Frequency domain data 48
Figure 31. Ident toolbox in MATLAB 50
Figure 32. Neural Network representation 51
Figure 33. NARMA-L2 parameters for speed control 52
Figure 34. Block Diagram of NARMA-L2 controller [78] 53
Figure 35. Final form of NARMA-L2 NN [78] 53
Figure 36. NARMA-L2 Simulink model [78] 54
Figure 37. General schematic of Predictive NN [80] 54
Figure 38. Structure of plant model [80] 55
Figure 39. Model predictive control process [78] 56

Figure 40. Predictive control parameters 56
Figure 41. Predictive control NN training parameters 56
Figure 42. Precision and Significance scenarios [80] 57
Figure 43. Fuzzy vs Non fuzzy [82] 58
Figure 44. Triangular and Trapezoidal MFs [81] 59
Figure 45. Sugeno process [80] 59
Figure 46. Neuro-Fuzzy control 60
Figure 47. Speed and Valve to Flowrate fuzzy system 61
Figure 48. Neuro-Fuzzy Designer 62
Figure 49. Membership function selection 62
Figure 50. Response surface 63
Figure 51. Neuro-Fuzzy rules 63
Figure 52. Efficiency of the centrifugal pump [83] 64
Figure 53. Pressure rise vs Flowrate [83] 65
Figure 54. Efficiency vs Temperature rise 66
Figure 55. Noise in the system 66
Figure 56. Power consumption in the pump 67
Figure 57. Response graph for Efficiency 68
Figure 58. Vibration amplitude 70
Figure 59. Response graph for max amplitude frequency 71
Figure 60. Response graph for temperature rise. 72
Figure 61. Response graph for noise 73
Figure 62. Response graph for temperature rise 75
Figure 63. Vibration amplitude fitted line 80
Figure 64.Vibration max amplitude's frequencies fitted line 81
Figure 65. Temperature rise fitted line 81
Figure 66. Noise fitted line 81
Figure 67. Efficiency fitted line 82
Figure 68. Surface plot for vibration amplitude at valve angle 40 (degrees) 83
Figure 69. Surface plot for vibration amplitude at valve angle 60 (degrees) 83
Figure 70. Surface plot for vibration amplitude at valve angle 80 (degrees) 84
Figure 71. Surface plot for vibration max amplitude's frequencies at valve angle 40 (degrees) 85
Figure 72. Surface plot for vibration max amplitude's frequencies at valve angle 60 (degrees) 85
Figure 73.Surface plot for vibration max amplitude's frequencies at valve angle 80 (degrees) 86
Figure 74.Surface plot for temperature rise at valve angle 40 (degrees) 87
Figure 75.Surface plot for temperature rise at valve angle 60 (degrees) 87
Figure 76.Surface plot for temperature rise at valve angle 80 (degrees) 88
Figure 77.Surface plot for noise at valve angle 40 (degrees) 88
Figure 78.Surface plot for noise at valve angle 60 (degrees) 89
Figure 79.Surface plot for noise at valve angle 80 (degrees) 89
Figure 80.Surface plot for efficiency at valve angle 40 (degrees) 90
Figure 81.Surface plot for efficiency at valve angle 60 (degrees) 91

Figure 82.Surface plot for efficiency at valve angle 80 (degrees) 91
Figure 83. Vibration amplitude at 4.5 inches 92
Figure 84.Vibration maximum amplitude's frequencies at 4.5 inches 93
Figure 85. Temperature rise at 4.5 inches 93
Figure 86. Noise of the pump at 4.5 inches 94
Figure 87. Efficiency of the pump at 4.5 inches 94
Figure 88. FMEA graph 98
Figure 89. Spectral diagram of vibration signals [85] 100
Figure 90. Spectrum of vibration data of misalignment [86] 100
Figure 91. Taguchi experiment 1 spectrum results 101
Figure 92. Taguchi experiment 2 spectrum results 101
Figure 93. Taguchi experiment 3 spectrum results 101
Figure 94. Taguchi experiment 4 spectrum results 102
Figure 95. Taguchi experiment 5 spectrum results 102
Figure 96. Taguchi experiment 6 spectrum results 102
Figure 97. Taguchi experiment 7 spectrum results 103
Figure 98. Taguchi experiment 8 spectrum results 103
Figure 99. Taguchi experiment 9 spectrum results 103
Figure 100. Vibration spectrum at 12000 rpm 105
Figure 101. Vibration spectrum at 10 degrees' valve angle 105
Figure 102. Vibration spectrum when NPSHa<NPSHr 105
Figure 103. Experimental data for input (u1) speed and output (y1) flowrate 107
Figure 104. Step response of speed transfer function 108
Figure 105. Bode plot for speed transfer function 109
Figure 106. Model versus Experimental data output 109
Figure 107. Training data results 110
Figure 108. Validation data results 111
Figure 109. Testing data results 111
Figure 110. Model fit data for Narma-L2 112
Figure 111. Validation performance curves 112
Figure 112. Speed controller results. 113
Figure 113. Speed controller results 114
Figure 114. Valve angle controller results 115
Figure 115. Valve angle controller results 115
Figure 116. Fuzzy-Neuro controller response 117
Figure 117. Error in the Fuzzy-Neuro controller 117

List of Tables

Table 1. Losses in centrifugal pump system [10] 5
Table 2. Full Factorial Setup 32
Table 3. Standard orthogonal arrays [69] 35
Table 4. Structure of ANOVA table [70] 36
Table 5. Factors and level used 37
Table 6. L9 design 37
Table 7. L4 Orthogonal array 38
Table 8. CCF design 41
Table 9. Severity level definition [73] 44
Table 10. Frequency of occurrence [73] 44
Table 11. Optimal response for Efficiency 69
Table 12. ANOVA table for Efficiency 69
Table 13. Optimal levels for vibration amplitude 70
Table 14. ANOVA for vibrations amplitude 70
Table 15. ANOVA table for max amplitude frequency 71
Table 16. Optimal settings for max amplitude frequency 72
Table 17. ANOVA table for temperature rise 72
Table 18. Optimal settings for temperature rise 73
Table 19. ANOVA table for noise 73
Table 20. Optimal settings for noise 74
Table 21. ANOVA table for temperature rise 76
Table 22. Optimal settings for temperature rise 76
Table 23. ANOVA for vibration amplitudes 78
Table 24. ANOVA for maximum vibration amplitude's frequency 78
Table 25. ANOVA for noise 79
Table 26. ANOVA for temperature rise 79
Table 27. ANOVA for efficiency 80
Table 28. Common failures and their percent contributions in some phenomena in centrifugal pump [84] 95
Table 29. Failure mode effects analysis for this system 97

Abstract

Centrifugal pumps are the most commonly used pumps in industry. Therefore, maintenance is a very important part of the pump's life cycle. This work presents a systematic robust condition-based monitoring process for diagnostics and prognostics of centrifugal pumps. The process includes industrial design of experiments; data acquisition software and hardware; transient modeling using transfer functions, artificial intelligent control methods; and spectral analysis using Fast Fourier Transform. Industrial design of experiments used in this work includes orthogonal arrays or Taguchi method, full factorial design, and response surface methodology. As for the data acquisition system, NI DAQ (National Instruments) hardware were used interactively with LabVIEW software to collect the data from the different sensors. Transient modeling using time domain data was established using MATLAB's modeling toolbox, identification toolbox. Artificial intelligent control methods used were NARMA-L2 and Predictive Neural Networks, Fuzzy Logic control method, and Neuro-Fuzzy control method. Lastly, spectral analysis using Fast Fourier Transform was performed on the vibrations of the system.

1. Introduction

Energy needs in the world is expected to increase by 30% from 2016 to 2030, going from 162,500 ZW to 198,654 ZW [1]. Electric motors by themselves consume 46% of the electrical energy in the world. This number represents 70% of the whole industrial electricity usage [2]. shows the world's energy consumption by applications. The figure shows that pumps consume 22% of the total energy, 16% of that is used by centrifugal pumps. Therefore, minimizing energy waste in centrifugal pumps minimizes the overall energy loss. Less energy waste requires efficient pumping systems and smarter maintenance methods.

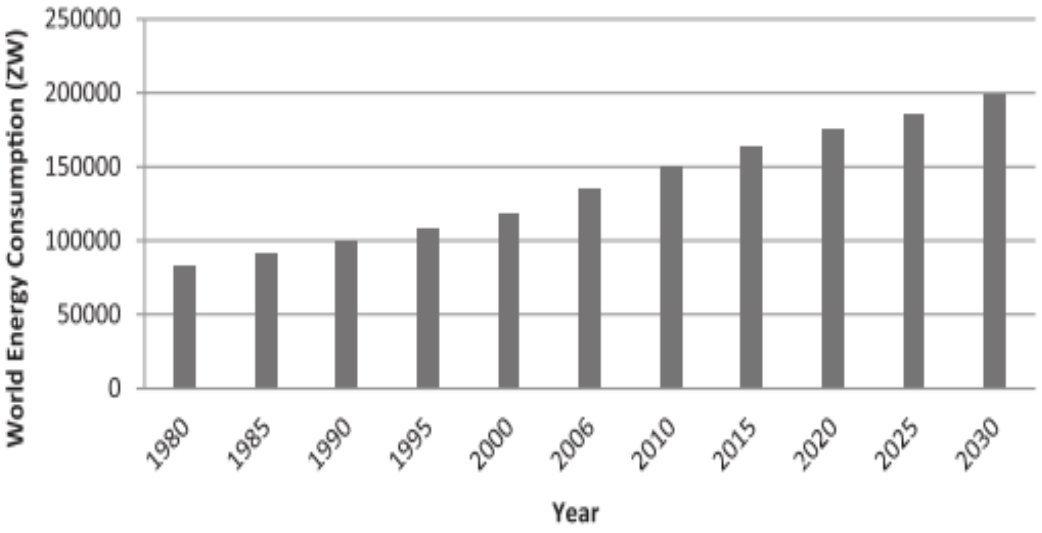

Figure 1.Global energy consumption from 1980 to 2030 [1]

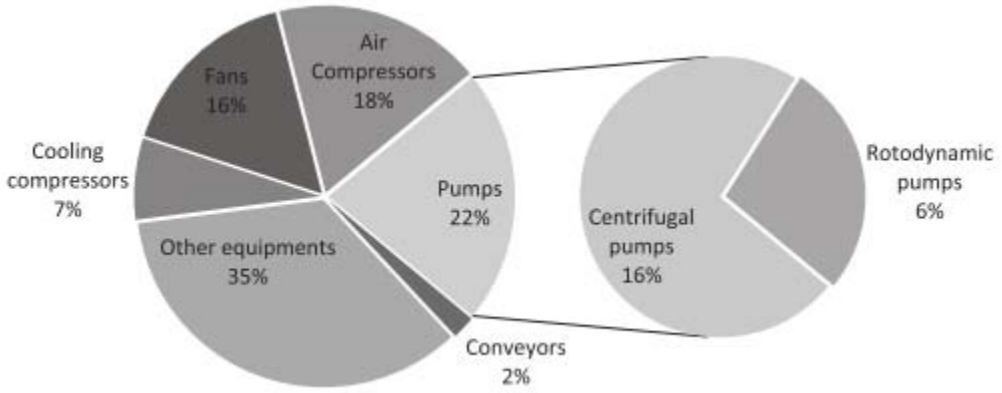

Figure 2. Energy consumption in world's applications [3]

Centrifugal pumps are turbomachinery systems that transfer electrical energy to mechanical energy using motors. Figure 3 shows the components of a centrifugal pump. The impeller rotates using electrical motor creating a low-pressure area around the center. The suction side of the pump is connected to a fluid that needs to be transferred. When low pressure is present, the fluid travels through the suction side into the impeller. After that, the trapped fluid in the impeller is forced to follow a certain path, this path is decided by the design of the volute. The volute is then connected to a discharge side where the fluid exists the pump. Centrifugal pumps increase the hydraulic energy of the fluids; this means increasing the pressure and flowrate. The transferred fluid can be in form of multiple liquids or gases. Figure 4 shows a centrifugal pump system components. Main components to mention are bearing, sealing, shaft and casing.

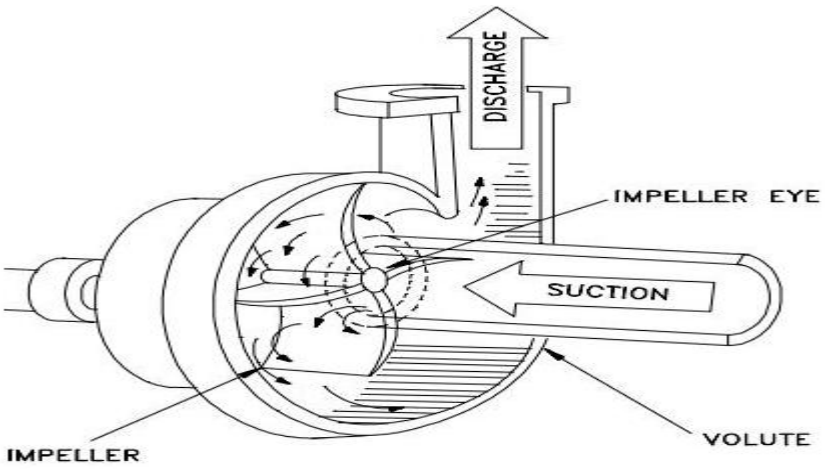

Figure 3. Centrifugal pump components [4]

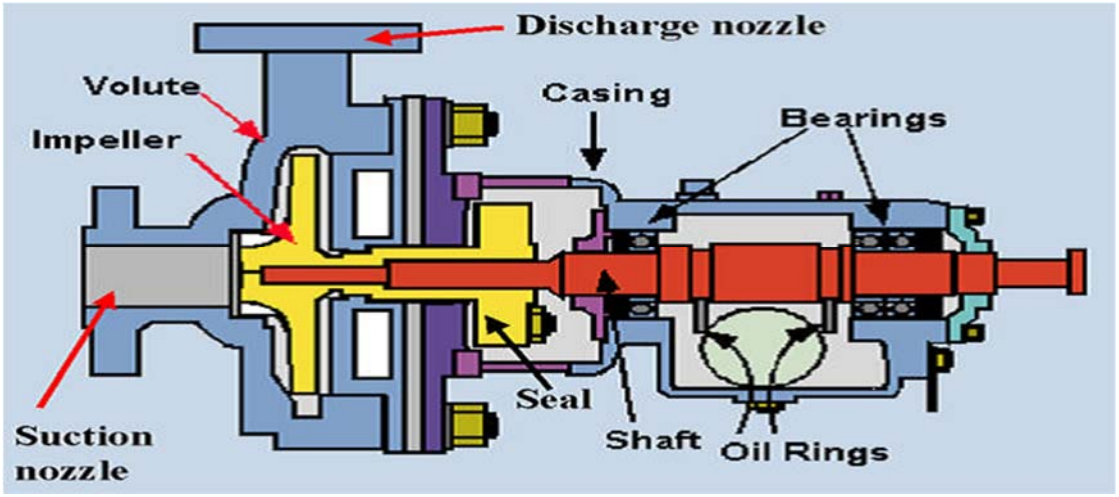

Figure 4. Centrifugal pump system components [5]

Centrifugal pumps are used in multiple industries. It is used in wastewater, chemicals, petroleum, natural gas, irrigations, drilling, and painting. Multiple devices use centrifugal pumps, such as boilers, pneumatic actuators, and many more. In fact, 80-90 % of petroleum plants use centrifugal pumps. The reason being is that centrifugal pumps have high efficiency, different ranges of flowrates and pressures, smoother flows, simplicity in design, and they are easily operated [6].

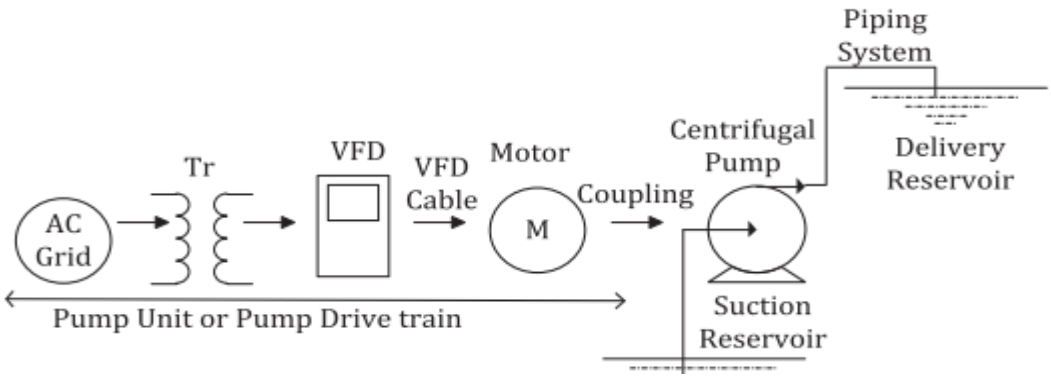

Figure 5. Centrifugal pump system [7]

Figure 5 shows a centrifugal pump system. The system consists of AC electrical power source, transformer or drive train, VFD (Variable Frequency Drive), motor, pipes, couplers, suction reservoir, delivery reservoir, and finally, the pump. VFD is a device used to control the speed of the pump by varying the supply frequency to the motor [8]. Because of the multiple components of centrifugal pump systems, there are multiple sources of energy loss. Table 1 shows the average efficiency of each component in the system, and the percent of energy loss. As shown, most of the losses come from piping systems, motors, and the pump itself. The rest of the components does not have high losses. Motor and piping losses are studied thoroughly in the literature, and for each application, there are several motors and pipe designs that can be used. As far as the pump itself, the manufacturer can guarantee the initial efficiency of the pump, and recommends a safety measures for operation. But, it will not be able to control and monitor the health of the pump and make decisions all the time. In fact, as soon as the pump is installed, its efficiency becomes a function of process conditions. Pump health can be affected by system components, control methods used, maintenance cycles, and overall system design. In many industries, the cost of maintaining healthy operation of a pump can be twenty times the purchasing cost [9]. Therefore, finding ease to use, simple, and efficient maintenance system can have tremendous savings.

Table 1. Losses in centrifugal pump system [10]

Sl.	Component in pumping system	Efficiency (%)	Losses (%)
1.	Piping system	50–60	40–50
2.	Pumps	85–90	10–15
3.	Coupling	~99	~1
4.	Motors	>90	<10
5.	VFD cables	~98	~2
6.	VFDs	95–98	2–5
7.	Transformers	~99	~1

$$LCC = C_{ic} + C_{in} + C_e + C_0 + C_m + C_s + C_{env} + C_d \quad \text{Equation 1}$$

Equation 1 represents the life cycle cost (LCC) for a pump system. C_{ic} is the initial cost, C_{in} is installation cost, C_e is energy cost, C_o is operation cost (labor), C_m is maintenance and repair costs, C_s is downtime cost, C_{env} is environmental cost, C_d is disposal costs. Environmental cost may be caused by contamination of the liquid being transferred. Disposal costs might include discarding of auxiliary devices or services. The significant of each cost term differs from one industry to another. For example, petrochemical industries cannot afford a downtime cost. As being down means losing millions of dollars. Therefore, close attention is paid for maintaining or replacing the pump systems. In some industries, environmental rules might be strict, and disposal cost might be more important than others [11].

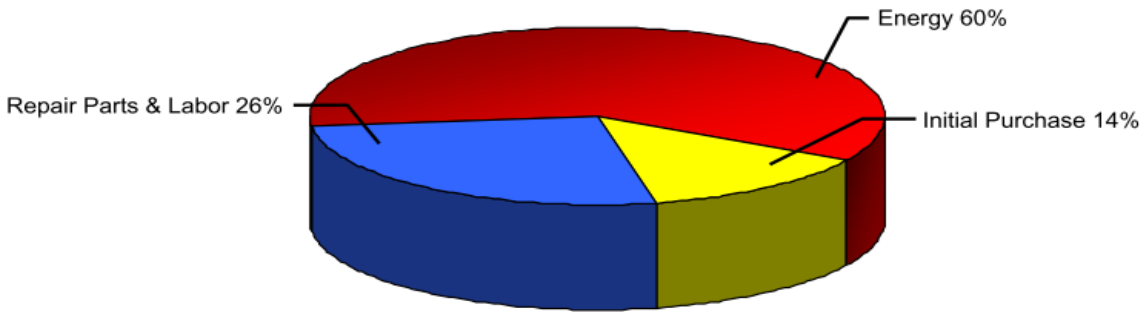

Figure 6. Centrifugal pump life cost [11]

Figure 6 shows the total life cost of a centrifugal pump that was running for seven years. As shown above, most of the cost is going for energy usage, and the other part is going for maintenance and labor. Meanwhile, the initial cost of purchase is not as significant as others.

This work presents a systematic method for health monitoring of a centrifugal pump. It contains modeling of system components, designing industrial testing methods, estimating failure modes, and testing multiple intelligent control methods. The goal of this work is to design a robust autonomous condition based maintenance system, to increase the life of centrifugal pumps and minimize the life cost. The main objective of this work is to create simple, robust intelligent system to diagnose future failures, and suggest the appropriate methods of solving them.

2. Literature Review

2.1 Centrifugal Pump Problems

Centrifugal pumps are highly dynamic components. Therefore, centrifugal pump systems often suffer multiple problems that affect performance and life of the pump. Before introducing methods to monitor the pump's health, it is useful to understand the main problems associated with the pump. These problems can be categorized in three categories; hydraulic failures, mechanical failures and other failures. Hydraulic problems can be in the form of cavitation, pressure pulsations, radial thrust, axial thrust, and suction and discharge recirculation. Mechanical problems can be in the form of bearing and seal failures, excessive vibrations, lubrication and fatigue failures. Other failures might include erosion, corrosion, and excessive power consumption [12]. In the following, those failures are introduced, thoroughly.

Cavitation is the formation of vapor bubbles in a moving fluid when the pressure of the fluid drops under its vapor pressure. This vapor pressure might be created due to a reduce in the inlet pressure, high inlet temperature, or increase in the flowrate [13]. Best efficiency point (BEP) is the goal that most centrifugal pump users try to achieve. Running centrifugal pumps at BEP is not always achievable. Therefore, operating outside of the BEP point will introduce bubbles to the system [14].

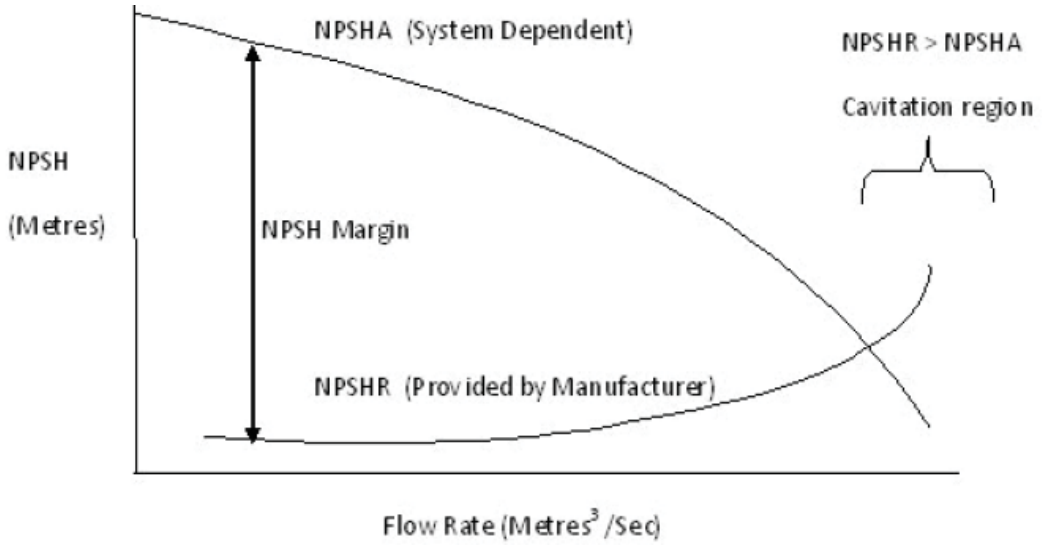

Figure 7. NPSH vs flowrate [12]

Figure 7 shows net positive suction head (NPSH) versus flowrate. NPSH stands for amount of liquid in the inlet side. NPSH is divided into two type; NPSHa and NPSHr. NPSHa stands for the available or actual head in the suction side of the pump, where NPSHr stands for the suction head required by the pump manufacturer. The figure shows that cavitation occurs when NPSHa < NPSHr. Furthermore, increasing flowrate will reduce NPSHa, therefore, creating cavitation. The reason behind that is, increasing flowrate will increase the fluid temperature and reduce the pressure [15].

Cavitation can be catastrophic to any system. It will produce erosion which is the breakdown of the vapor bubbles when the pressure in the system increases. The energy of that collapse creates stresses on the areas where cavitation is occurring, and therefore damaging those surfaces [16]. The risk of having erosion will be four times higher when the flowrate increases by 20% of the shockless flow. Shockless flow occurs when the flow is 10 to 30 % higher than the flowrate required to run the pump at BEP [17].

Cavitation can also be associated with noise. As the bubbles explode, they create a high pitch and random noise [18]. There are three different cavitation noises; sheet cavitation, cloud cavitation, and vortex cavitation. Sheet cavitation is associated with low amplitude, and low frequencies between 2 kHz to 40 kHz. It is usually occurring in the vane area of the pump. Cloud cavitation is the highest amplitude noise between all three, and the frequency range is between 20 kHz to 40 kHz. Vortex cavitation occurs in the suction area, while the flowrate of the pump is low. It is not stable and has low damage, because the bubbles occur in the inlet side and not around the pump. It is associated with low amplitude and low frequencies of 1 to 4 Hz [19].

Mechanical vibrations are also created by cavitation. Vibrations caused by cavitation is associated with high amplitude and low frequencies in the range of 0 to 10 Hz [17].

Pump's efficiency is highly reduced when cavitation exists. Bubbles created around the pump acts as gates that blocks the flow [20]. Reduced efficiency is a clear sign of cavitation occurrence, as the rest of the signs (noise, vibration) do not last. It is shown that in some scenarios, efficiency will increase just before cavitation occurs, then it will drop drastically [21].

Radial thrust is another hydraulic issue associated with centrifugal pumps. It is the thrust in the direction of the center of rotation. Radial thrust can cause the shaft to move and deflect, and eventually causing failure. Radial thrust can also create temperature rise in the bearings, reducing the life span. High radial thrust can also cause unbalance. Radial thrust can be reduced by increasing the flowrate or creating a feedback path to the system to allow the flow to return to the suction side [18].

Axial thrust can be problematic, too. Axial thrust occurs in the direction of the shaft axis. It usually introduces bearing fatigue failures. These failures are caused by the cycle loading accompanied

with axial thrust. It will cause failures in shafts and bearings. Shaft problems can be avoided by increasing the area of the output flow thus reducing the pressure on the axial or by the feedback path mentioned earlier. To detect axial loads, an accelerometer can be installed in the base where the pump exists.

Bearing failure is described as a mechanical failure. There are three reasons for this failure, solid particles trapped inside the oil, mixing the oil with other liquids, and increase in the temperature. The reasons of those problems vary [22]. Mixing the running oil with solid particles or other liquids can be due to leakage of unproperly sealed bearing. This mixture can create stresses on the shaft, causing an overload on the bearings. This also leads to misalignment between the pump and the driver, causing the pump to operate far away from its BEP. Proper sealing will help reduce bearing problems [23].

Seal problem is the second mechanical defect to study. The main reason for this problem is the dryness of the pump due to lack of lubrication. To solve this issue, most of the seals are pressurized to keep the lubrication for extended periods [24]. When the seal starts to fail, solid particle invades the pump causing scratches on the impeller or the sealing of the pump. This phenomenon will create wear in the impellers and the casing. To avoid sealing problems, temperature should be kept within the specifications of the manufacturer, and also to use sufficient lubrication methods [22].

Lubrication failure is another mechanical problem. The goal of a lubricant is to reduce wear by reducing friction in moving parts. Clean oil (no mixers) can prevent wear in the components up to thirty years in 30° C environment. If the temperature rises 10 degrees C, this will reduce fifteen years of the components life. Heat can be caused by overloads in the bearing as mentioned earlier.

If high temperature exists, viscosity of the lubricant will be reduced causing lubrication failure [25].

Excessive vibration is also an unwanted mechanical phenomenon. There are multiple sources of vibration in centrifugal pump. Impeller imbalance causes high vibration due to unbalanced forces coming from loose impellers. Baseplates can also cause increase in vibration when it is made from a material than does not have high rigidity. For example, cast iron causes higher vibration than steel if used as the baseplate material. Hydraulic imbalance is also a source of high vibrations. It is formed because of the irregular flow motion in the casing of the pump. Increasing the NPSHa will help eliminate this problem [18].

Shafts can be a source of high vibrations. Vibrations from the shaft is mainly occurring due to the imbalance in the weight of the components or misalignment in the shaft. This will cause radial force, therefore, creating high source of unwanted vibrations [26].

Beebe, discussed in his work multiple sources of vibration in centrifugal pumps and the causes behind it. He tested different speeds, and diagnosed the issues related with it. He changed temperatures to detect the misalignment caused by thermal expansion. He cut some parts of the pump to analyze the unbalance. Finally, he applied impact forces to test the bearing and casing housing frequencies [27].

Fatigue is another major problem in pumps. Most of pumps run for several hours without stopping. Therefore, fatigue is a common problem. Fatigue failures have three steps; crack initiation, crack propagation, and final failure. To reduce fatigue failure, higher corrosion resistance material can be used [18].

The last problem discussed in this work is the excessive power consumption. If the pump is using higher input power than needed, this means there are multiple problems causing this issue. First problem might be the contamination of the fluid. Running fluids might have solid particles accompanied with it. These particles will cause wear in the pumps components, reducing efficiency by demanding higher inlet power. This is a very common problem, and almost every centrifugal pump system faces this issue [28]. Other issues causing excessive power consumption can be summed as liquid density is higher than recommended, liquid viscosity is higher than specified, speed is higher than recommended, misalignment of the shaft, and some damage in the impeller [29].

3.2 Health Monitoring Methods

As mentioned earlier, centrifugal pumps are one of the largely used pumps in industry. For that reason, maintenance methods are studied heavily. There are three types of centrifugal pump maintenance methods; breakdown, preventive, and condition-based maintenance. Breakdown maintenance is the oldest method of maintenance. In this method, there is nothing done until the pump breaks or it fails and requires a repair. Preventive maintenance was introduced in 1950s after the breakdown method produced high cost and time waste. This waste came because replacing the equipment and repair it when it fails, became highly expensive and time consuming. In the preventive method, there are a periodic inspection and maintenance, even if, the machine does not have a fail [30].

Bazovsky started the preventive method by introducing mathematical optimization by using maintenance policies [31]. Jardine presented prevention method by analyzing reliability information, such as breakdown history of a machine and cost of repair, and presented models for

selecting the best replacement or repair method [32]. Nevertheless, periodic maintenance did not find acceptance by many users because it is labor concentrated, and it will not prevent terrible failures.

Condition-based maintenance (CBM) is the future vision of preventive maintenance using intelligent systems. CBM monitors the pump condition using measurements that do not affect the daily operation of the pump. CBM have three components; data acquisition system to take measurements using different sensors, data processing techniques to acquire the needed signals, and decision making by identifying which area is affected and what is the best maintenance method to use. CBM tries to monitor the machine health and compare it to the normal running conditions. If the machine reports unusual activity, then it means failures are starting to happen. Vibration and acoustic data are introduced to the system as a monitoring methods. With CBM advancing, new type of data using new technologies are introduced. Those types of data might be too advanced and not fully explored yet. Therefore, it will be a challenge to the analysis team to fully understand what to do with it. To avoid that, automated systems should be installed to autonomously diagnose and control the machine. This process is known as prognostics. Prognostics provides multiple advantages and savings in time and cost by reducing labor hours and downtime [30].

There are many studies conducted in the past regarding prognostics and diagnostics methods. Vachtesvaneo et al created intelligent failure detection methods for machines using different examples [33]. Pusey and Roemer introduced new aspects for developing prognostics in turbo-machinery [34]. Jardine focused on creating a collection of publications regarding data acquisition and failure prognostics of different systems [35]. In summary, there are three different methods to predict malfunction in rotary machines; event based, condition based, and prediction and event based. Event based prediction methods use the past data until failure to analyze the performance

of a machine. It uses reliability functions to model the machines performance. This method is useful for a company that makes high volume identical units; as diagnosing the history of machine's performance is only helpful if the same machine is used with the same specifications. Another setback of this method is that the information provided are for the overall production units and not for a specific unit. This means, for an individual unit, this method is not hundred percent accurate. Condition data based prediction is more general than the event data based prediction. Condition monitoring (CM) provides ongoing information about the health of the machine. This information is particularly useful for engineers who are monitoring the behavior of the machine, and based on the information given, a decision will be made. CM enables engineers to create models to predict the failure of the machine. These models can be physics based models or data-driven models. Physics based models can be useful in predicting stresses, cracks, and other type of physical failures in the system. Physics models do not require big database from the operating system. On the downside, physical models assume system conditions to stay the same. This assumption in many cases is not a valid one, as dynamic systems can change rapidly. Also, physical models can be computationally expensive. Data-driven models do not require physical assumptions nor it is computationally expensive. But, it requires large amount of information of the system's operation. Combining event and CM methods together provide higher accuracy and longer prediction ranges [30].

Some researchers investigated the physical prediction models. Lee used finite element model based on Paris law to investigate the crack growth and stresses on gear tooth [36]. Loparo used Forman law of linear elastic fracture mechanics to model shaft crack increase. This model was not as sufficient, as it required stopping the machine's operation, and taking measurements of the instantaneous defect size [37]. Sentient Corporation provided a finite element based model to

obtain the life cycle of a machine by measuring the stress field. The program is called Contact Analysis for Bearing Prognostics [38]. Qiu et al. investigated the failure natural frequency and vibration amplitudes and related them to the running and failure times [39]. All the above physics based models require numerous assumptions, those assumptions in some cases would make the system unrealistic. Also, some parameters used in those models require aborting the machine, therefore, loss of time and cost.

Just like the physical model method, data-driven models are intensively studied in literature. Data-driven method creates models from directly collected condition monitoring data rather than models that are physics dependent. There are two main models used; smoothing and autoregressive models. These two models are common because of their simplicity. But, the main disadvantage in those two model is that they assume the system's operation to have some stability. This assumption might not be valid in all cases [40]. Cempel suggested a Tribo-vibroacoustical (TVA) model that approximates the failure time of the system. His model could approximate the vibration amplitudes, but could not estimate the unexpected variation in the system's life operation [41].

Artificial neural network (ANN) is the furthermost used data-driven method. ANN uses layers and nodes to train network to create a relationship between inputs and outputs. ANN depends on inputs and outputs data to make that relationship. ANN have multiple components associated with it; layers of input nodes, layers of hidden nodes, and one layer of output nodes. These layers are adjusting information by weights. There are multiple advantages of using ANN. It performs quicker than traditional methods [42]. It is very similar in performance to statistical methods but without the need to make distribution assumptions [43]. Also, it can make complicated mathematical relationships without previous knowledge [44].

Figure 8 shows similarity between the biological and artificial neural network. Neurons in the biological network are connected by axons, each link can modify a signal depending on the activation status. Artificial networks are also consisting of neurons that are connected to each other, and the information between each neuron is modified using weights. These weights can decide on the importance of each neuron. Each of these neurons have an activation function associated with it. Activation functions build the relationship between inputs and outputs in the network [45].

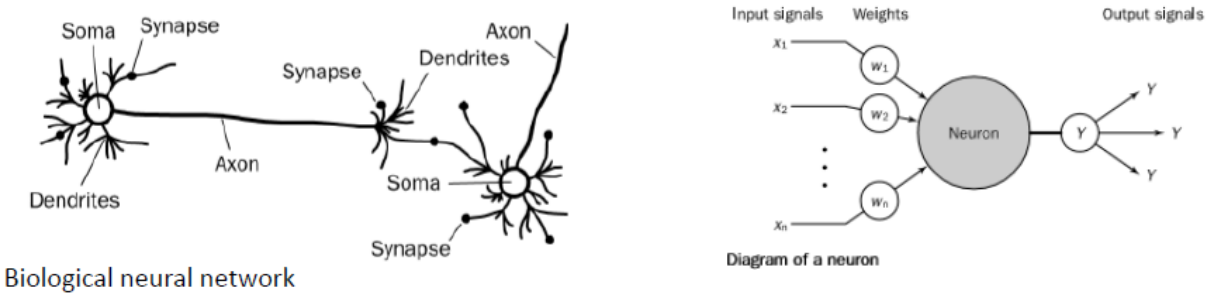

Figure 8. Biological (left) and artificial (right) neural networks [45]

In health monitoring techniques, ANN are used with time series estimation models. Yam et al used RNN (recurrent neural network) to decide on the suitable CM method from the input signals [46]. Wang and Vachtsevanos created a wavelet neural network (RWNN) to estimate crack propagation in bearings [47]. Shao and Nezu used feed forward neural network (FFNN) to create a single step ahead estimation of defects in bearing's elements [48]. Gabraeel et al. estimated the genuine bearing failure time by using exponential function as the crack growth, and he used FFNN to compute the exponential function parameters [49].

The third method of failure prediction methods is the integrated CM and reliability methods. CM is useful, and it is the most used method in failure prediction. Nevertheless, it does not give reliability information of a system. Therefore, integrating reliability with CM models will solve

that issue [30]. Goode et al. used Weibull distribution to predict the failure in hot strip steel mill accompanied with a model based on vibration data [50]. Jardine et al. created Proportional Hazards Model (PHM) to predict the reliability of elements in bearings and engines. His model used CM data to use in the reliability model [51]. Sun et al. suggested a Proportional Covariates Model (PCM) that predicts the failure in mechanical parts. He used PCM to create reliability functions to predict failure while the machine is operating [52]. Wang developed PHM and PCM models to create an overall residual time distribution to predict the life of bearing elements [53]. Cempel et al. defined reliability in symptom's condition domain. He assumed that defected parts have a uniform failure value. Then, he used that value to create a function that estimates the failure of a part based on the symptoms [54].

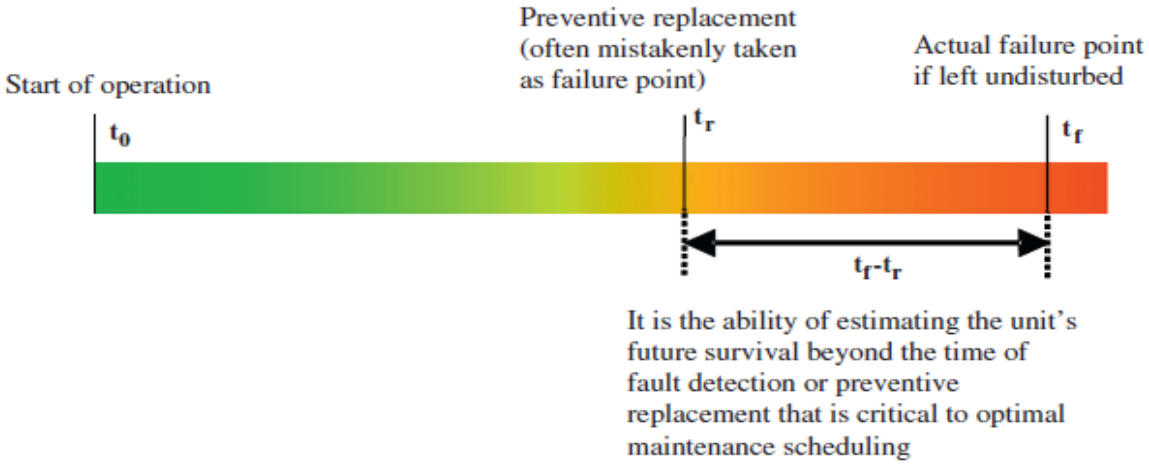

Figure 9. Timeline of the operational life of a part [30]

Figure 9 shows the timeline of a product life. The figure shows that, often, the preventive methods in detecting failures do not guarantee the accurate failure point. This concludes that failure prediction methods have difficulties. These difficulties can be summed in few points. First, the ways of capturing the system's data need to be entirely discovered. Second, because of the changing behavior of an operating machine, the need for accurate models to predict that change is

a must. Lastly, expanding the prediction methods to different types of machine can be challenging [30].

Samer proposed an algorithm based on using FFT (Fast Fourier Transform) to create a CBM system to identify acoustic emissions for fault diagnosis. He claims that his algorithm overcomes the problems associated with artificial intelligent. The algorithm has a 100% failure detection accuracy [55].

Fardin claimed a novel bearing condition monitoring technique (BCM) method to detect failures in bearings. His method is based on analyzing the instantaneous frequency of motor voltage. He said that this method is better than other methods that are based on analyzing vibration and current. He said that this method is much more efficient and less time consuming [56].

Abtin used two methods to apply CBM, ANN and Support Vector Machine (SVM). He focused merely on detecting failures using common features in centrifugal pumps. These features are flow, temperature, inlet pressure, outlet pressure, and vibration. He optimized the performance using Genetic Algorithm (GA) [57].

McKee suggested a vibration cavitation sensitivity parameter to detect cavitation in centrifugal pumps. He used adaptive octave band analysis accompanied with statistical methods. He used water pumps to perform the experiments following ISO 10816 classifications [58].

Senthilkumar created a fault diagnosis tool using Shape Memory Alloy Based ATDVA. He used vibration data on three axes using accelerometers. The tool could detect unbalance, misalignment, hydraulic pulsation and bearing defects in the system. He claimed that 60% of vibration amplitude could be reduced when varying frequencies from 335 to 340 Hz [59].

Kostyukov used vibration detection method in adaptive measurements. The goal of his work was to increase the accuracy of CBM using spectral analysis. He claimed that he was able to separate the spectral data for the defects, opening the way to make precise health monitoring decisions [60].

Luo developed a sensorless cavitation detection method based on the current signals. This method reduced number of sensors used and the time required to install them. Because of the new idea of sensorless data, this work provided study of motor current usage in detection cavitation [61].

There are few disadvantages of the above models. First, they are concerned with a single component or a single failure. Second, they present highly complicated methods to follow or apply in real industry. This work suggests a systematic health monitoring technique that can be followed and applied easily. This work has four stages. The first stage is characterization of a centrifugal pump to identify the running conditions, and obtaining the normal operation schemes. The second stage is modeling the system conditions using MATLAB. In this stage, transfer functions are created to relate inputs to outputs. The third stage is designing industrial experiments to understand the effects that the system's parameters have on some outputs. The last stage is the control methods. In this stage, intelligent control methods are introduced, such as ANN and fuzzy logic. The goal of this control is to avoid the settings that create defects in the system.

3. Investigation Approach

To create a systematic robust method to monitor the safety of a centrifugal pump, few steps have been taken. First, experimental rig containing sensors to measure flowrate, pressure, vibration and temperature have been installed in a setup like what Boeing (Aircraft Company) has for their fuel system. Second, industrial design processes such as Taguchi (Orthogonal Array) and Response Surface Methods (RSM) were used to plan the experimental procedure, and to analyze the results. The third step was to model the system using classical Transfer Function (TF) methods with the help of the programming language MATLAB. Lastly, control methods were used to keep the pump from operating in the low efficiency, high risk regions. Those control methods are based on Artificial Intelligent (AI) methods. These methods are Artificial Neural Network (ANN) and Fuzzy Logic (FL).

3.1. System Design

3.1.1. Hardware

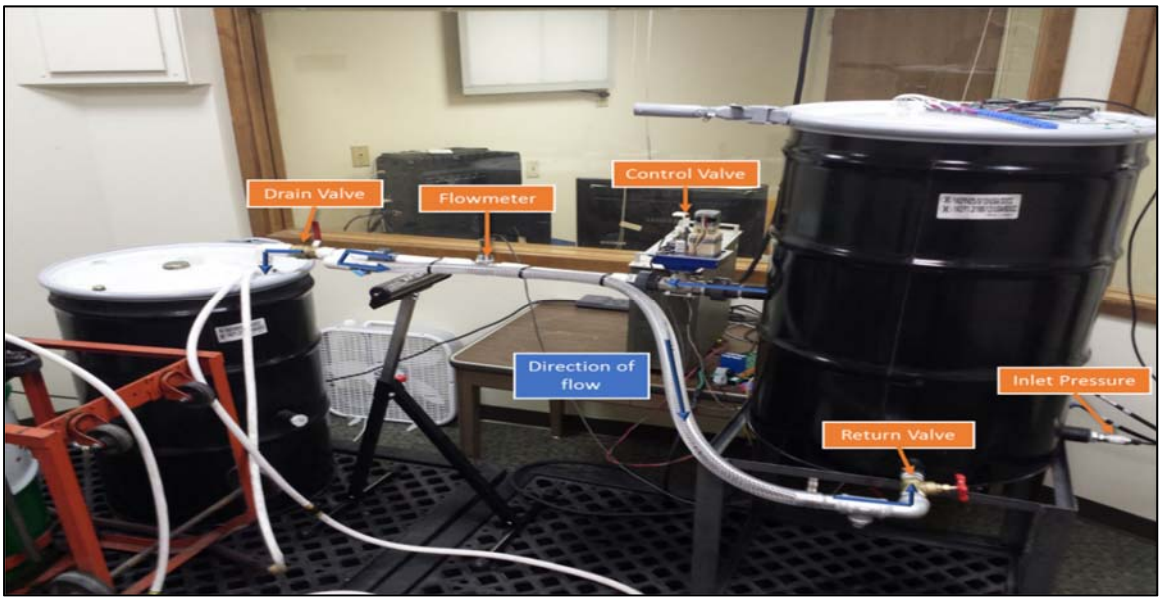

Figure 10. Experimental rig used in this research [62].

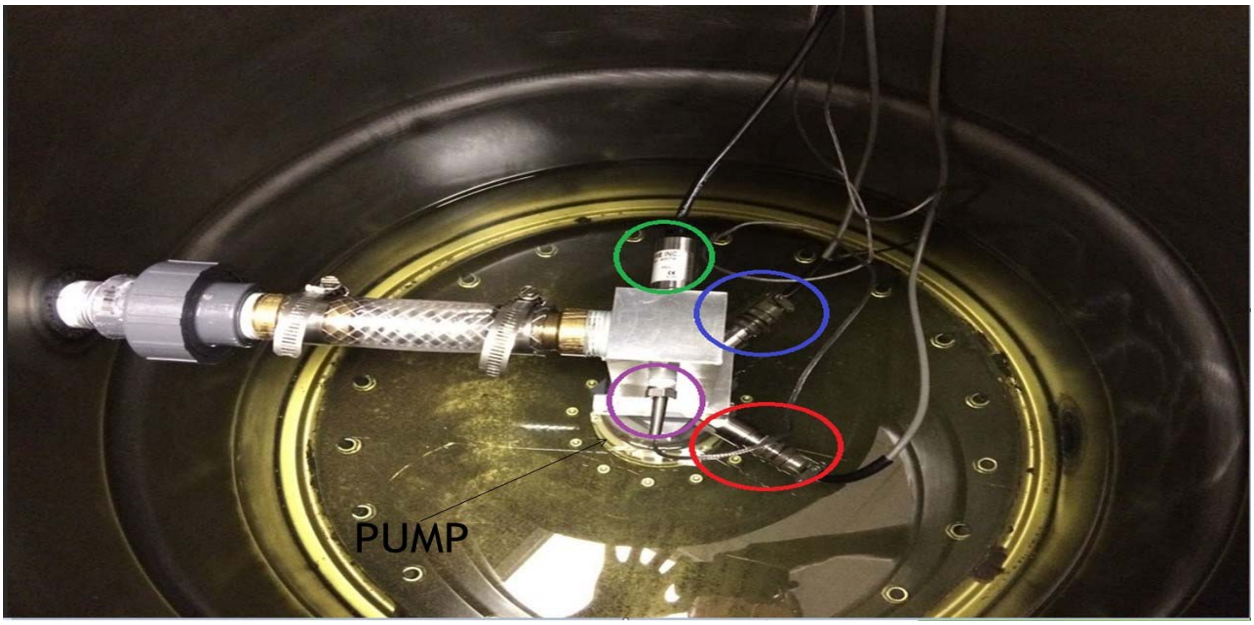

Figure 11. Inside the main tank

Figure 10 shows the experimental rig used in this work. The setup contains two tanks, primary (one on right) and secondary; pressure transducers to measure inlet and outlet pressures in the pump; flowmeter to measure the outlet flow of the pump; and electro-mechanical control valve that can be controlled using data acquisition system. Figure 11 displays the inside of the main tank. It contains centrifugal pump in the bottom of the tank, and it is contained by a special casing; accelerometers (red and blue circles); pressure transducer (outlet pressure, green circle); and RTD (Resistor Temperature Detector, purple circle) to measure the fluid temperature as it leaves the pump (outlet temperature). Another accelerometer lays on the bottom of the tank (not shown) that measures the vibrations perpendicular to the two accelerometers shown in the figure. The pump used was manufactured by the French company, Intertechnique. The fluid used in this work is MIL-PRF-6081, Grade 1010 Mineral oil with a specific gravity of 0.85. PVC pipes with 1 inch diameter are used in the connections. Full description of the system components can be found in the appendix.

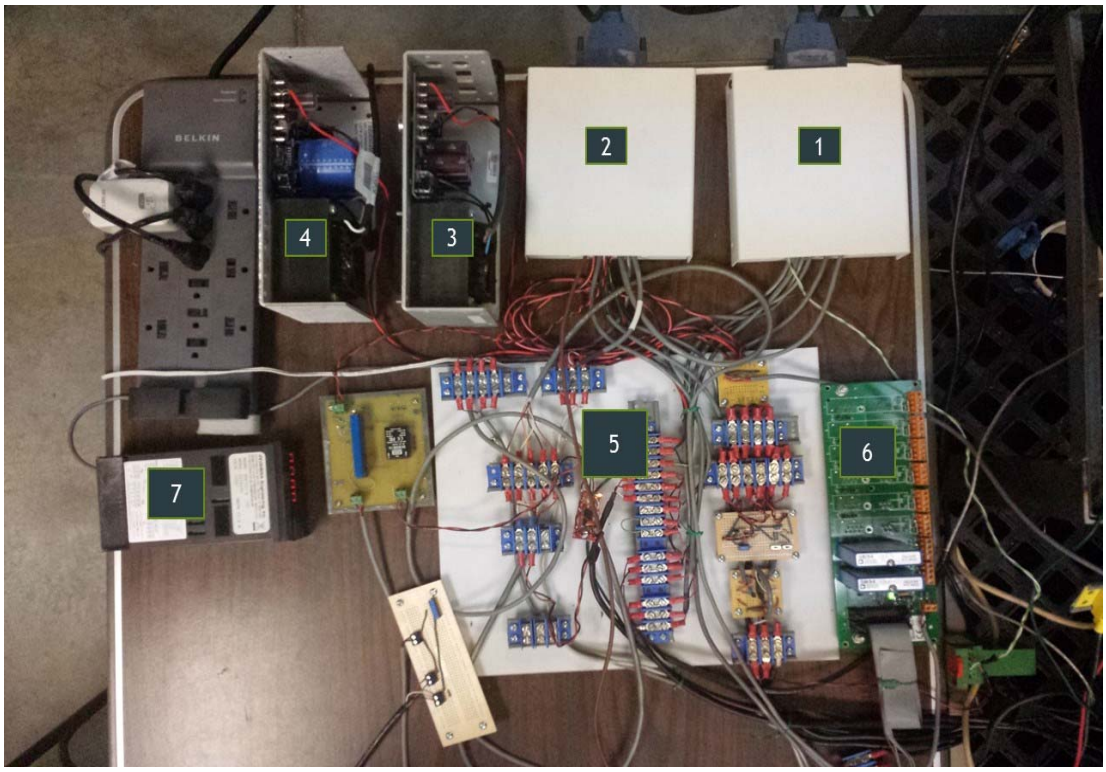

Figure 12. Electrical setup

Figure 12 shows the electrical components used in the experimental rig. All the data from the sensors are connected through this electrical setup. Numbers one and two (Figure 14) correspond to the modules used to connect the sensors. All the signals used in this work are analog signals. So, to connect it to a computer, PXIe device was needed (Figure 13). Numbers three and four are two 24 VDC power supplies to activate the sensors, as most of the sensors run from 0-10 volts. Five is an electrical junction for connecting the wires coming from the sensors and going to the DAQ (Data Acquisition) device. Number six is a current source to activate the RTD sensors, as those sensors are resistance based, and need a current source activate them. The other sensors are voltage based. So, they only need the voltage coming from the power supply. Lastly, number seven corresponds to a frequency converter. This converter will convert the frequency signal coming from the flowmeter to voltage. The turbine flowmeter used in this work uses rotational movement

of blades to calculate how fast those blades are rotating. Then, it uses the frequency of the rotation and sends it to the frequency converter. The frequency is then calibrated by the converter into a flowrate measurement such as GPM (Gallons Per Minute).

Figure 13. DAQ Assistance NI PXIe-1078

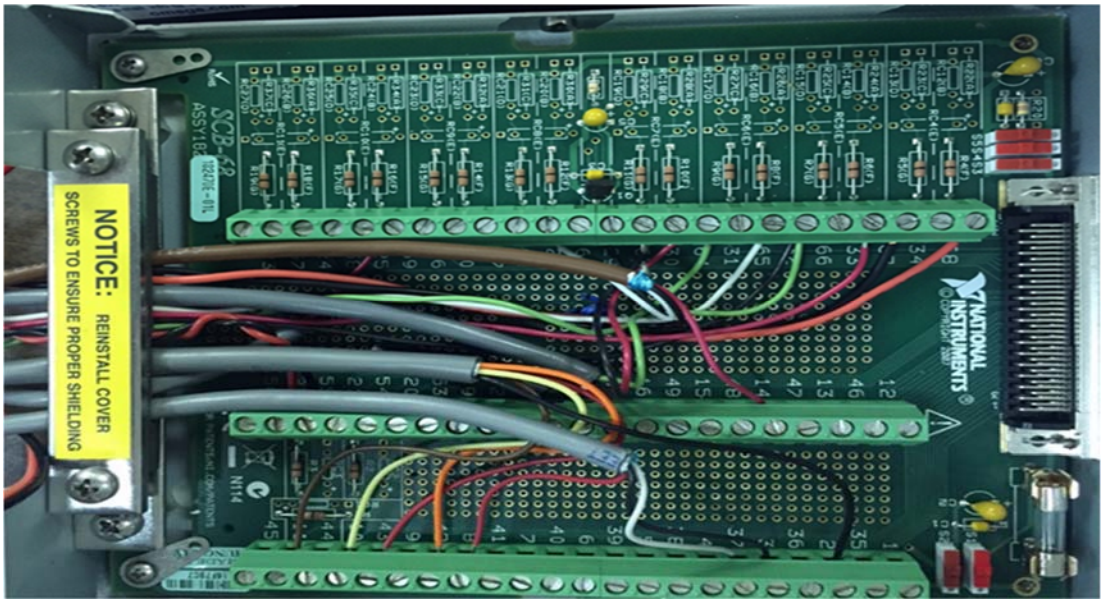

Figure 14. Signals modules

3.1.2 Software

To interact with the hardware devices, a software package that can provide DAQ interaction is necessary. So, LabVIEW (Laboratory Virtual Instrument Engineering Workbench) is chosen. LabVIEW software has the ability of receiving and sending signals from and to a workstation machine such as a computer. LabVIEW was created by National Instruments (NI), it is the same company that manufactured the DAQ hardware used in this work. Having the same manufacturer for the hardware and software means less complications in the interaction between the two.

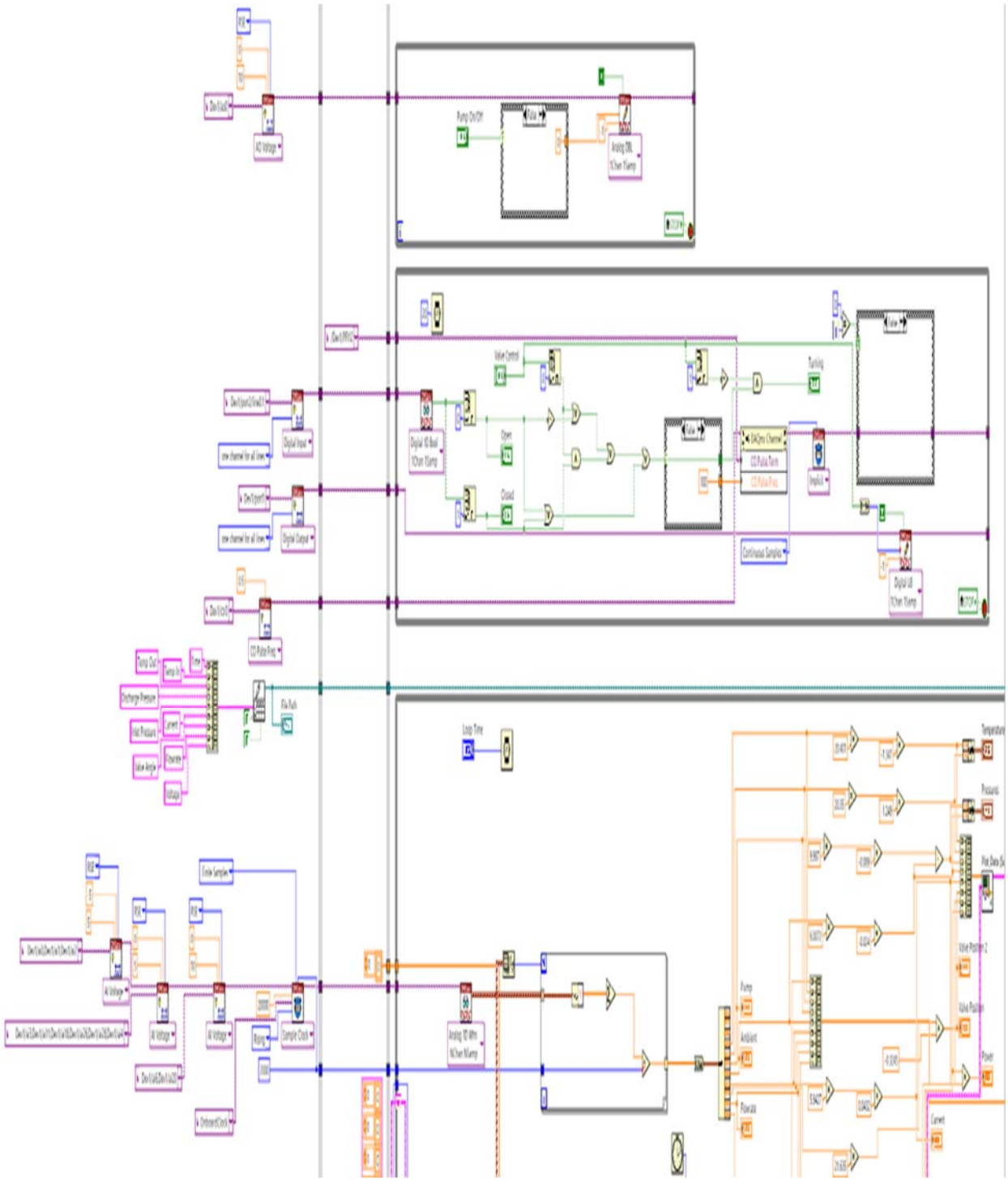

Figure 15. LabVIEW interface

Figure 15 shows the LabVIEW program used in this work. The image does not do justice to the program. So, the following paragraphs will have explanation of the main tools used in the program, these descriptions are taken from the LabVIEW manual created by NI [63].

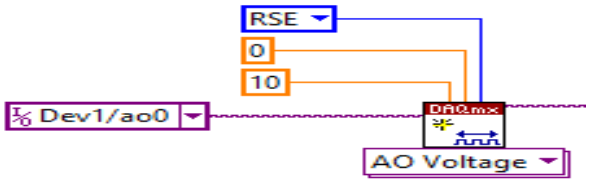

Figure 16. DAQmx Create Channel

The icon above associated with creating a virtual channel that allows the user to create either a receiving channel from the card reader of the DAQ hardware or a sender channel. The main thing to keep in mind when using this tool is the type of signal that the sensor is recoding, whether it is a single ended referenced (RSE) or differential (DIFF).

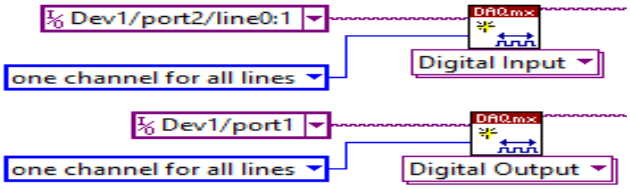

Figure 17. DAQmx Create Channel - Digital Input/Output

The above two icons create a virtual digital input and output channels. If multiple sensors are to be connected in the same line with different ranges of voltages, then the order of the icons will determine which channel will be used first.

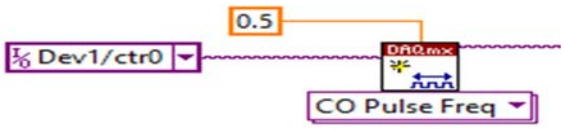

Figure 18. CO Pulse Frequency

The above icon allows the user to create digital pulses for a defined frequency.

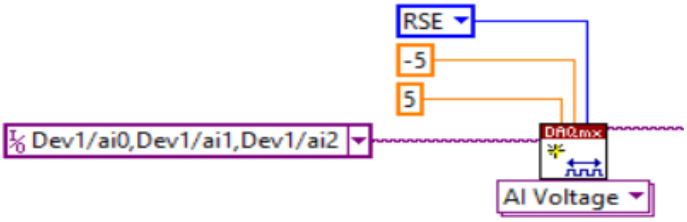

Figure 19. Analog Input Channel

The above icon allows taking measurement from an analog source, such as pressure or temperature. Each physical channel will have the shortcut, ai0, which corresponds to analog input, and the number attached to it corresponds to the number of the channel. For example, if the pressure sensor is connected to physical analog channel 6, then the analog input channel for it will be ai5. As the number of the channels starts from zero and not one.

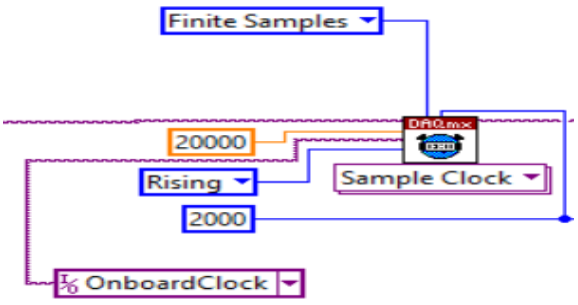

Figure 20. Sample Clock

The above icon controls the sample rate of the data. Sample rate is the number of samples collected in seconds. The higher the sample rate, the more information sent to the user. But, the main problem with increasing the sample rate is the ability to store the data. Furthermore, higher sample rate mainly depends on the DAQ hardware used. In general, the higher the sample rate, the more expensive the DAQ device will be.

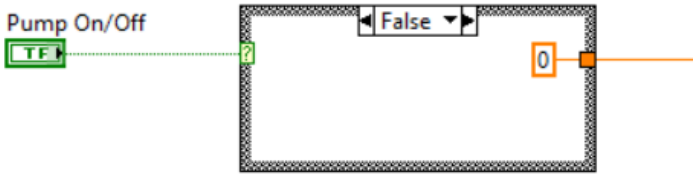

Figure 21. Case Structure

The above icon serves as a conditional statement. If the condition on the question mark icon is met, then what is inside the square will be active. This special icon can be used to decide when the data are being collected. In General, data in the beginning and end of the physical operation is not of an interest because it contains large sources of error. So, the use of this icon decides when to record the data.

Figure 22. Single Tone Extraction

The above icon collects the phase, frequency, and period of the time signal. This is helpful when spectral analysis is needed. The use of this icon in this work allowed to convert time domain information to frequency domain using FFT (Fast Fourier Transform). FFT computes the DFT

(Discrete Fourier Transform) of a function. DFT converts the finite samples of equal distances to an equivalent sample of same distances [64].

$$X_k = \sum_{n=0}^{N-1} x_n \cdot \left(cos\left(-2\pi k \frac{n}{N}\right) + isin\left(-2\pi k \frac{n}{N}\right)\right), k \in Z \qquad \text{Equation 2}$$

Equation 2 shows the FFT of a discrete data. This equation is implemented in LabVIEW using the icon in Figure 22. The frequency domain information is much simpler method to explain vibrations. The plots from the time domain will not show clearly the amplitude and frequency of the signals involved, but the frequency domain data will do. Finally, all the data gathered are stored in excel.

3.2. Experimental Design and Procedure

After the installation setup, it is time for the experiments. The main goal of the experiments is to find the conditions and parameters that ensures the safety and health of the centrifugal pump. In this work, there are four main control factors to study, fluid height in the main tank, speed of the pump, valve angle and time. Valve angle term used in this work refers to the amount of opening the valve has. If the valve is half way open, then the valve angle will say 50°, and fully closed will be 90°. The speed range used is between 6000-11000 RPM (Revolutions Per Minute). The time is measured in minutes, and it is between 0-20 minutes. Fluid height level is between 3-6 inches.

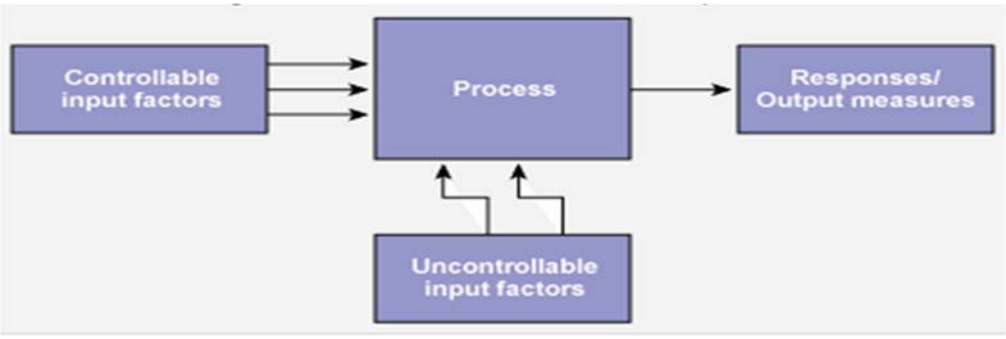

Figure 23. Components of Design of Experiments

Figure 23 shows the main components of the design of experiments (DOE. DOE is a systematic method to investigate the relationship between the factors and the results of a process. To fully understand the pump operation, full factorial experiments were conducted. These experiments will characterize the pump and system operations. Maximum efficiency at different speeds will be determined. Factors levels were these efficiencies occur will also be known [65].

Industrial design of experiments such as Taguchi (Orthogonal Array) method and Response Surface Methods (RSM). Taguchi methods saves time and cost while keeping accuracy of the experiments. It minimizes variation of the samples while keeping ensuring robustness. It also based on engineered quality and not added value. The main disadvantage of the Taguchi method that it does not explain the interaction between the factors accurately because of the small sample size. [66]. To fix that issue, RSM methods are used. RSM can serve not only as a valid way to explain interaction between factor but also as an optimization tool [67].

3.2.1. Full Factorial Design

In this section, the full factorial DOE used in this work is explained. The main goal of the full factorial experiments is to investigate all the factors with all of the levels. This process gives the ability to explore the maximum efficiency of the pump.

$$Y_{ij} = \mu + A_i + B_j + AB_{ij} \ldots Z_k + \varepsilon_{ij} \qquad \text{Equation 3}$$

Equation 3 explains the model used in the full factorial design. Where i=1,2,3..., n and j=1,2,3…n, correspond to the levels of each factors. A and B up to Z, are the factors used, ε_{ij} is the error term confounded with A and B interactions [65]. In this design, two factors were considered, speed of

the pump and valve angle. Speed of the pump have six levels, and the valve angle have seven levels. The schematic of the experiments is presented in the table below.

Table 2. Full Factorial Setup

Speed (rpm)	6000	7000	8000	9000	10000	11000
	Valve Angle (Degree)					
	30	30	30	30	30	30
	40	40	40	40	40	40
	50	50	50	50	50	50
	60	60	60	60	60	60
	70	70	70	70	70	70
	80	80	80	80	80	80
	90	90	90	90	90	90

Table 2 shows the full factorial design setup used in this work. The table shows that for each speed there are seven valve angles, totals in 42 experiments. The sole purpose of these experiments as mentioned above was to characterize the pump and to find the maximum efficiency.

$$\eta = \frac{P_T Q}{EI} * 0.435 \qquad \text{Equation 4}$$

Equation 4 describes the efficiency of a centrifugal pump [62]. P (psi) is the head, Q (gpm) is the output flowrate, E (volts) is the voltage and I (ampere) is the current. E and I are associated with the motor that runs the pump. So, the efficiency is the ratio of the output power (Hydraulic Power) represented in flowrate and pressure divided on the inlet power (Electrical Power) represented in the current and voltage supplied to the motor. The number 0.435, is the conversion ratio to horsepower.

3.2.1. Taguchi Method (Orthogonal Array)

Genichi Taguchi added multiple benefits to industrial statistics. Some of his contributions were reducing variations around a targeted value, suggested experiments to design a product that is insensitive to changes in it is own components, he used loss functions to study the economic aspect of a product variation, and he insisted that the quality must be engineered to the system and cannot be added to it. The Taguchi approach to any engineering design had three steps. System design; which focuses on the technical aspects of a product. Second, parameter design; which focuses on the performance of a product that is insensitive to changes in it is own components and the environment around it. Lastly, tolerance design; which focuses on optimizing the parameter design to achieve lower variation [66].

Taguchi methods, like any other statistical design method, have few parameters associated with it. The goal of these parameters is to explore the effect of each factor individually without the interaction term. The main goal of orthogonal array is to find the optimum set of conditions that brings the optimum results. Taguchi methods are pre-defined experiments depending on the number of factors used and their levels.

Table 3 shows the standard orthogonal arrays used. L_4, means that there are four experiments in this setup. The table also shows the number of factors allowed in L_4 are three, each factor with two levels. There are two types of problems associated with Taguchi method; static and dynamic

problems. Static problems occur when the signal or the source takes a fixed value. Dynamic problems occur when the signal and the response have a linear relationship [68].

Signal to noise ratios (S/N) are log functions that determine the desired outcome from the Taguchi experiments. It can be viewed as the objective function for optimization, S/N helps in the analysis and prediction of the optimal values. There are three different scenarios where S/N analysis is of interest; smaller the better, lager the better, and nominal the best. Smaller the better is used when the characteristic variable or the response needs to be minimized. For example, defects in a product. Larger the better is the opposite, were the response needs to be maximized. Such as, strength of a material. Nominal the best, is used when the response needs to be as close as possible to a desired value. Equations 5-7 show the mathematical interpretation of each scenario. Measured data, are the values of the characteristic variable.

$$Smaller\ the\ better = -10\ Log_{10}[mean\ of\ sum\ of\ squares\ of\ measured\ data] \quad \text{Equation 5}$$

$$Larger\ the\ better = -10\ Log_{10}[mean\ of\ sum\ of\ squares\ of\ reciprocal\ of measured\ data] \quad \text{Equation 6}$$

$$Nominal\ the\ best = -10\ Log_{10}[\frac{square\ of\ mean}{variance}] \quad \text{Equation 7}$$

Table 3. Standard orthogonal arrays [69]

Orthogonal array	Number of rows	Maximum number of factors	Maximum number of columns at these levels			
			2	3	4	5
L_4	4	3	3	-	-	-
L_8	8	7	7	-	-	-
L_9	9	4	-	4	-	-
L_{12}	12	11	11	-	-	-
L_{16}	16	15	15	-	-	-
L_{16}'	16	5	-	-	5	-
L_{18}	18	8	1	7	-	-
L_{25}	25	6	-	-	-	6
L_{27}	27	13	-	13	-	-
L_{32}	32	31	31	-	-	-
L_{32}'	32	10	1	-	9	-
L_{36}	36	23	11	12	-	-
L_{36}'	36	16	3	13	-	-
L_{50}	50	12	1	-	-	11
L_{54}	54	26	1	25	-	-
L_{64}	64	63	63	-	-	-
L_{64}'	64	21	-	-	21	-
L_{81}	81	40	-	40	-	-

After finding the S/N ratios for all the experiments, it is time to find the optimum level for each factor. This process takes two steps. First, finding the average value of each level. Second, plotting those averages on a response graph or tabulate them in a response table. S/N is a log based value, this means, the bigger the value, the better the response. So, for each factor, the optimal level is associated with the higher S/N value. After that, those optimal levels are added together to find the optimum S/N ratio for the characteristic variable.

$$Optimum\ value = mean + a_i + b_j + \cdots + z_n + error \qquad \text{Equation 8}$$

Equation 8 calculates the optimal overall value. Where $a_i\ and\ b_j$ are the optimal factors minus the overall S/N mean, and the error term corresponds to the experimental error. The next step is to use

the ANOVA tables (Analysis of Variance). ANOVA tables quantifies the contribution of each factor to the results.

Table 4. Structure of ANOVA table [70]

Source of Variation	SS	df	MS	F ratio
Between Samples	SSB	k - 1	$MSB = \frac{SSB}{k-1}$	$F = \frac{MSB}{MSW}$
Within Samples	SSW	n - k	$MSW = \frac{SSW}{n-k}$	
Total	SST = SSB+SSW	n - 1		

Table 4 shows the structure of ANOVA table. Where SS is the sum of squares, df are the degrees of freedom, MS is the mean square value, and F ratio is the statistical value to find the effect of each factor. Between Samples stands for the factors and Within Samples represents the error in the experiment. Total, shows the total values for df and SS.

$$SS = \sum_{i=1}^{N}(y_i - T)^2 \qquad \text{Equation 9}$$

$$df = (\#\ of\ levels\ of\ Factor - 1) \qquad \text{Equation 10}$$

Equation 9 calculates the sum of squares of the factors. Where y_i is the average value of the factor at a certain level, T is the overall average, and N is the number of levels for each factor. The error or within samples can be viewed in two perspectives. First, statistical error, which comes from subtracting the total sum of squares and the sum of squares for each factor. The second error, is the experimental error, were the factors with the lowest affects can be assumed as an error source.

In this work, Taguchi method were used twice. First, L_9 was used to determine five characteristic variables; efficiency of the centrifugal pump, amplitude and frequency of the pump in z-direction (vertical to the alignment of the pump), noise of the pump, and temperature rise. The factors used were fluid height in main tank, speed of the pump, and valve angle. Each of these factors have three levels. Table 5 shows the factors and levels used in the experiment. Table 6 shows the full L_9 design. The main goal of this experiment was to find the percent contribution of each factor to the characteristic variables.

Table 5. Factors and level used

Levels	Fluide Height (in)	Speed (RPM)	Valve Angle (Degrees)
1	3	6000	40
2	4.5	8000	60
3	6	11000	80

Table 6. L9 design

Expeirment #	Fluide Height (in)	Speed (rpm)	Valve Angle (Degrees)
1	3	6000	40
2	3	8000	60
3	3	11000	80
4	4.5	6000	60
5	4.5	8000	80
6	4.5	11000	40
7	6	6000	80
8	6	8000	40
9	6	11000	60

Second Taguchi experiment used was L_4. In this experiment, the goal was to find the contribution of time and speed to the five characteristic variables mentioned above. Table 7 shows experiments and the associated levels for each factor.

Table 7. L4 Orthogonal array

Experiment #	Time (min)	Speed (rpm)
1	5	6000
2	5	11000
3	20	6000
4	20	11000

3.2.2. Response Surface Methodology

Response surface method (RSM) is a process of creating an empirical model [71]. The main goal of the model is optimizing the response of the characteristic variable. The first step in the RSM is to find the appropriate approximation to the actual relationship between the inputs and outputs. The most common method is the low-order polynomials. In RSM, as in every design of experiment, the mathematical models or functions that describe the relationship have unknown formulation. Therefore, the design of the experiment is unique for every problem. The other goal of RSM is to notice the direction of change in the response. Those relationships can be fully described using either surface plots or contour plots [67].

There are multiple models that RSM use; First Order Model, Multi Regression Model, and Orthogonal First Order Design. Those models were developed based on the steepest ascent method. The main idea is to run a simple experiment to determine a surface of very small samples, then

extend it to create more complex surfaces. To find the equation of the surface, the experiments must follow specific order [71].

$$Y = B_0X_0 + B_1X_1 + B_2X_2 + \epsilon \quad \text{Equation 11}$$

$$Y = B_0X_0 + B_1X_1 + B_2X_2 + B_{11}X_1^2 + B_{12}X_1X_2 + B_{22}X_2^2 + \epsilon \quad \text{Equation 12}$$

Equation 11 represents the simplest surface model, two-dimensional plane. Y is the observed value; B's are coefficients that will be determined using the least square method. Those coefficients minimize the sum of squares of the error, ϵ. X's are the different variables used. Equation 12 shows a second order surface, this will be used if the experiments are expected to have a second order surface.

Central composite designs (CCD) are used to fit data into a second order response shape. It creates experiments based on a central point if the distance from the center point to any other design point is ± 1. Usually, CCD contains two times central points than the factors in the experiment. So, if the total number of factors is three, then there should be at least six central points. There are three different CCD designs; CCC (Central Composite Circumscribed), CCI (Central Composite Inscribed), and CCF (Central Composite Face-centered). CCC, is the most original form of CCD. The star points are extreme values that represent low and high levels for any factor. They are usually in a distance, α, from the central points. With the additional low and high levels suggested by the user, these star points are additional points to add in the experiments. CCI is a scale down design from CCC. CCI is used when the low and high levels of the factors are the actual limits of the experiment. Both CCC and CCI need at least five levels for each factor. CCF is used when the star points are at the center of each face of the factorial design. This means when α is actually ± 1. CCF requires at least three levels for each factor. Figure 24 shows the three different CCD methods.

Square points are the star points and the circular points are the levels of each factor. Equation 13 shows how α is calculated.

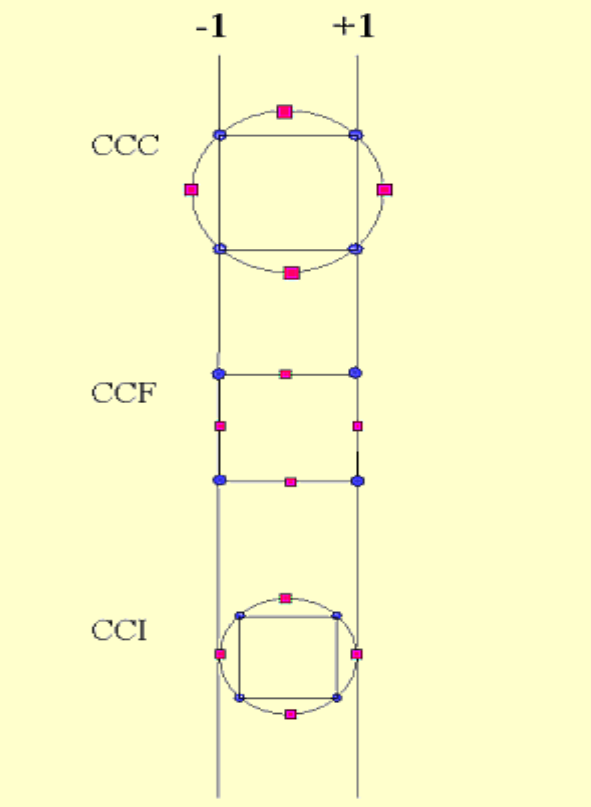

Figure 24. Types of CCD methods [70]

$$\alpha = [number\ of\ factorial\ runs]^{(\frac{1}{4})} \qquad \text{Equation 13}$$

In this work, CCD is used with CCF method. The goal of doing these experiments was to determine the relationship between the five characteristic variables, z-direction vibration's amplitude and frequency; temperature rise in the system; efficiency of the pump; and noise of the pump. Three factors with three levels are used, fluid height in the main tank (3,4.5 and 6) inches; speed of the pump (6000,8500, and 11000) rpm; and valve angle (40,60 and 80) degrees. The biggest advantage

RSM method have over Taguchi method, is the ability of creating a response surface between the factors(interaction), and between the characteristic responses and the factors.

Table 8. CCF design

Expeirment #	Fluid Height (in)	Speed (rpm)	Valve Angle (Degrees)
1	3.0	6000	40
2	3.0	6000	80
3	3.0	11000	40
4	3.0	11000	80
5	6.0	6000	40
6	6.0	6000	80
7	6.0	11000	40
8	6.0	11000	80
9	3.0	8500	60
10	6.0	8500	60
11	4.5	6000	60
12	4.5	11000	60
13	4.5	8500	40
14	4.5	8500	80
15 (C)	4.5	8500	60
16 (C)	4.5	8500	60
17 (C)	4.5	8500	60
18 (C)	4.5	8500	60
19 (C)	4.5	8500	60

Table 8 shows the CCF used in this work. There are nineteen experiments with five experiments repeated around the central point.

3.2.2. Failure Mode Effects Analysis

Failure Mode Effects Analysis or FMEA, is a step by step method of capturing all the possible failures in a system or a product. FMEA was developed by the aerospace and automotive industries. Failure Mode corresponds to the ways a system or a product might fail. Effect Analysis corresponds to the results of those failures or defects. FMEA requires the knowledge of the system or a product used, and, the dangerous scenarios it might occur while using the product or system.

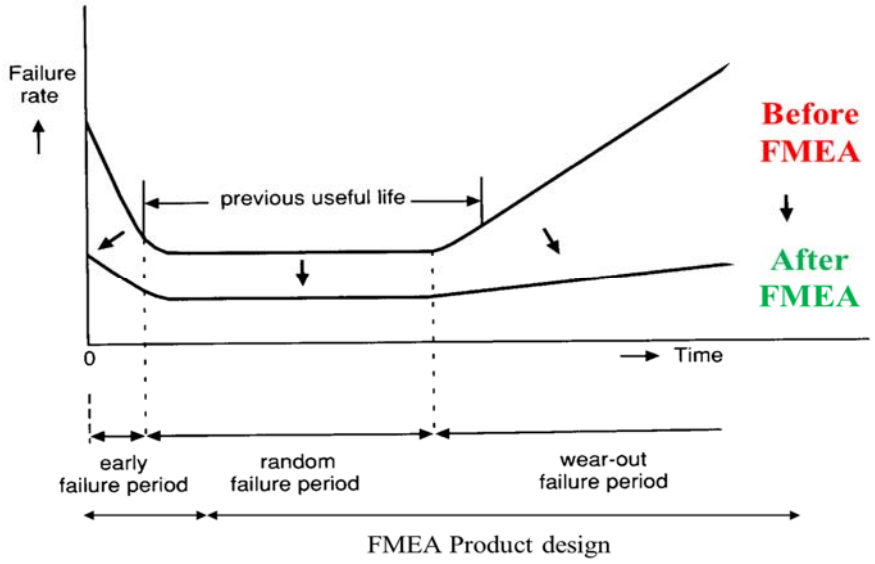

Figure 25. Failure Rate Curve [72]

Figure 25 shows the failure rate curve. The figure shows the benefit of using FMEA in the design process. FMEA increases the length of the useful life of a product or a system, slows the wear out failure, increases the early failure period, and increases any random failure period.

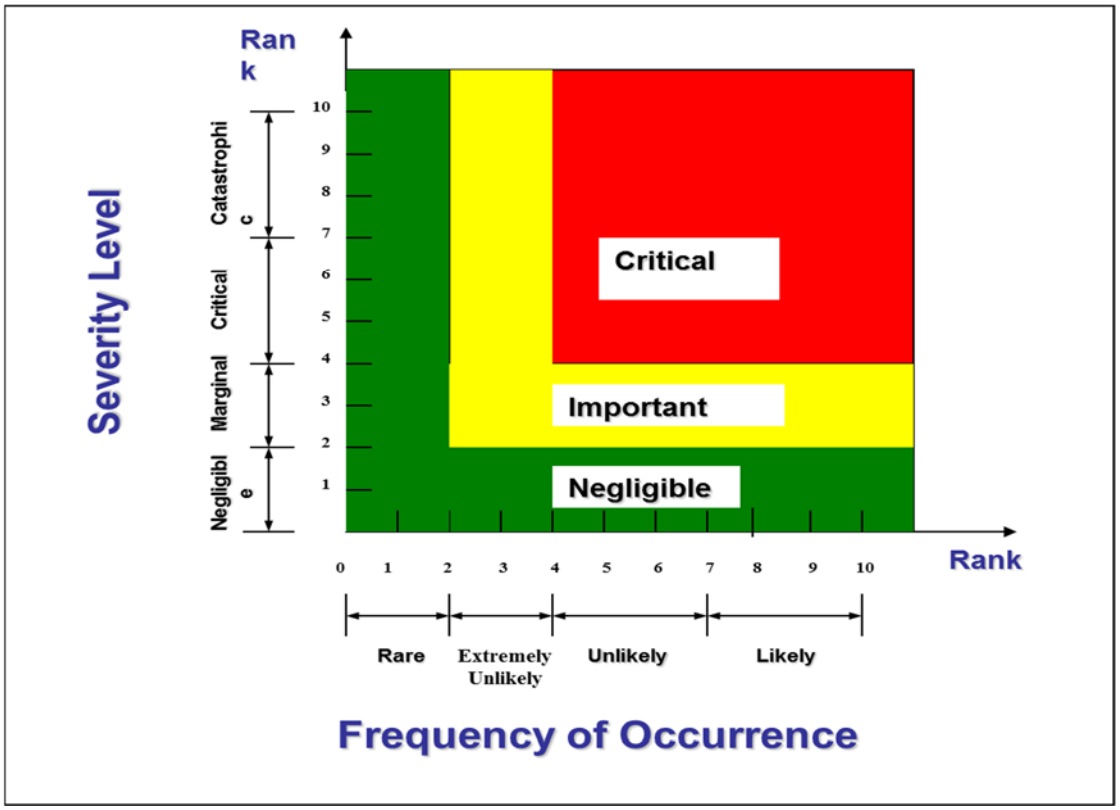

Figure 26. Risk Ranking Matrix [72]

Figure 26 shows the risk ranking matrix. This chart indicates two variables; frequency of occurrence and severity level. Frequency of occurrence is associated with how many times the failure might occur, while the severity level is associated with how dangerous that failure is. Green color in the chart shows safety region were the failure is not that dangerous. Yellow color shows that the failure is going to the red zone were the failure is catastrophic. Explanations of the scales of these failures are shown in the tables below.

Table 9. Severity level definition [73]

Hazard Categories	Rank	Consequences to the safety of users, workers and product performance
Catastrophic	7-10	May cause death, loss of the facility or operation, or severe impact on the environment (non compliance with regulation)
Critical	4-7	May cause severe injury, major damage to a facility or operation, or major impact on the environment (high degree of customer dissatisfaction)
Marginal	2-4	May cause minor injury or minor impact on the environment (cause some customer dissatisfaction)
Negligible	1-2	Will not result in injury (very little effect on customer satisfaction and product performance)

Table 10. Frequency of occurrence [73]

Frequency	Rank	Occurrence Per Year
Likely (Failure is inevitable)	7-10	Greater than 1 in 100
Unlikely (Occasional failure)	4-7	Less than 1 in 100 and greater than 1 in 10,000
Extremely Unlikely (very few failures might occur)	2-4	Less than 1 in 10,000 and greater than 1 in 1,000,000
Rare	1-2	Less than 1 in 1,000,000

FMEA was used in this work after discussing the results from the experimental design.

3.3 Vibration Analysis

Vibration is a useful method of detecting failures in any dynamic system. In centrifugal pumps, they serve as a tool for health monitoring and safety triggers. Vibration is a periodic movement; this means that it repeats itself after some time. Figure 27Figure 28 show the basic components of vibration. T in the figures, is the period. The period, is the time it takes a wave to complete one cycle. X_0 is the amplitude. The amplitude, is how high the wave can get. In other words, amplitude is the distance from zero to the highest point in a wave. Frequency (f), is how many times a certain wave is repeated over a period. Figure 28 shows a simple mass-spring dynamic system. The mass is attached to a spring and it is moving up and down. The mass crosses the same point repeatedly. This repeated motion is expressed as vibration. So, the basic components to describe a vibration is frequency, amplitude, and phase. Phase is meaningful if there are two signals with the same frequency but different amplitudes. It describes how far the signals are from each other. If the two signals have different frequencies, then there is no meaning for the phase value [74].

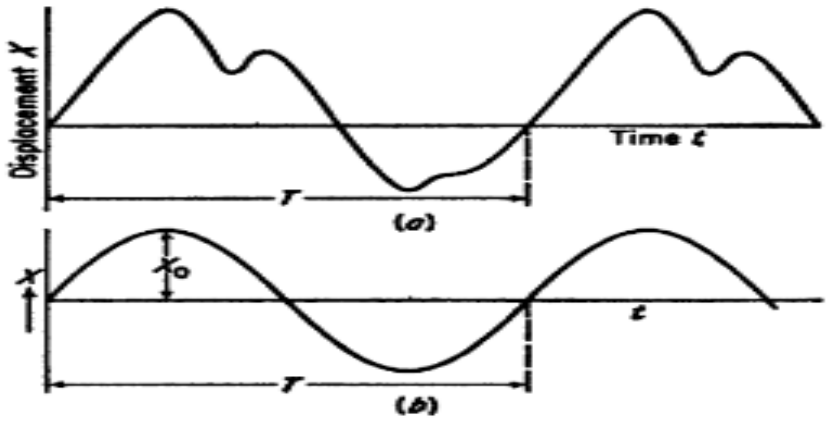

Figure 27. Periodic function

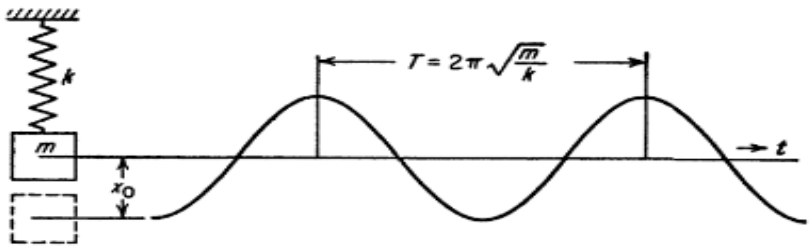

Figure 28. Simple mass-spring system

Fourier transform separates a time signal to the frequency signal that constructed this signal. It is the generalize form of the complex Fourier series in the limit from L to infinity [75].

$$F(\omega) = \sqrt{\frac{|b|}{(2\pi)^{1+a}}} \int_{-\infty}^{\infty} f(t) e^{ib\omega t} dt \qquad \text{Equation 14}$$

$$f(t) = \sqrt{\frac{|b|}{(2\pi)^{1+a}}} \int_{-\infty}^{\infty} F(\omega) e^{-ib\omega t} d\omega \qquad \text{Equation 15}$$

Where, F is the Fourier transform; f is the inverse Fourier transform; a and b are the Fourier parameters; ω is the frequency; and t is the time. Fast Fourier transform (FFT) is a fast method for computing the Fourier transform. Furthermore, converting time domain signal to a frequency domain signal.

Figure 29 shows a time domain data for two sine waves of frequencies 15 and 20 Hz. As shown in the figure, the analysis of the data is difficult as the two waves are on top of each other. Plus, the information of each wave is imbedded in one other. Therefore, FFT is a better way to understand these two sine waves. Figure 30, shows the frequency domain information for these two waves. As shown from the frequency domain information, the two spikes represent the two frequencies in the data and their associated amplitudes. Therefore, if complicated signals with multiple waves are

involved in a system, using FFT to represents it in frequency domain will be more meaningful than time domain.

In centrifugal pump systems, there are multiple components, such as, bearings; pump casing; bolts; base plate; and the pump itself. All those components have different movements. Some, have high amplitude, low frequency motion; others will have low amplitude, high frequency movement; and some have low amplitude, low frequency motion. Therefore, predicting the motion of each of those components in a time domain data is very complicated. Therefore, FFT is used in this work to identify the motion of each component and the effects it adds to the system. Multiple failures can be detected using the frequency information of these components. Those failures can be in the shape of unbalance, misalignment, and looseness.

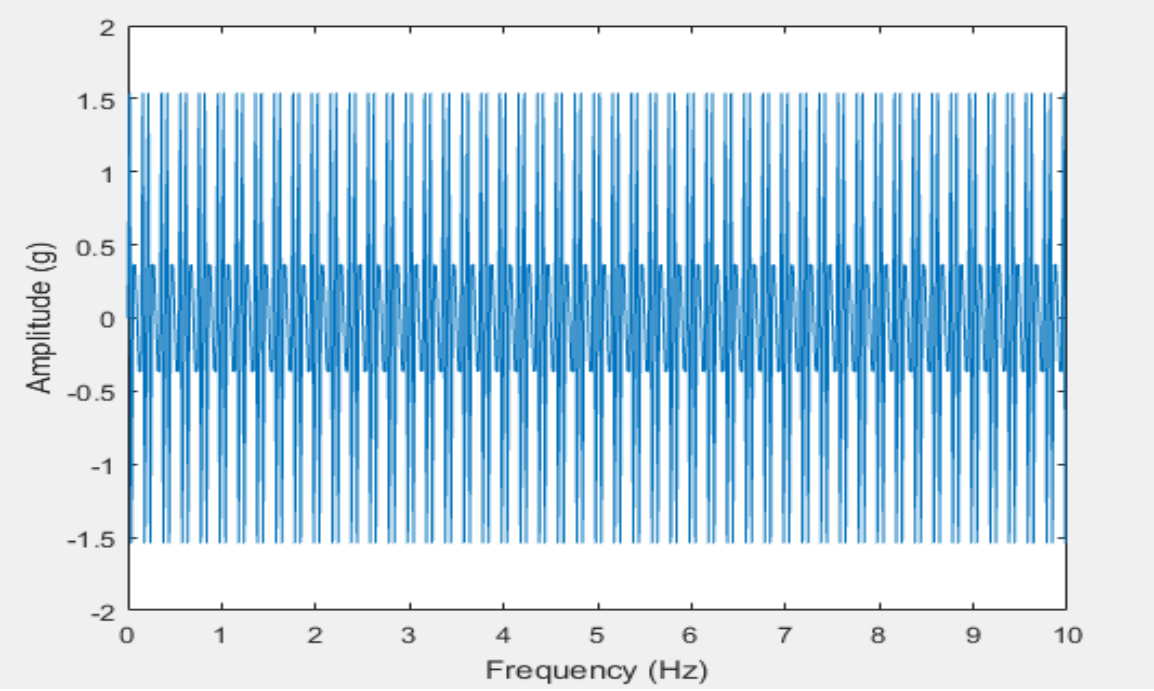

Figure 29. Time domain data

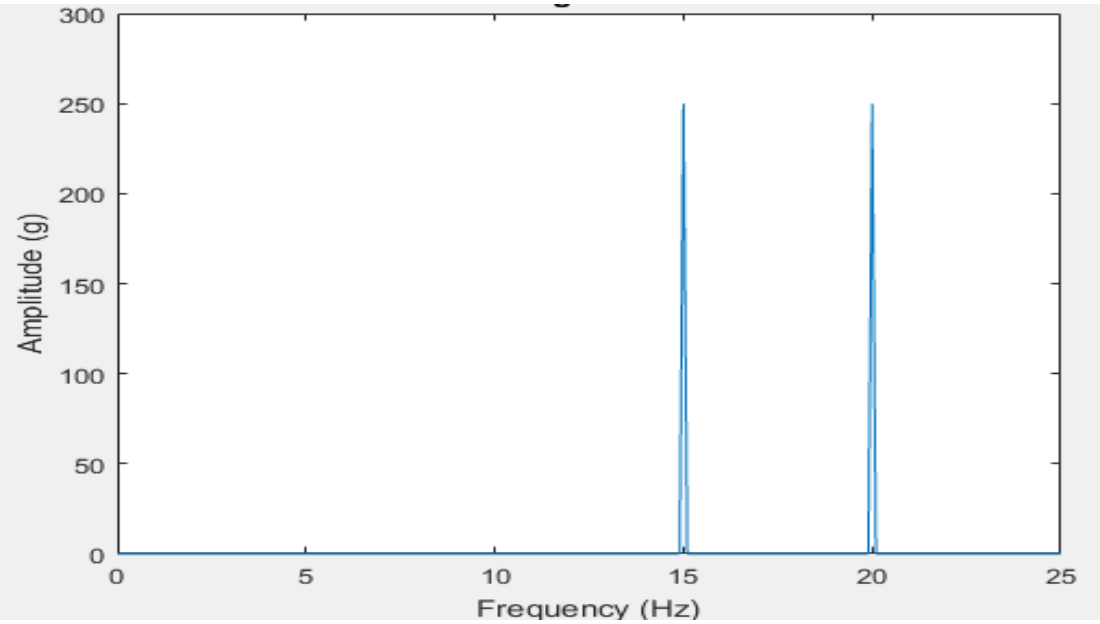

Figure 30. Frequency domain data

3.4. Control Methods

3.4.1. Modeling Speed and Valve angle

After characterizing the system, the control is needed. The main objective of the control is to maintain a healthy life for the pump. This requires running the pump in the no fail zones. Fail zones are ranges of speeds, valve angles, fluid heights, and times that create the most unwanted vibrations; temperature rise; and noise.

The first step in the control method is modeling. There are multiple methods to model a dynamic system; transient response, state space modeling, frequency response, neural network, and many others. Transfer functions (TF) are one of the main modeling methods. TF is a convenient method to represent the relationship between inputs and outputs. If TF for a system is obtained, then this function can be used to represent the system. Obtaining TF for a system could be a difficult task.

Therefore, many methods are suggested as mentioned in chapter 3. In this work, the transient response method is used to obtain TF for the system [76].

TF models the relationship between the speed of the pump and valve angle to the output flow. Output flow can then be related to efficiency of the pump and the head (pressure rise). Transient response applies an input (step) to the system and observes the output. Flowmeter values are observed when a change in the input is applied. Two transfer functions were needed in this work; speed of the pump and valve angle. Both models relate speed and valve to flowrate. To model both devices, each is kept constant while the other is changing. So, when speed is modeled, valve angle is kept constant and vice versa. Then, flowrate data is collected and sent to the computer. After that, identification toolbox is used in MATLAB. Identification toolbox uses a transient analysis between inputs and output, and creates a TF to express the relationship. First, the valve angle is kept fully open (90 degrees), and the speed is changed. Then, the flowrate data is collected when the speed is changed. These data are inserted in the identification toolbox in MATLAB to create a discrete transfer function to fit the data. Same is done with the valve angle; the speed is kept constant while the valve angle is changed. Then transfer function is created for both [77].

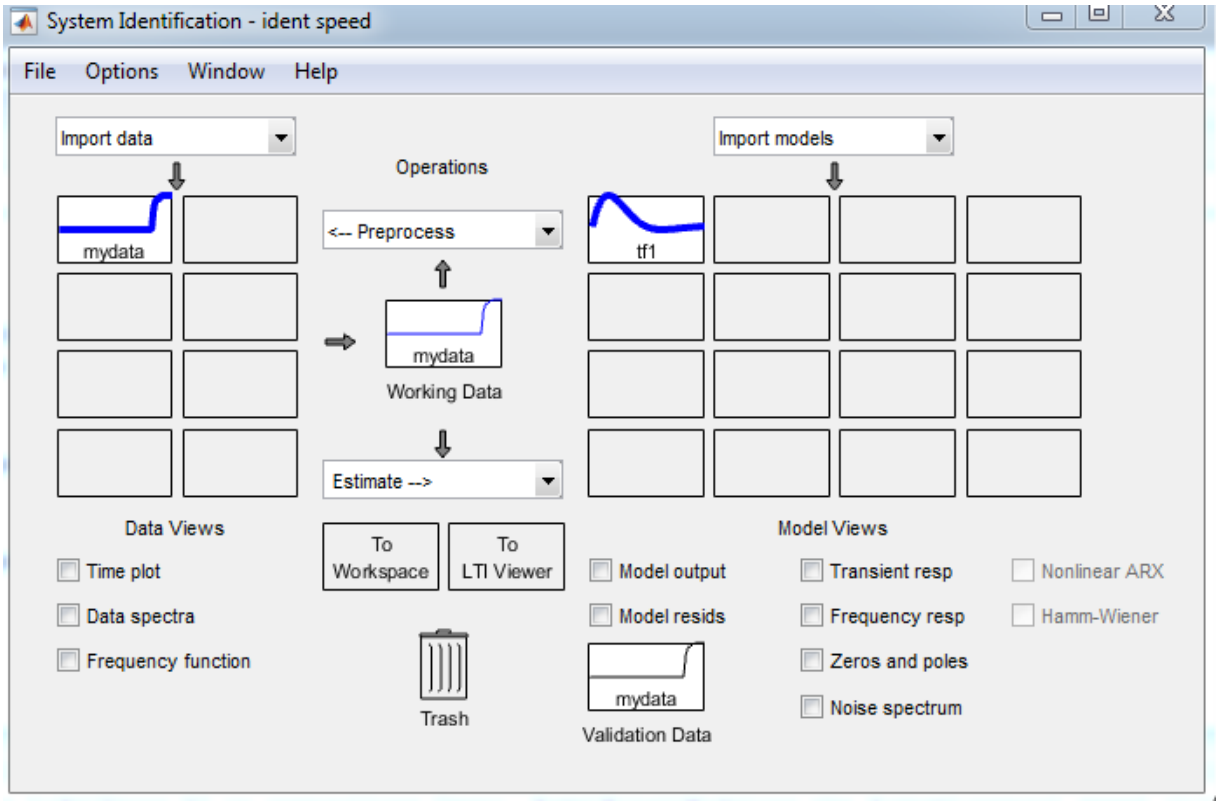

Figure 31. Ident toolbox in MATLAB

3.4.2. NARMA-L2 Neural Network

NARMA-L2 neural network or sometimes is called feedback linearization, is used when the plant has a particular form (companion form). The main idea of this type of NN (neural network) is to linearize the nonlinear dynamics in a system. This type of network works in two step; identification and control. In the identification step, the companion function is presented to model the system. In the control step, the identified NN will establish a control based on companion function [78].

$$y(k+d) = N[y(k(, y(k-1), \dots, y(k-n+1), u(k), u(k-1), \dots u(k-n+1)] \quad \text{Equation 16}$$

Equation 16 describes one of the standard models used to represents the nonlinear dynamics. Where u(k) is the system input, y(k) is the system output, k is number of steps, and n is the sample count. This equation represents the forward dynamics of the system.

$$u(k) = G[y(k(, y(k-1), \dots, y(k-n+1), y_r(k+d), u(k-1), \dots u(k-m+1)] \quad \text{Equation 17}$$

Equation 17 represents the controller model used in NARMA-L2 NN. G is a function created by the network to minimize mean square error. Reducing this error is done in several ways; increasing the training epochs, increasing the sample size, changing the relationship function, and repeated training [79].

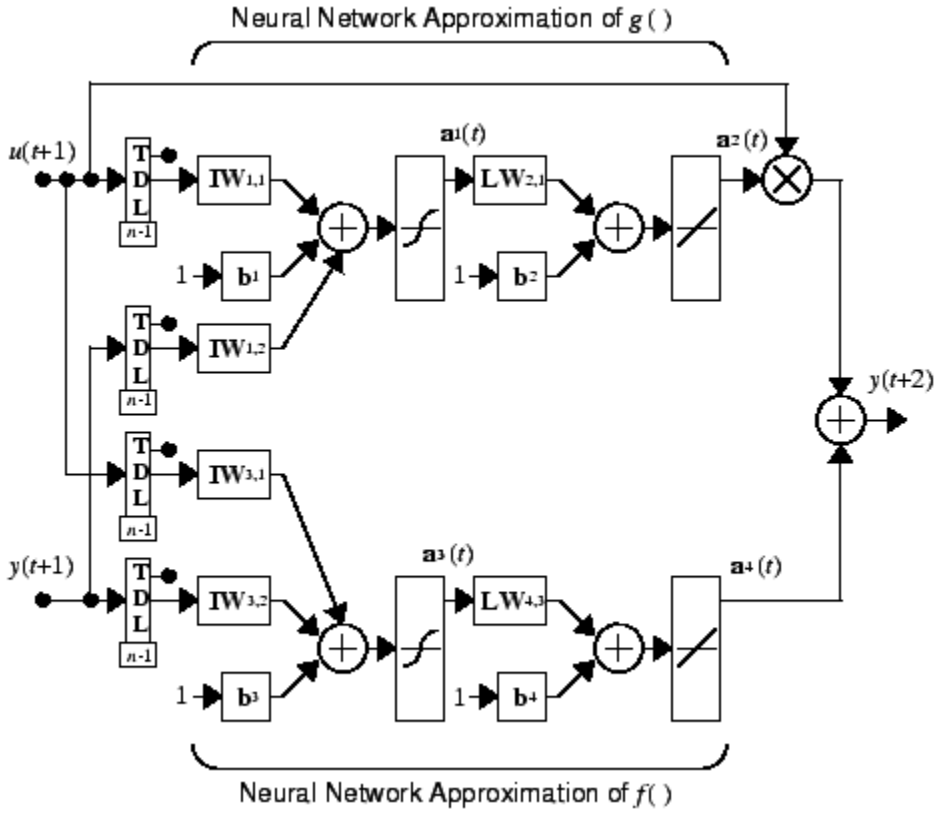

Figure 32. Neural Network representation

Figure 32 shows a general schematic of a NN. The main thing to get from the figure is the weights which are represented by IW, f represents the suggested fitting polynomial to approximate the model of the system, and g represents the actual response from the system. The network will be judged by the error between g and f. The following figures show the general schematic of NARMA-L2 controller and the final form of NARMA-L2 NN respectively. In this work, MATLAB is used to construct and train the NN. The parameters used to train the speed controller for the pump are shown in Figure 33. Valve control is the same and it is shown in the appendix. The figure shows 8000 samples used for training, and the sampling interval is 0.01 second. The rest of the parameters are changed frequently until a good response was achieved. Simulink plant model used the transfer function created by the identification toolbox for the speed controller.

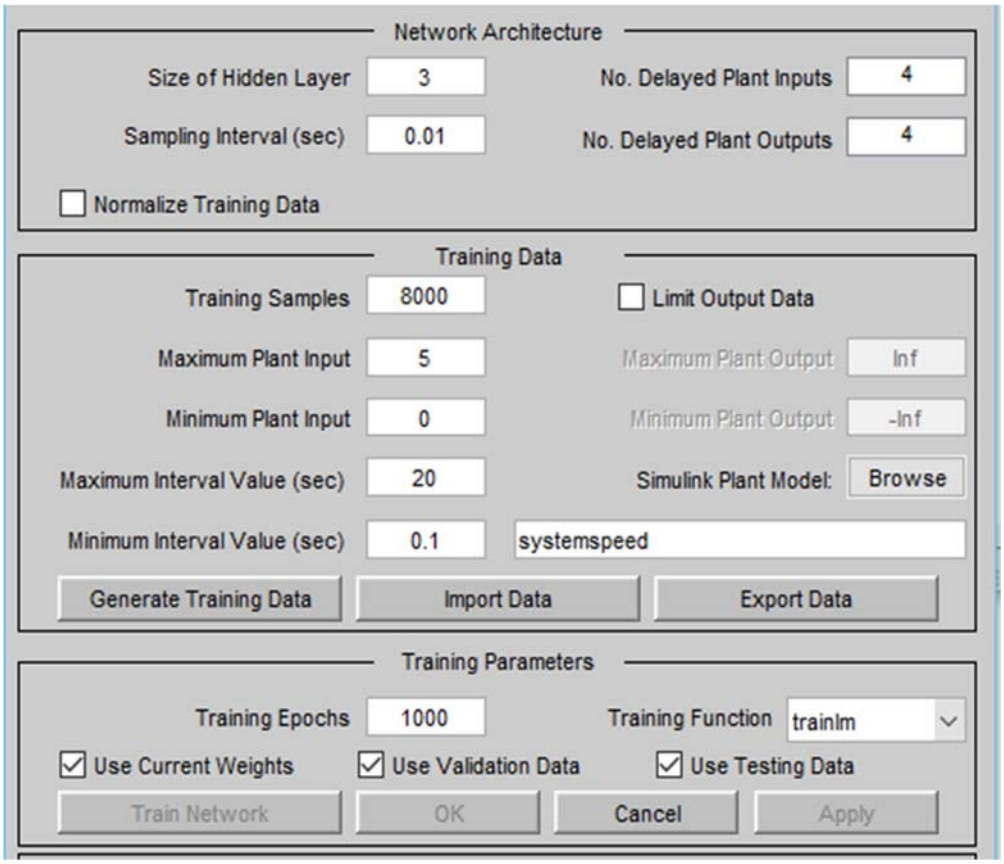

Figure 33. NARMA-L2 parameters for speed control

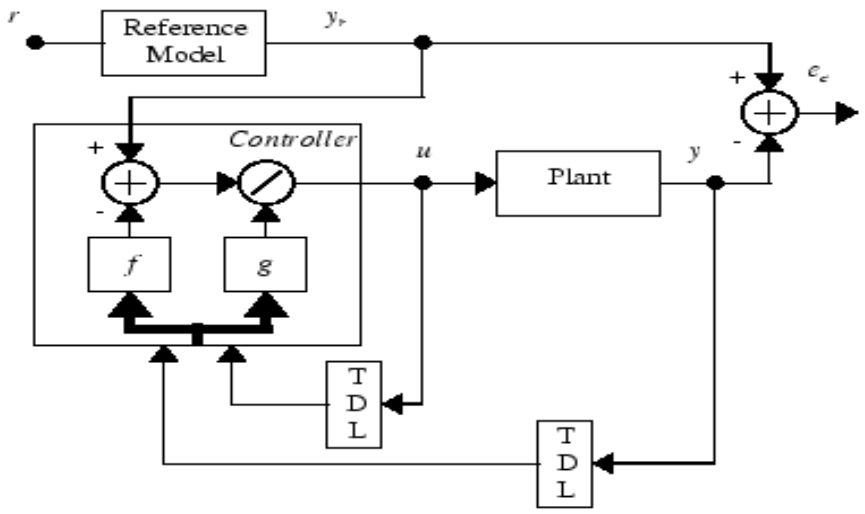

Figure 34. Block Diagram of NARMA-L2 controller [78]

Figure 34 shows the block diagram of NARMA-L2 NN controller.

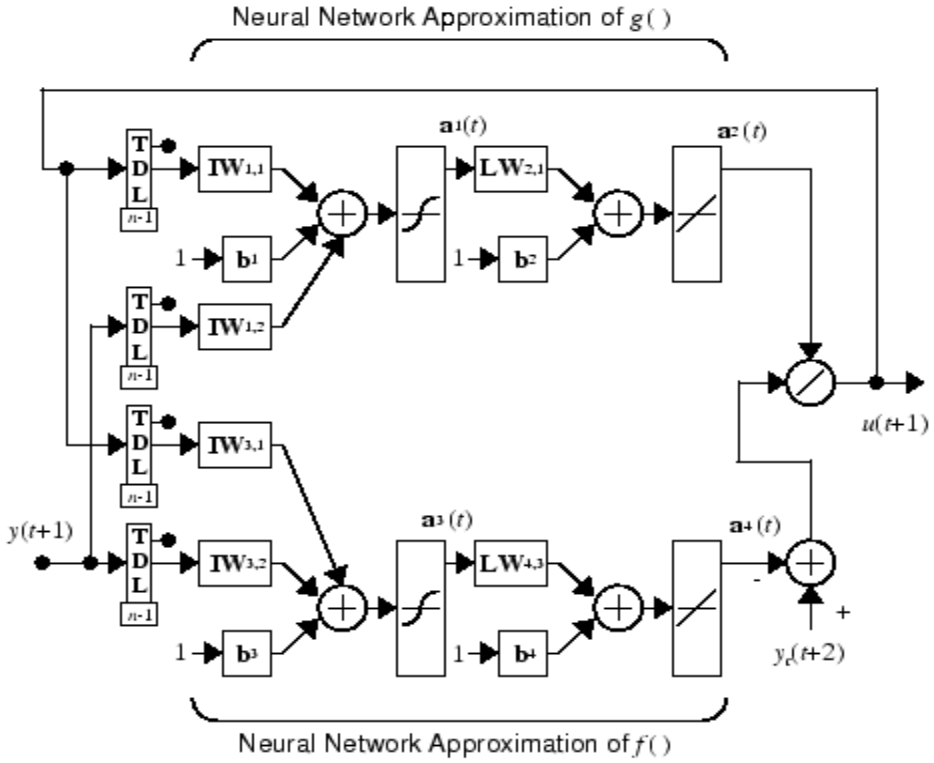

Figure 35. Final form of NARMA-L2 NN [78]

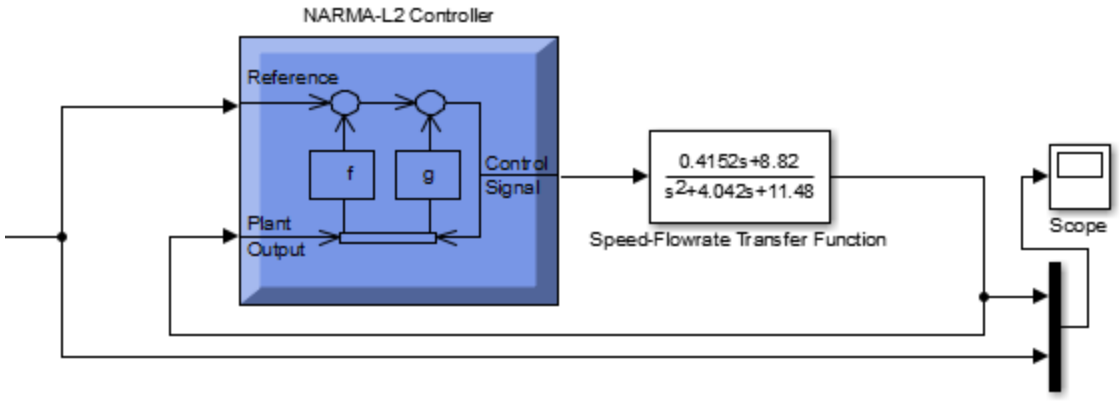

Figure 36. NARMA-L2 Simulink model [78]

3.4.3. Predictive Neural Network

Predictive neural network as the name suggests, uses a model of nonlinear plant to estimate future plant performance. It is separated into two steps; determining the plant model and creating a control to keep the plant response as desired. Figure 37 shows a schematic of predictive NN. The predictive NN is trained by forward dynamics. The approximation error between the plant output and the NN output is used as a feedback to train the network again. Figure 38 shows the structure of the predictive NN plant. This structure uses the previous input and output from the plant to predict future plant output [78].

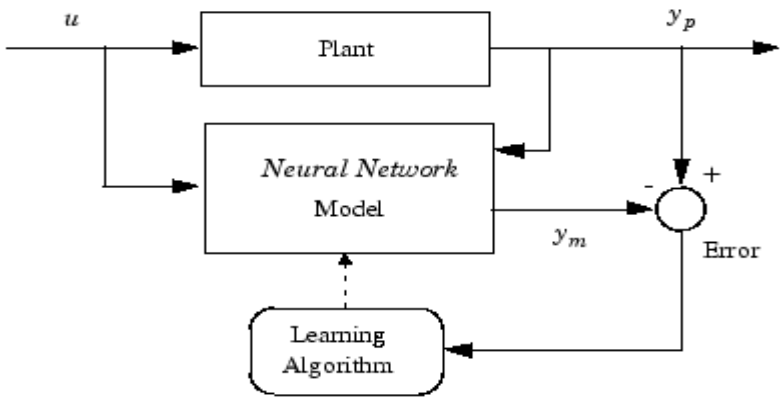

Figure 37. General schematic of Predictive NN [80]

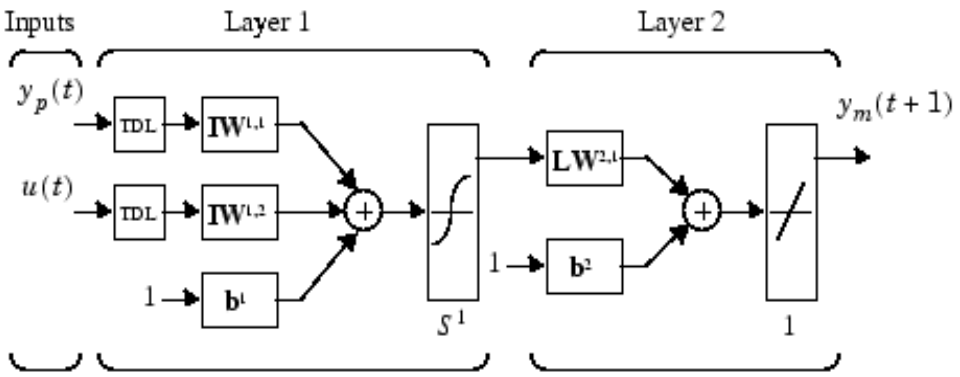

Figure 38. Structure of plant model [80]

$$J = \sum_{j=N_1}^{N_2}\left(y_r(t+j) - y_m(t+j)\right)^2 + \rho \sum_{j=1}^{N_u}\left(u'(t+j-1) - y_m(t+j-2)\right)^2 \quad \text{Equation 18}$$

Equation 18 shows the performance criterion over specified horizon, J. The goal of the predictive NN is to minimize that criterion. N_1, N_2, and N_u define the horizon at which the tracking error and control increments are evaluated. u' is the control signal, y_r is the desired response, y_m is the NN model response, and ρ determines the contribution that the sum of squares of both the control increment and performance index have [79]. Figure 39 shows the model of predictive control process. There are two main components, plant model and optimization block. Optimization block calculates the values of u' that minimizes the function J. After that, u' is used as an input to the plant [79].

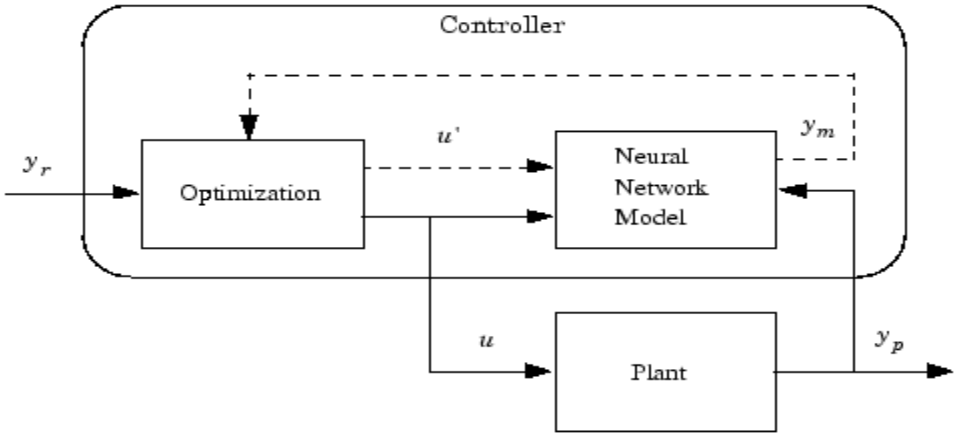

Figure 39. Model predictive control process [78]

Figure 40. Predictive control parameters

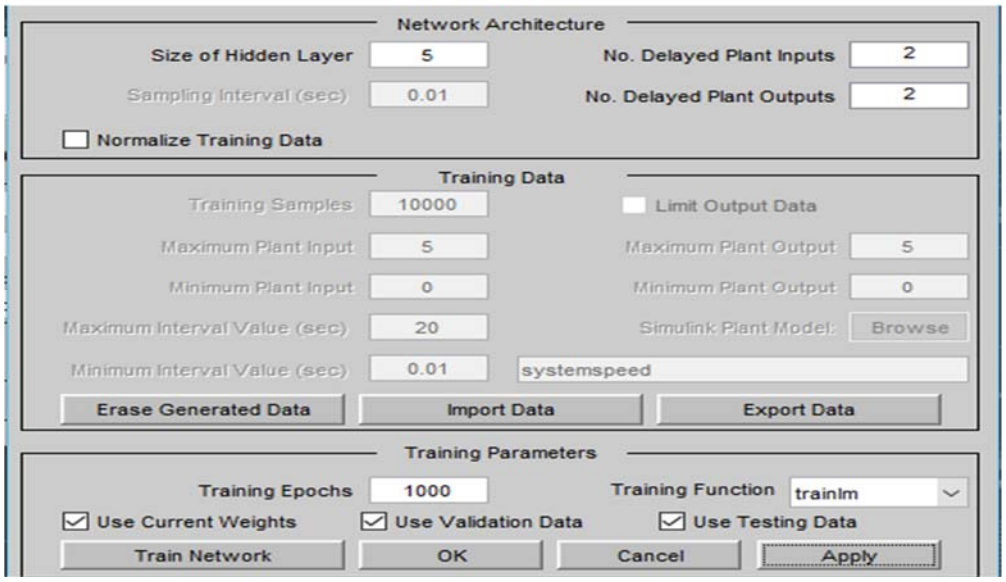

Figure 41. Predictive control NN training parameters

Figure 40 shows the control parameter used in this work to create a control for the speed of the pump. Figure 41 shows the parameter used to train the predictive NN. These parameters are changed frequently until a desired response is achieved.

3.4.4. Fuzzy Logic Control

Fuzzy logic (FL) in general is a theory that classifies objects with boundaries. FL is based on linguistic variables. This means, the variables used are words and not numbers. The basic idea of FL is common sense. Therefore, expert person or expert data is needed. Figure 42 shows the difference between precision and significance. FL falls between these two statements; it does not have the full precision and in the same time it is not fully significance. It uses common sense to produce a solution that satisfies precision and significance in the same time. So, the basic idea of fuzzy will be in this short question; how important is to be exactly right when a rough answer will do? The answer will decide whether to use FL or not. If the answer is "very", then FL is not the path to follow. But, if the answer is "not much", then FL works perfectly [81].

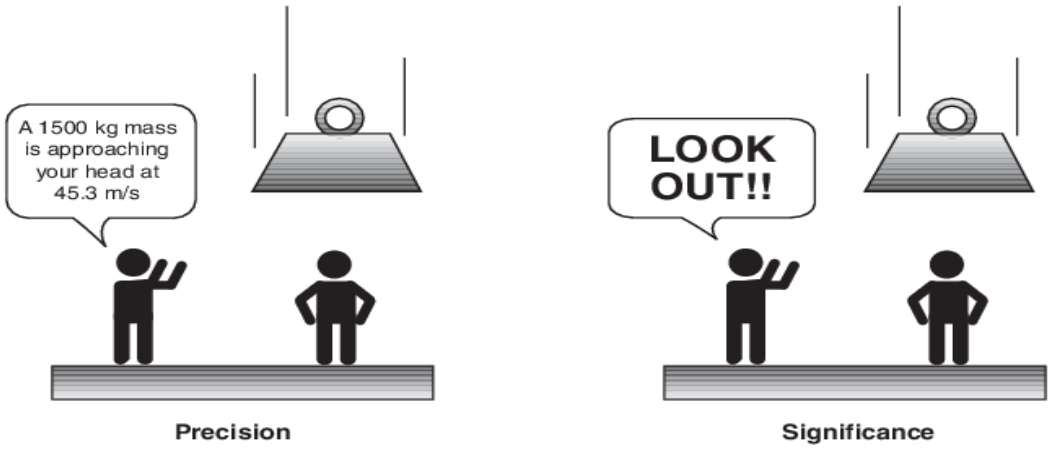

Figure 42. Precision and Significance scenarios [80]

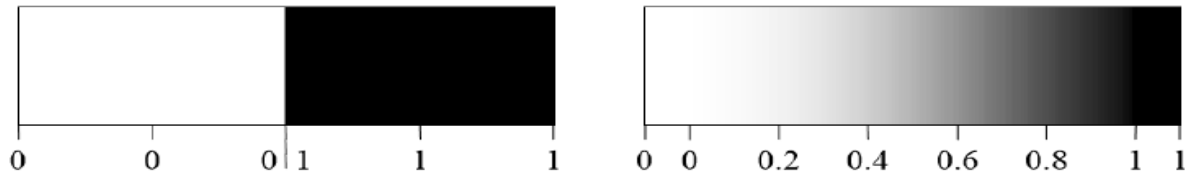

Figure 43. Fuzzy vs Non fuzzy [82]

Figure 43 shows a difference between two valued operation vs fuzzy language. The scale on the left shows only two answers; white or black. The scale on the right shows that anything can be partially white and partially black. For instance, in the middle it will say 0.5, this means the scale reads 50% white and 50% black. Moving further to the right will increase the black color percent and reduce the white color percent. This is how fuzzy logic works. Everything has a percent related to it, nothing is absolute.

Membership function (MF) is a function that describes how important is each value (degree of membership), and it falls between 0 and 1 [81]. There are many MFs; traingular, trapozoidal, gaussian, sigmoidal and many more. Figure 44 shows traingular and trapazoidal MFs, the x-axis represents the input space or universe of discourse. Each of these inputs has an importance contribution to the system and it ranges between 0 and 1. The choice of MF is up to the user and the system. Some MF might work with some scenarios and others might work for others. As mentioned earlier, FL is based on expert inputs from either the user or the data. MF has the job of taking the numerical values and convert them into a lingustic values and vice versa. Changing from numerical values to linguistic varaibles is called Fuzzification. Defuzzification is the opposite. The lingustic variables created must be converted to numerical values to quantify the problem [82].

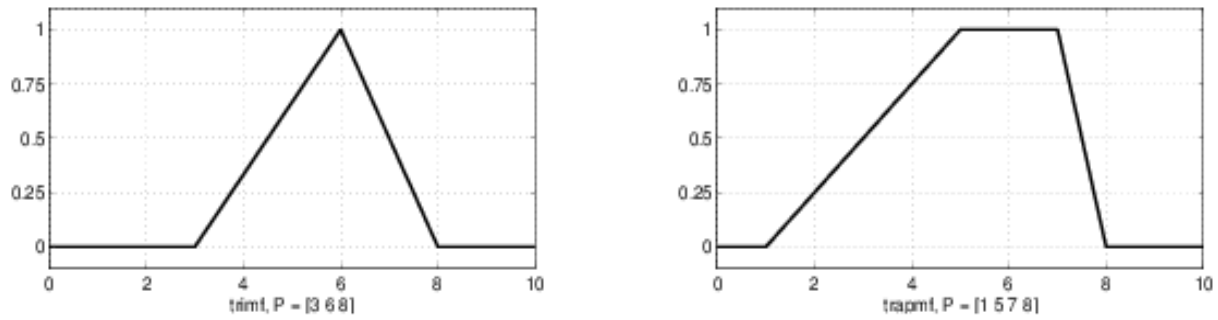

Figure 44. Triangular and Trapezoidal MFs [81]

For FL to perform correctly, relationship between inputs and outputs must be defined. FL rules are a method that relates inputs and outputs in fuzzy logic. It is based on conditional statements in the form of: IF something is C, then Another is B.

There are two types of fuzzy systems; Mamdani and Sugeno. These two types relate to the output parameter of the fuzzy system. Each of these systems represent the output differently than the other. Mamdani system has a range of output to any input. Sugeno, has only one output for a set of inputs. Mamdani is used mostly in linear and optimization techniques, and it is well suited to mathematical analysis, and it is computationally efficient. Sugeno is used with nonlinear control problems [82]. Figure 45 shows a schematic of Sugeno design process.

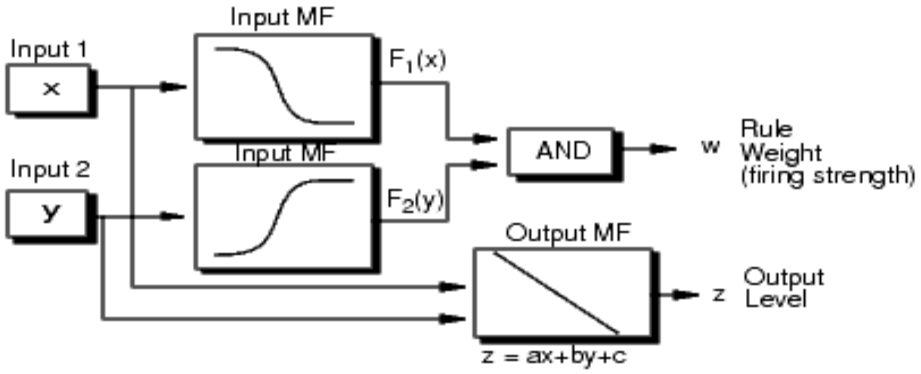

Figure 45. Sugeno process [80]

In control problems, FL can be of a great help. Mamdani and Sugeno both can be used to control and model a dynamic system. But, because of the uncertainty in the results of FL, it should be combined with another control method. In this work, Neuro-Fuzzy control has been used. Neuro comes from neural network. ANFIS or adaptive neuro-fuzzy inference system is a fuzzy system with a modified MF parameters using NN. NN is trained as discussed earlier to create and modify the MFs and the rules that are used in the fuzzy system. ANFIS uses Sugeno fuzzy system as the output scheme. MATLAB Neuro-Fuzzy toolbox is used to train and construct the ANFIS system [80].

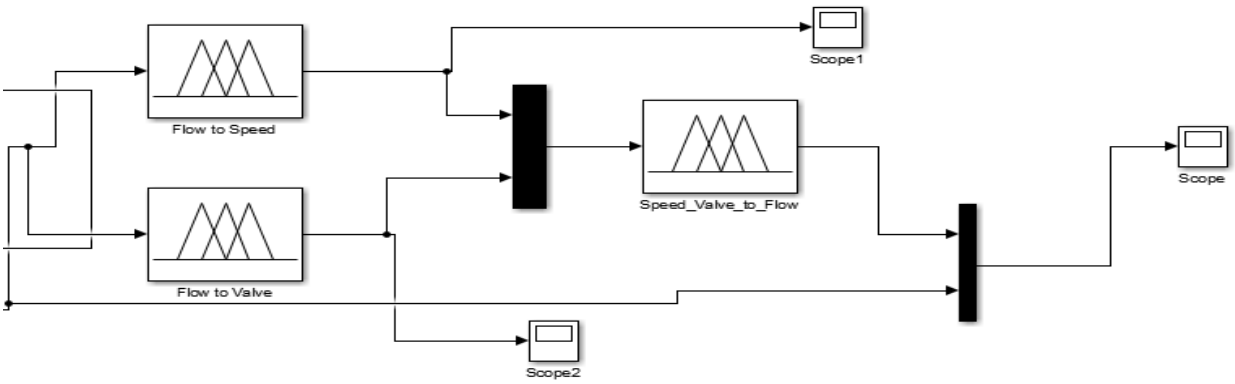

Figure 46. Neuro-Fuzzy control

Figure 46 shows the Neuro-Fuzzy control system used in this work. There are two steps used in this control. First, modeling the flow as a feedback to the first two controllers, speed and valve. Each of these fuzzy systems has one input (flowrate) and one output (speed or valve). Then, this signal is sent to the third fuzzy system that consists of two inputs (speed and valve) and one output (flowrate). So, the user decides on a reference flowrate, then the first set of fuzzy systems takes this signal as an input, and sends it to the first two controllers. After that, this system outputs speed and valve necessary to achieve the reference flowrate. Furthermore, the computer or DAQ device

takes these speed and valve angle values, and feeds it to the system modeled (Speed_Valve_to_Flow) in the figure above. Figure 47 shows the third fuzzy system used. This system has two inputs and one output. The other systems are presented in the appendix.

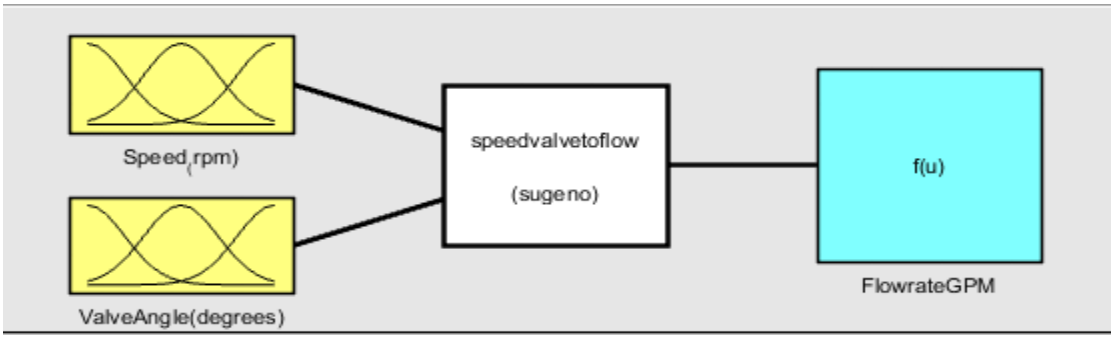

Figure 47. Speed and Valve to Flowrate fuzzy system

Figure 48 shows the Neuro-Fuzzy designer. This is the first step in constructing the fuzzy system. In this step, training data is used to train the network and construct the rules that will be assigned to the MFs of the fuzzy system. These rules are adjusted using NN, and the method used is hybrid. The data selected in this process are related to the analysis and results. To clarify, the goal of this work was to construct a system that reduces failure and ensures safety of the pump and the system as all. So, the data selected for training are the data that have less risk for the system. This means, data that have low vibrations, low cavitation, high efficiency, low noise, and low temperature rise. This will train the network to only send signals that are safe to the pump, and avoid the signals that have potential danger to it. If the system recognizes a dangerous signal, it will automatically reduce speed or valve angle to ensure safety. Figure 49 shows the selection of MF. Gaussian function was used for all the fuzzy systems in this work. The numbers 1 and 3 represent the rules that are used in the function. Figure 50 and Figure 51 show the response surface and the rules used in this work.

Response graph is a good presentation to the relationship between inputs and outputs. While, the rules are a method to get an exact numerical answer to the input.

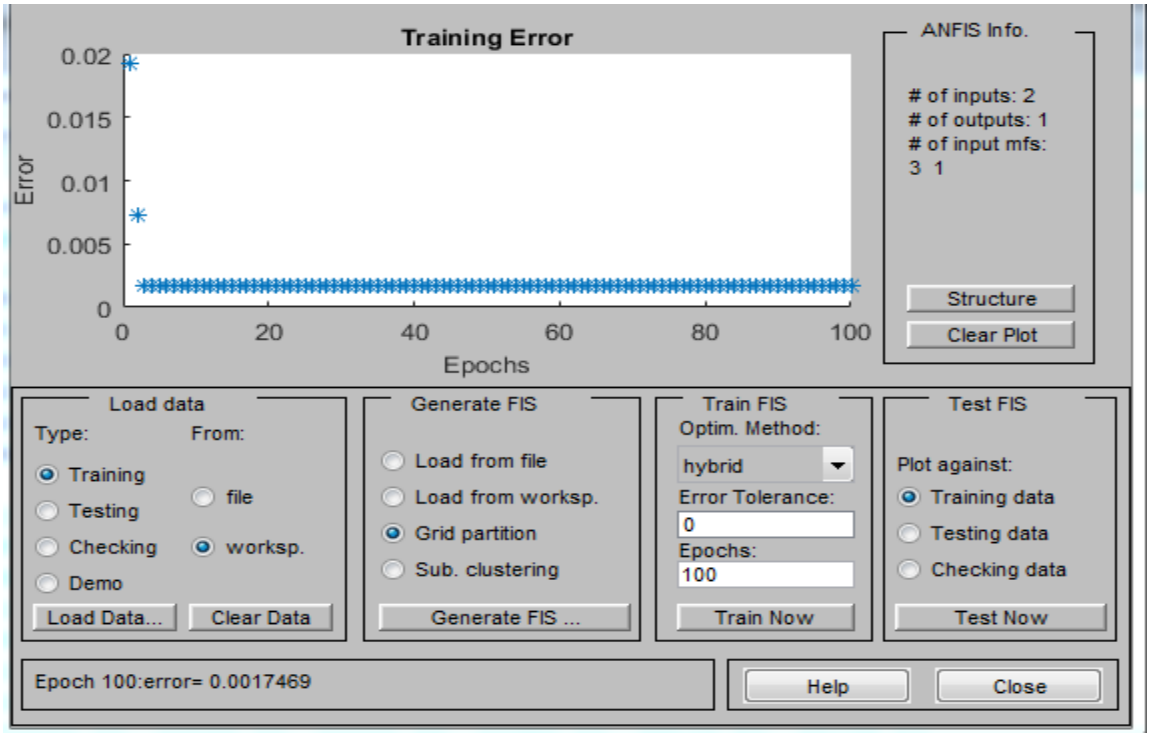

Figure 48. Neuro-Fuzzy Designer

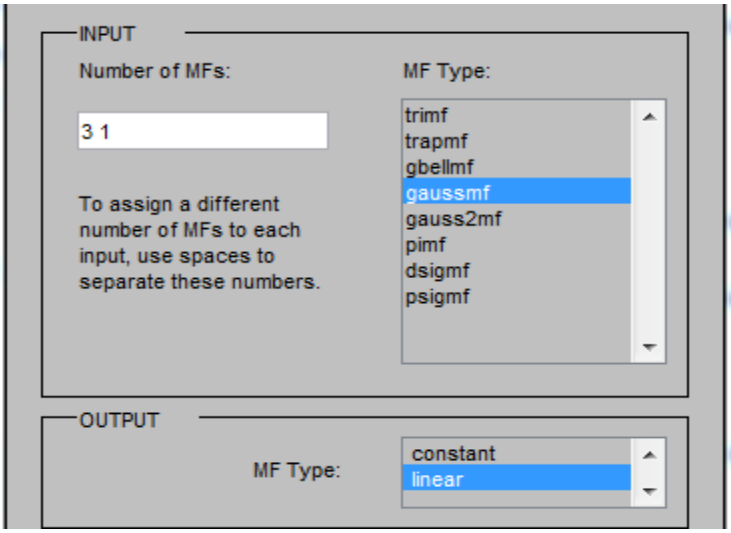

Figure 49. Membership function selection

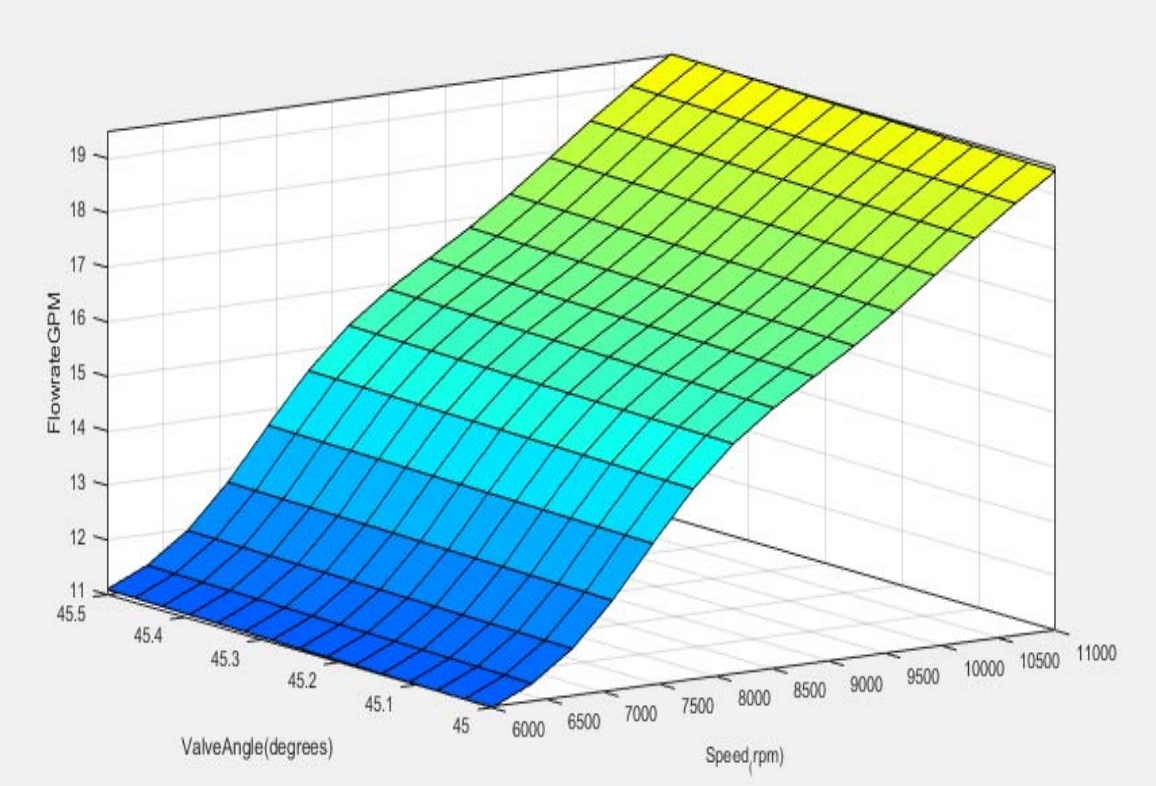

Figure 50. Response surface

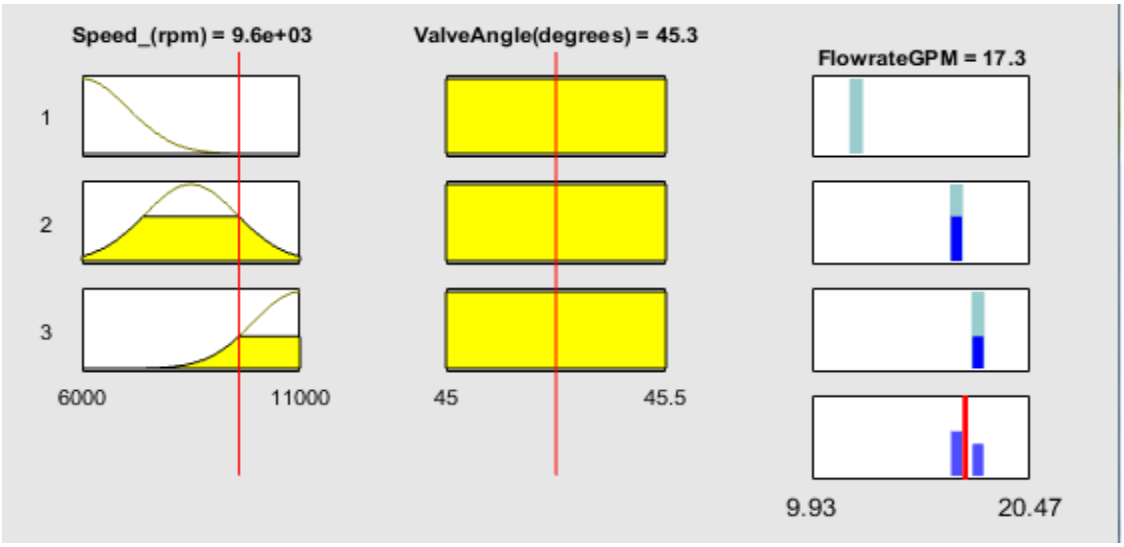

Figure 51. Neuro-Fuzzy rules

4. Results and Discussions

4.1 Experimental Results

4.1.1 Full Factorial Design

To recall, the main goal of the full factorial experiments was to characterize the system and identify the efficiency; flowrate; and pressure rise of the pump. To control the centrifugal pump, few steps should be taken; characterization of the pump and characterization of the system by finding the vibrations, noise, and temperature rise associated with it.

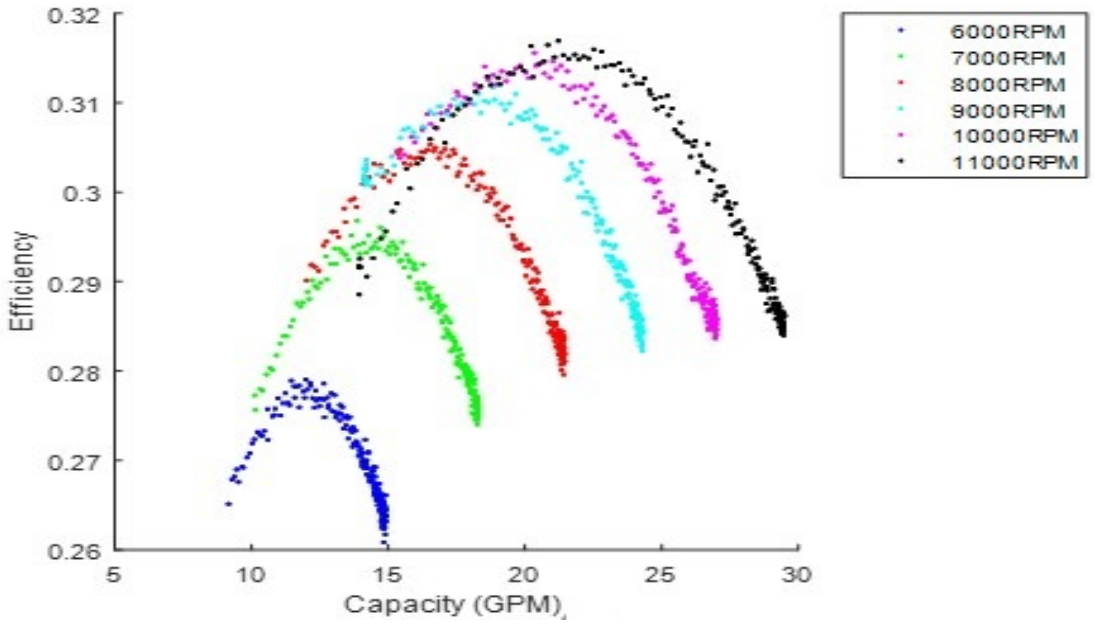

Figure 52. Efficiency of the centrifugal pump [83]

Figure 52 shows the efficiency of the centrifugal pump. Capacity is another term that describes flowrate. Flowrate in this work indicates the output flowrate of the pump. This plot is using the data from each speed with valve angles between 30-90 degrees. The efficiency is increasing as the

speed increases. The quadratic behavior of the efficiency indicates that the maximum efficiency of the pump at each speed is located at valve angles 40-50 degrees. Figure 53 shows the head (pressure rise) vs output flowrate. Pressure rise, is the difference between the outlet pressure of the pump and the inlet pressure measured as the height of fluid in the main tank. As indicated by the figure, the flowrate increases when the pressure rise decreases. This behavior matches the behavior of centrifugal pumps discussed in chapter 3. Furthermore, the flowrate changes with changing the valve opening. This means, going from left to right in the figure means opening the valve.

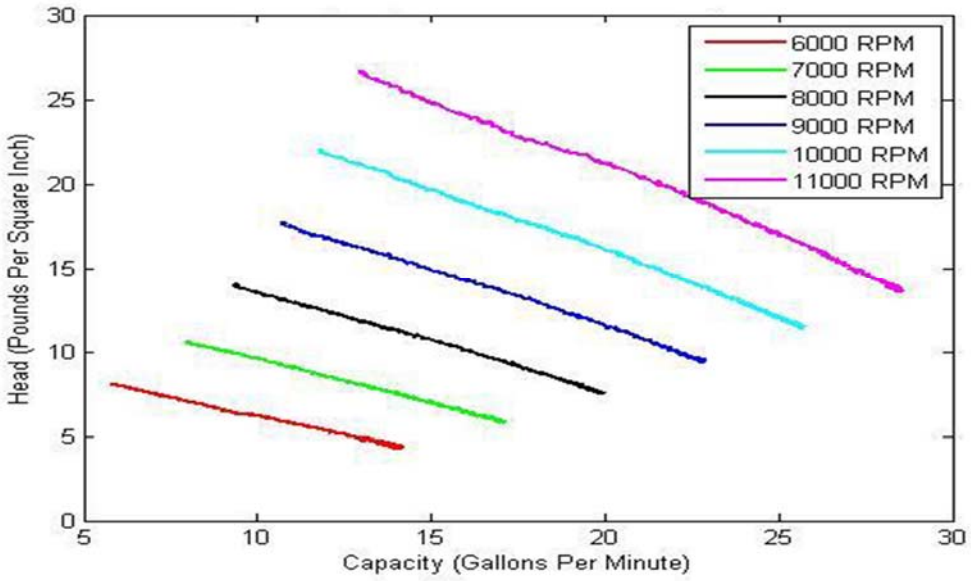

Figure 53. Pressure rise vs Flowrate [83]

Figure 54 shows the efficiency vs temperature. This figure shows a negative relationship between temperature rise in the fluid with the efficiency of the pump. As mentioned earlier, high temperatures will lead to cavitation created in the system. Plus, some of the fluid properties will change.

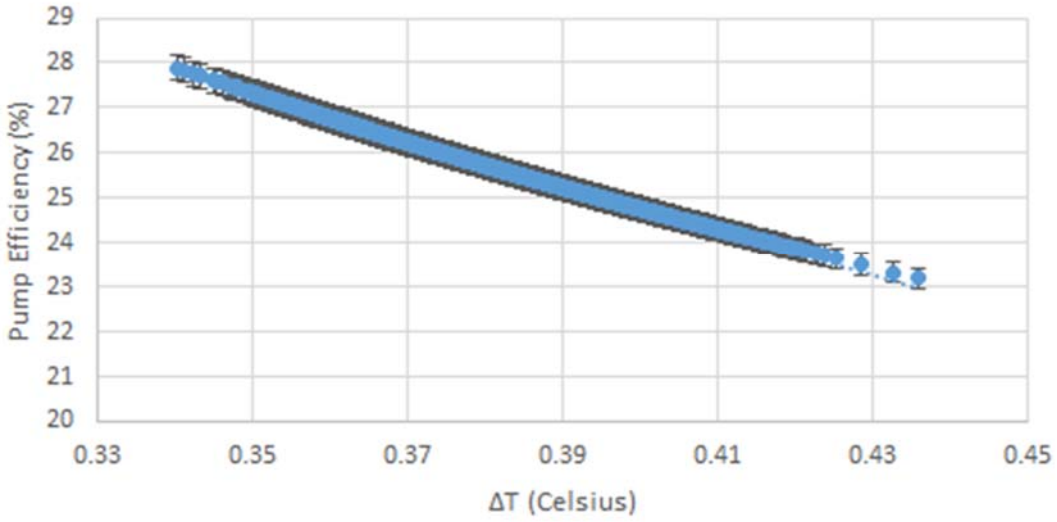

Figure 54. Efficiency vs Temperature rise

Figure 55 shows the change in noise of the system when the valve angle and speed change. The noise increases as the speed increases. Valve angle does not have a major effect on the noise except in the low valve openings.

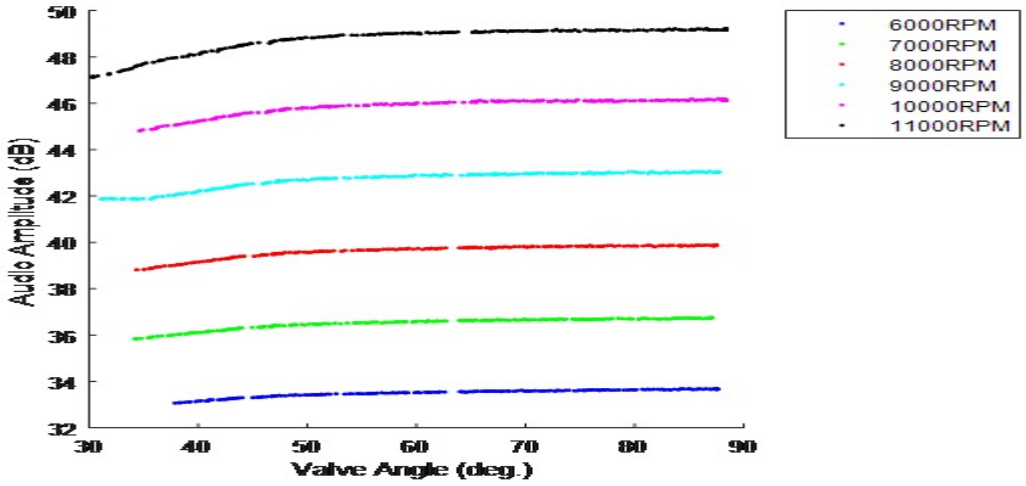

Figure 55. Noise in the system

Figure 56 shows the electrical power consumed by the pump. The figure shows when higher flowrate is necessary, higher speeds are required.

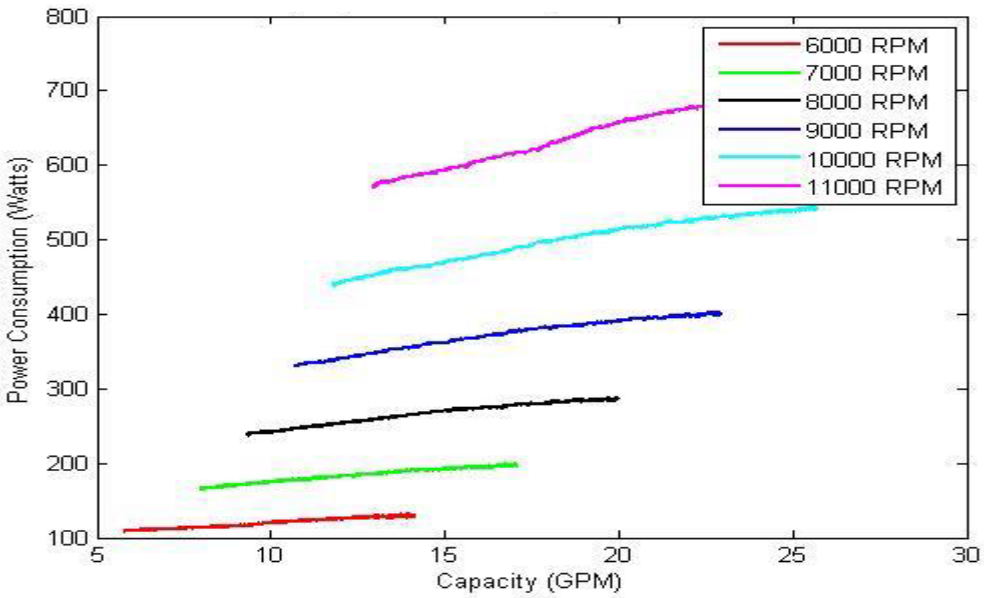

Figure 56. Power consumption in the pump

4.1.2 Orthogonal Array (Taguchi method)

After characterizing the pump, the need for identifying the important factors and their levels that affect the different responses. To do so, Taguchi method was implemented as mentioned earlier. First, five different responses or characteristic variables were considered; vibrations amplitude, vibrations frequency, temperature rise, noise and efficiency. To study the factors, two different orthogonal designs were followed. First, L9 orthogonal matrix was constructed to study three factors; speed of the pump, valve angle, and fluid height in the main tank. The results are shown below.

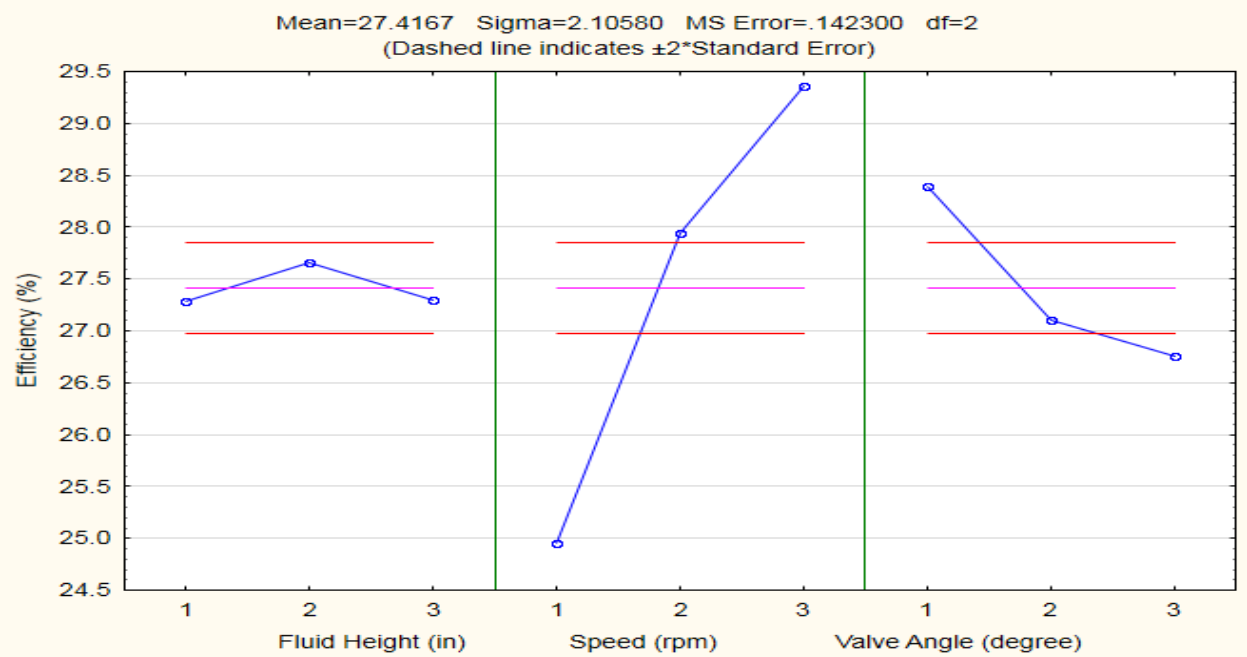

Figure 57. Response graph for Efficiency

Figure 57 shows the response graph for efficiency. The results show the S/N ratios with larger the better criteria. As the intend of the pump is to run at maximum efficiency, always. The figure clearly shows that fluid height is less significant than the other two factors. Speed has more effect on the efficiency than valve angle. One significant level was chosen for each factor and it is shown in

Table 11. The table shows that to achieve the optimal efficiency, the pump speed should be at level three (11,000 rpm), valve angle at level one (40 degrees), and fluid height at level 2 (4.5 inches). Table 12 shows the ANOVA table for efficiency. The results agree with the response graph for speed being the dominant factor. Because, the p-value is lower than 0.05 for 95% confidence intervals. Valve angle is very close to the required p-value; therefore, it is considered to have some effect on the efficiency.

Table 11. Optimal response for Efficiency

Factor	Mean = 27.4167 Sigma = 2.10580 Level	Effect Size	Standard Error
{1}Fluid Height (in)	2	0.24667	0.217792
{2}Speed (rpm)	3	1.94667	0.217792
{3}Valve Angle (degree)	1	0.97667	0.217792
Expected S/N		30.58667	

Table 12. ANOVA table for Efficiency

Effect	Mean = 27.4167 Sigma = 2.10580 SS	df	MS	F	p
{1}Fluid Height (in)	0.27407	2	0.13703	0.9630	0.509427
{2}Speed (rpm)	30.43307	2	15.21653	106.9328	0.009265
{3}Valve Angle (degree)	4.48327	2	2.24163	15.7529	0.059691
Residual	0.28460	2	0.14230		

Figure 58 shows S/N values for the second response, vibration amplitude. The results shows that speed is the most significant factor in changing the amplitude of the vibration. S/N used for the amplitude is following smaller the better criteria. This means, to achieve the lower amplitude the settings should be, level two for fluid height; level two for speed; and level one for valve angle as shown in Table 13. Table 14 shows the ANOVA table for vibration amplitude. The results shows that speed is the most signicant factor with p-value less than 0.05.

Figure 58. Vibration amplitude

Table 13. Optimal levels for vibration amplitude

Factor	Level	Effect Size	Standard Error
***Fluid Height (in)**	2	1.34009	
{2}Speed (rpm)	2	11.80608	1.700976
*Valve Angle (degree)	1	2.67204	
Expected S/N		34.76619	

Table 14. ANOVA for vibrations amplitude

	Mean = 22.9601 Sigma = 13.2302				
Effect	SS	df	MS	F	p
{1}Fluid Height (in)	10.272	2	5.1361	1.3111	0.432697
{2}Speed (rpm)	1348.235	2	674.1175	172.0822	0.005778
{3}Valve Angle (degree)	33.973	2	16.9864	4.3361	0.187402
Residual	7.835	2	3.9174		

For the rest of the responses, smaller the better criteria was followed and the results are shown in tables and figures below. Same conclusion can be drawn from each response.

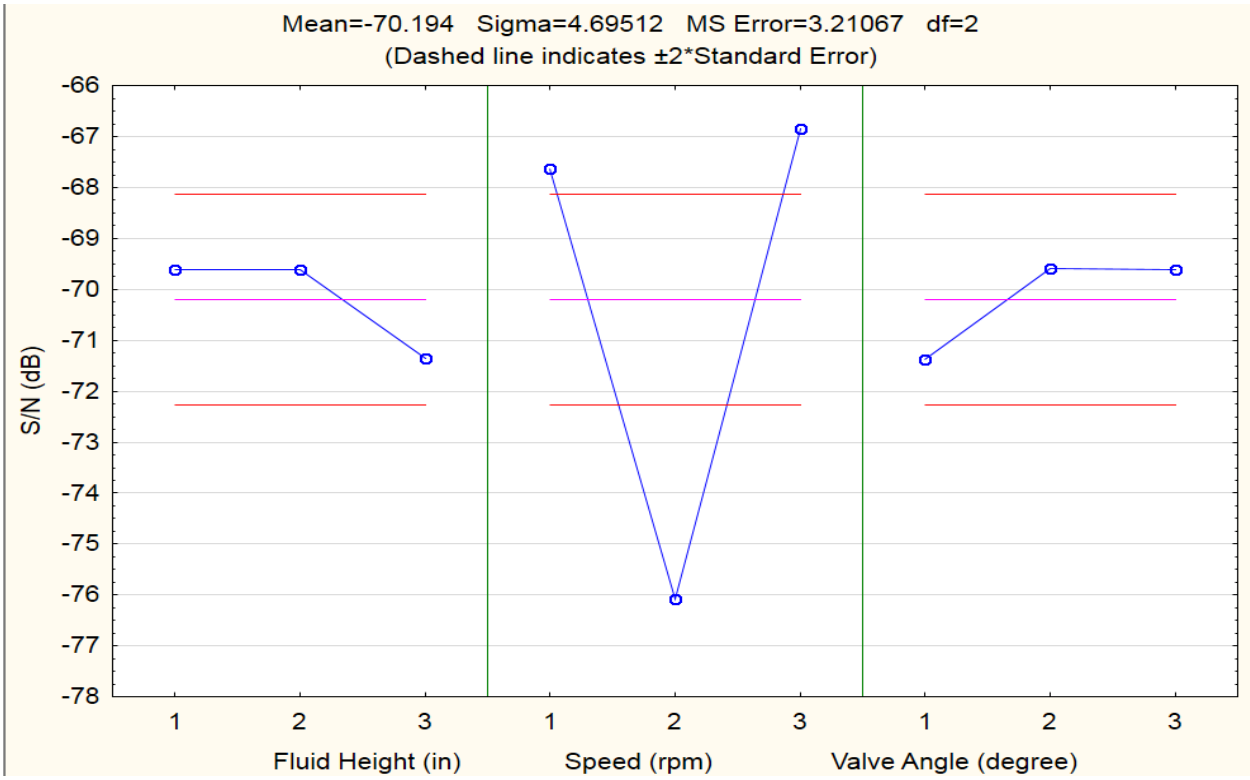

Figure 59. Response graph for max amplitude frequency

Table 15. ANOVA table for max amplitude frequency

Effect	Mean = -70.194 Sigma = 4.69512 SS	df	MS	F	p
{1}Fluid Height (in)	6.1415	2	3.07074	0.95642	0.511138
{2}Speed (rpm)	157.5076	2	78.75378	24.52878	0.039171
{3}Valve Angle (degree)	6.2830	2	3.14152	0.97846	0.505443
Residual	6.4213	2	3.21067		

Table 16. Optimal settings for max amplitude frequency

Factor	Mean = -70.194 Sigma = 4.69512 Level	Effect Size	Standard Error
{1}Fluid Height (in)	2	0.5851	1.034516
{2}Speed (rpm)	3	3.3452	1.034516
{3}Valve Angle (degree)	2	0.6094	1.034516
Expected S/N		-65.6538	

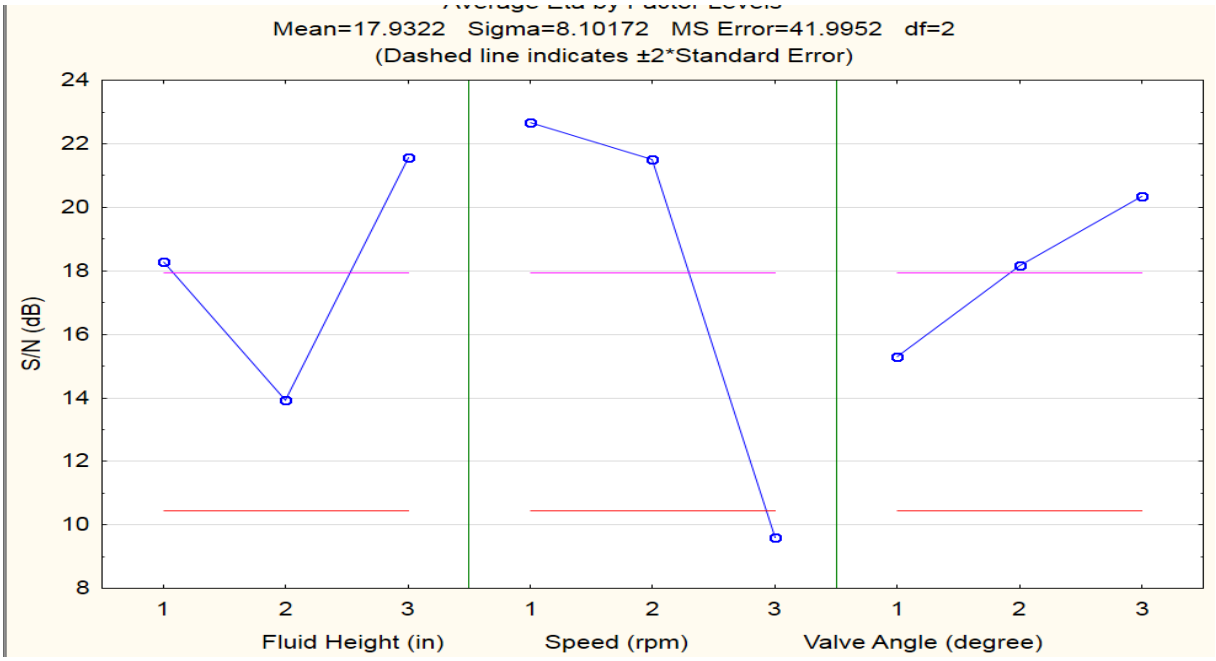

Figure 60. Response graph for temperature rise.

Table 17. ANOVA table for temperature rise

Effect	Mean = 17.9322 Sigma = 8.10172 SS	df	MS	F	p
{1}Fluid Height (in)	88.0804	2	44.0402	1.048696	0.488115
{2}Speed (rpm)	314.3893	2	157.1947	3.743156	0.210830
{3}Valve Angle (degree)	38.6428	2	19.3214	0.460085	0.684891
Residual	83.9904	2	41.9952		

Table 18. Optimal settings for temperature rise

Factor	Level	Effect Size	Standard Error
{1}Fluid Height (in)	3	3.64450	3.741444
{2}Speed (rpm)	1	4.74737	3.741444
{3}Valve Angle (degree)	3	2.41115	3.741444
Expected S/N		28.73525	

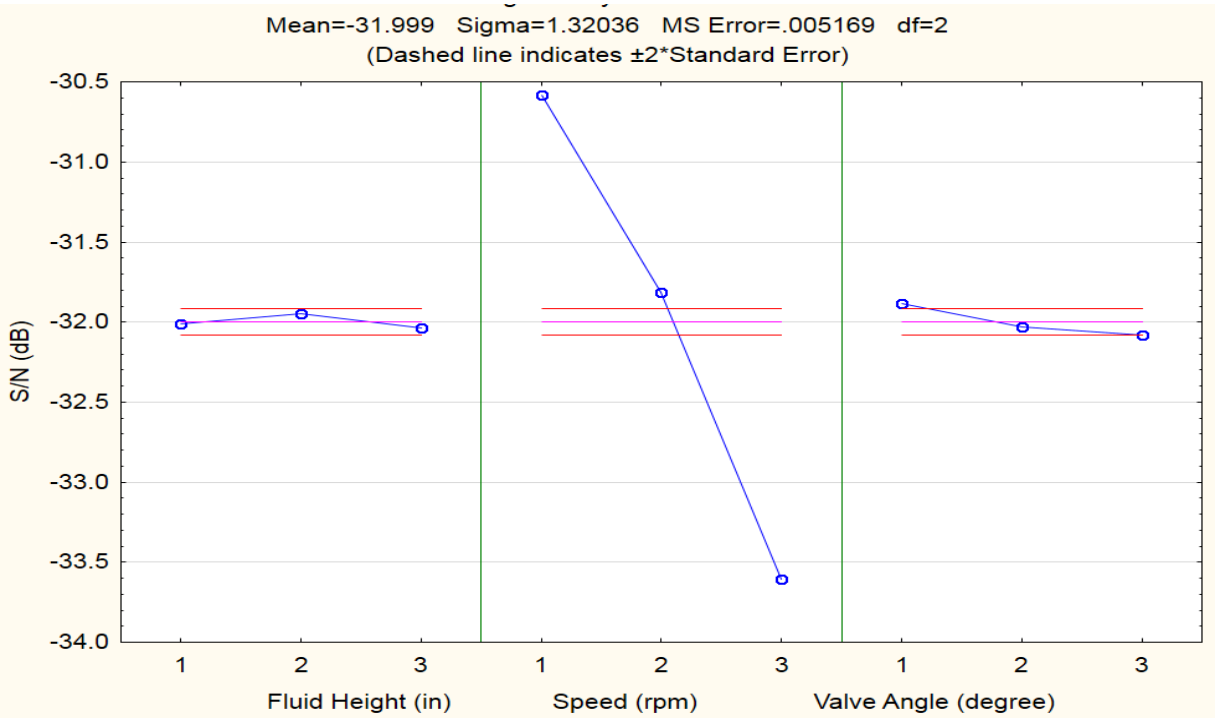

Figure 61. Response graph for noise

Table 19. ANOVA table for noise

Effect	Mean = -31.999 Sigma = 1.32036 SS	df	MS	F	p
{1}Fluid Height (in)	0.01223	2	0.006115	1.183	0.458076
{2}Speed (rpm)	13.85741	2	6.928707	1340.450	0.000745
{3}Valve Angle (degree)	0.06673	2	0.033364	6.455	0.134144
Residual	0.01034	2	0.005169		

Table 20. Optimal settings for noise

Factor	Mean = -31.999 Sigma = 1.32036 Level	Effect Size	Standard Error
{1}Fluid Height (in)	2	0.0507	0.041509
{2}Speed (rpm)	1	1.4185	0.041509
{3}Valve Angle (degree)	1	0.1179	0.041509
Expected S/N		-30.4114	

Few points can be interpreted from the analysis above:

To achieve high efficiency, the setting should be as follows: speed at level 3, valve at level 1, and fluid height at level 2.

To achieve low vibration amplitudes, the setting should be as follows: speed at level 2, valve at level 1, and fluid height at level 2.

To achieve low amplitude frequencies, the setting should be as follows: speed at level 3, valve at level 2, and fluid height at level 2.

To achieve low temperature rise, the setting should be as follows: speed at level 1, valve at level 3, and fluid height at level 3.

To achieve low noise, the setting should be as follows: speed at level 1, valve at level 1, and fluid height at level 1.

All the above analysis was done using steady state situation, where time was irrelevant. To determine the effect that time has on the above responses, L4 orthogonal design was constructed. The goal of this experiment is to find the effect time has on vibration, efficiency, temperature rise, and noise. In this experiment, two factors were considered; time and speed. Speed is selected from the results of the earlier L9 analysis because it was the most significant factor.

Figure 62 shows the response graph for temperature rise. Temperature rise was chosen, because the rest of the characteristic variables (efficiency, vibration and noise) were not affected by time. The figure shows that temperature increases with time and speed. Although the speed has the most significant slope but with more time the temperature will also increase.

Table 21 shows the ANOVA table for this experiment. The table shows that none of the factors are less than 0.05; which means they are not significant enough. But, the speed is very close to that. So, it influences the temperature. Table 22 shows the optimal levels to obtain the smaller values for temperature rise. The table suggests that to obtain the least amount of temperature rise, speed and time should be at level one. This means, speed should be at 6000 rpm and the pump should run for 5 minutes.

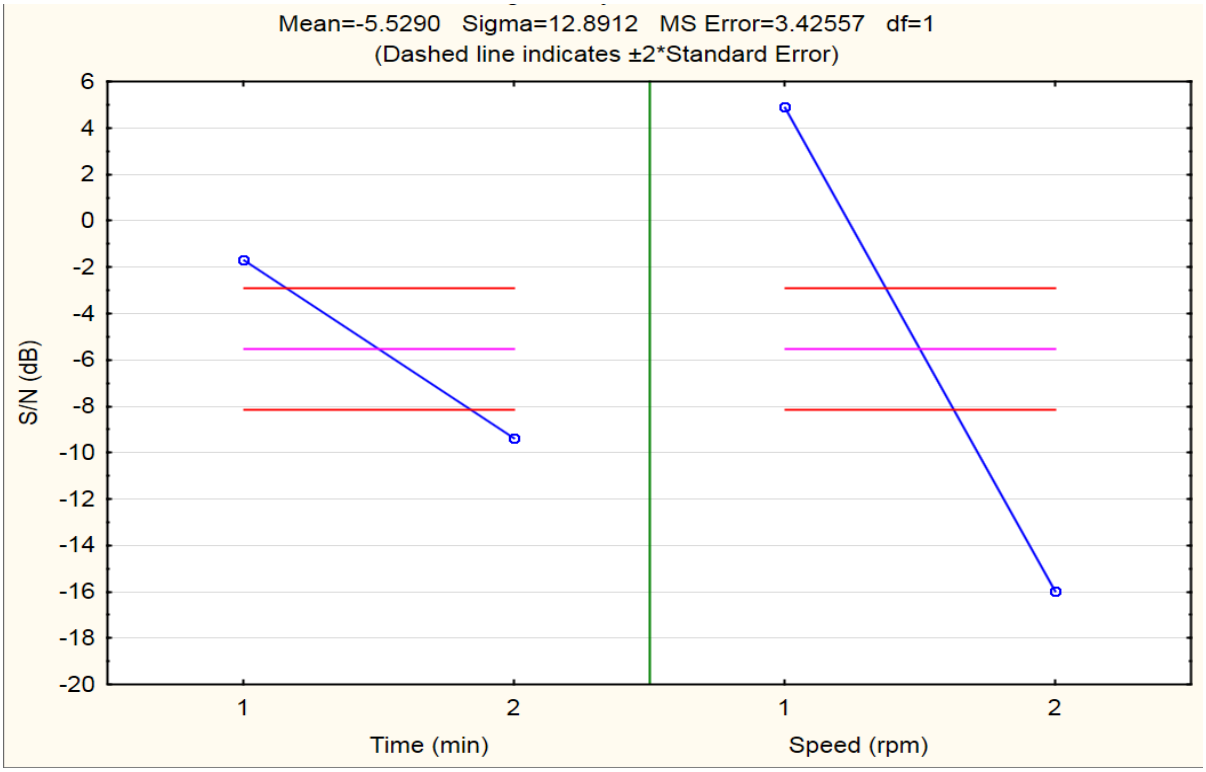

Figure 62. Response graph for temperature rise

Table 21. ANOVA table for temperature rise

	Mean = -5.5290 Sigma = 12.8912				
Effect	SS	df	MS	F	p
{1}Time (min)	59.2835	1	59.2835	17.3062	0.150182
{2}Speed (rpm)	435.8381	1	435.8381	127.2310	0.056292
Residual	3.4256	1	3.4256		

Table 22. Optimal settings for temperature rise

	Mean = -5.5290 Sigma = 12.8912		
Factor	Level	Effect Size	Standard Error
{1}Time (min)	1	3.84979	1.308733
{2}Speed (rpm)	1	10.43837	1.308733
Expected S/N		8.75917	

4.1.3 Response Surface Methodology

Taguchi does a great job in reducing time and cost for any industrial experiment. However, the big disadvantage of Taguchi method is the lack of explanation between variables themselves (interaction). Response Surface Methodology (RSM) method creates surfaces to explain the relationship between factors and results, and between factors themselves.

In this work, five responses are considered. These responses are vibration amplitude, vibration maximum frequencies, temperature rise, noise, and efficiency. Three factors were used; fluid height in main tank, speed of the pump, and valve angle. CCC was used to perform the RSM analysis with nineteen experiments as explained earlier in chapter four.

Table 23 shows ANOVA table for the first characteristic variable, vibration response. The table shows speed and valve angle are the most significant. Also, the interaction between the two is also significant. Table 24 shows the ANOVA table for the highest amplitude's frequencies. The table shows that speed and valve angle are also significant in the frequencies but their interaction is not.

Table 25 shows the ANOVA table for noise of the pump. Speed and valve are also the most significant in that process, and fluid height is not affecting the process. Table 26 on the other hand does a strange behavior. The table shows that temperature rise is not affected by speed or height, but it is affected by the valve angle and the interaction between fluid height and valve angle. This is not realistic as the speed clearly affects the temperature rise as shown from Taguchi methods and full factorial design. Therefore, these results cannot be analyzed. Another reason to ignore these results is the adjusted R-squared value. R-square value represents the how accurate the fitting curve between the predicted values from the model and the actual values taken. All of the other characteristic variables have at least a value of above 85%, while the temperature rise model has only 66%. This means the values from the predicted model does not fit well with the actual values.

Table 27 shows the ANOVA table for the efficiency of the pump. The table shows that efficiency is affected by all the three factors. Also, it is affected by the interaction between speed and vale, and speed and fluid height. But, not affected by the interaction of fluid height and valve angle.

Table 23. ANOVA for vibration amplitudes

ANOVA; Var.:Vibration Amplitude (g); R-sqr=.98268; Adj:.96535
3 factors, 1 Blocks, 19 Runs; MS Residual=.0014123
DV: Vibration Amplitude (g)

Factor	SS	df	MS	F	p
(1)Fluid Height (in)(L)	0.000413	1	0.000413	0.2928	0.601596
Fluid Height (in)(Q)	0.001816	1	0.001816	1.2861	0.286065
(2)Speed (rpm)(L)	0.427828	1	0.427828	302.9321	0.000000
Speed (rpm)(Q)	0.198848	1	0.198848	140.7982	0.000001
(3)Valve Angle (degrees)(L)	0.009303	1	0.009303	6.5868	0.030363
Valve Angle (degrees)(Q)	0.003146	1	0.003146	2.2277	0.169752
1L by 2L	0.001399	1	0.001399	0.9907	0.345569
1L by 3L	0.001529	1	0.001529	1.0827	0.325245
2L by 3L	0.010585	1	0.010585	7.4950	0.022934
Error	0.012711	9	0.001412		
Total SS	0.733702	18			

Table 24. ANOVA for maximum vibration amplitude's frequency

	ANOVA; Var.:Vibration Frequency (Hz); R-sqr=.94296; Adj:.88592 3 factors, 1 Blocks, 19 Runs; MS Residual=212424. DV: Vibration Frequency (Hz)				
Factor	SS	df	MS	F	p
(1)Fluid Height (in)(L)	484000	1	484000	2.27846	0.165461
Fluid Height (in)(Q)	461628	1	461628	2.17315	0.174536
(2)Speed (rpm)(L)	125440	1	125440	0.59052	0.461906
Speed (rpm)(Q)	15334237	1	15334237	72.18692	0.000014
(3)Valve Angle (degrees)(L)	1466890	1	1466890	6.90548	0.027456
Valve Angle (degrees)(Q)	538578	1	538578	2.53539	0.145783
1L by 2L	605000	1	605000	2.84808	0.125755
1L by 3L	583200	1	583200	2.74545	0.131911
2L by 3L	594050	1	594050	2.79653	0.128800
Error	1911816	9	212424		
Total SS	33515811	18			

Table 25. ANOVA for noise

	ANOVA; Var.:Noise (dB); R-sqr=.99695; Adj:.9939 3 factors, 1 Blocks, 19 Runs; MS Residual=.01989 DV: Noise (dB)				
Factor	SS	df	MS	F	p
(1)Fluid Height (in)(L)	0.06084	1	0.06084	3.058	0.114269
Fluid Height (in)(Q)	0.00927	1	0.00927	0.466	0.512031
(2)Speed (rpm)(L)	42.10704	1	42.10704	2116.504	0.000000
Speed (rpm)(Q)	2.83302	1	2.83302	142.401	0.000001
(3)Valve Angle (degrees)(L)	11.77225	1	11.77225	591.730	0.000000
Valve Angle (degrees)(Q)	0.64738	1	0.64738	32.541	0.000293
1L by 2L	0.03251	1	0.03251	1.634	0.233100
1L by 3L	0.07031	1	0.07031	3.534	0.092812
2L by 3L	0.97301	1	0.97301	48.908	0.000064
Error	0.17905	9	0.01989		
Total SS	58.70118	18			

Table 26. ANOVA for temperature rise

Factor	ANOVA; Var.:Temperature Rise (°C); R-sqr=.80038; Adj:.6007 3 factors, 1 Blocks, 19 Runs; MS Residual=.0142529 DV: Temperature Rise (°C)				
	SS	df	MS	F	p
(1)Fluid Height (in)(L)	0.000425	1	0.000425	0.02983	0.866707
Fluid Height (in)(Q)	0.010480	1	0.010480	0.73529	0.413426
(2)Speed (rpm)(L)	0.000046	1	0.000046	0.00324	0.955830
Speed (rpm)(Q)	0.024391	1	0.024391	1.71131	0.223237
(3)Valve Angle (degrees)(L)	0.092333	1	0.092333	6.47820	0.031440
Valve Angle (degrees)(Q)	0.009896	1	0.009896	0.69432	0.426259
1L by 2L	0.048969	1	0.048969	3.43572	0.096799
1L by 3L	0.153098	1	0.153098	10.74158	0.009568
2L by 3L	0.058294	1	0.058294	4.08999	0.073839
Error	0.128276	9	0.014253		
Total SS	0.642600	18			

Table 27. ANOVA for efficiency

Factor	ANOVA; Var.:Efficiency (%); R-sqr=.99993; Adj:.999 3 factors, 1 Blocks, 19 Runs; MS Residual=.003665 DV: Efficiency (%)				
	SS	df	MS	F	p
(1)Fluid Height (in)(L)	0.1261	1	0.1261	34.4	0.000239
Fluid Height (in)(Q)	0.0172	1	0.0172	4.7	0.058646
(2)Speed (rpm)(L)	478.8014	1	478.8014	130621.4	0.000000
Speed (rpm)(Q)	1.2106	1	1.2106	330.3	0.000000
(3)Valve Angle (degrees)(L)	0.9788	1	0.9788	267.0	0.000000
Valve Angle (degrees)(Q)	0.2140	1	0.2140	58.4	0.000032
1L by 2L	0.0011	1	0.0011	0.3	0.605364
1L by 3L	0.0552	1	0.0552	15.1	0.003723
2L by 3L	0.2443	1	0.2443	66.7	0.000019
Error	0.0330	9	0.0037		
Total SS	481.5524	18			

Figure 63Figure 67 show the fitting line that describes the relationship between the model's predicted data and the actual experimental data (observed data). All of the data fit within the

predicted line except for temperature rise data. This conclusion also matches the results from ANOVA table. This concludes that this model is not a good model to analyze temperature rise. To solve this issue, more data point can be taken.

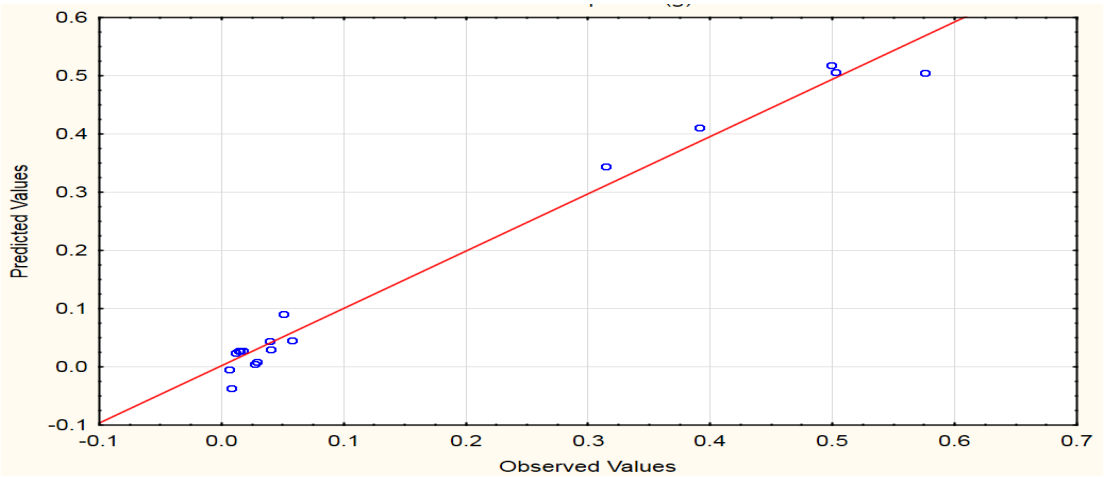

Figure 63. Vibration amplitude fitted line

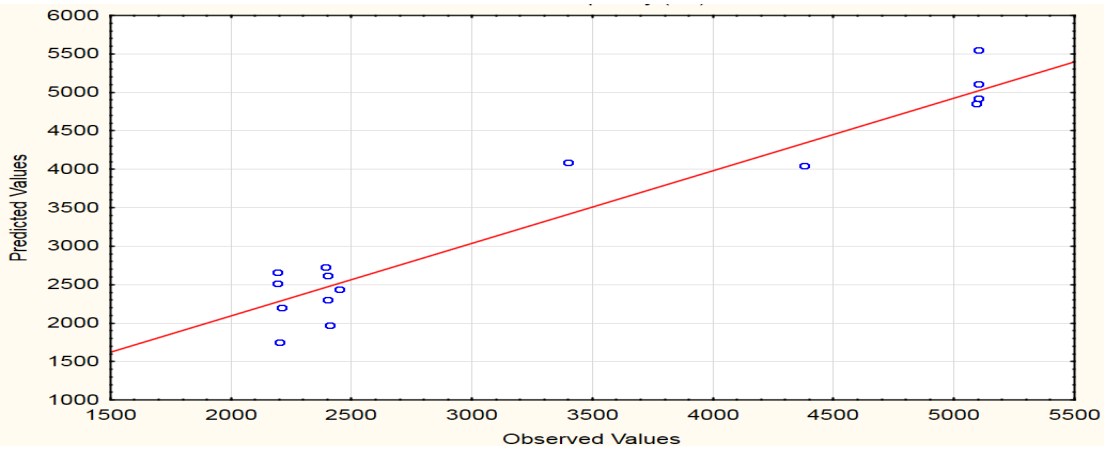

Figure 64.Vibration max amplitude's frequencies fitted line

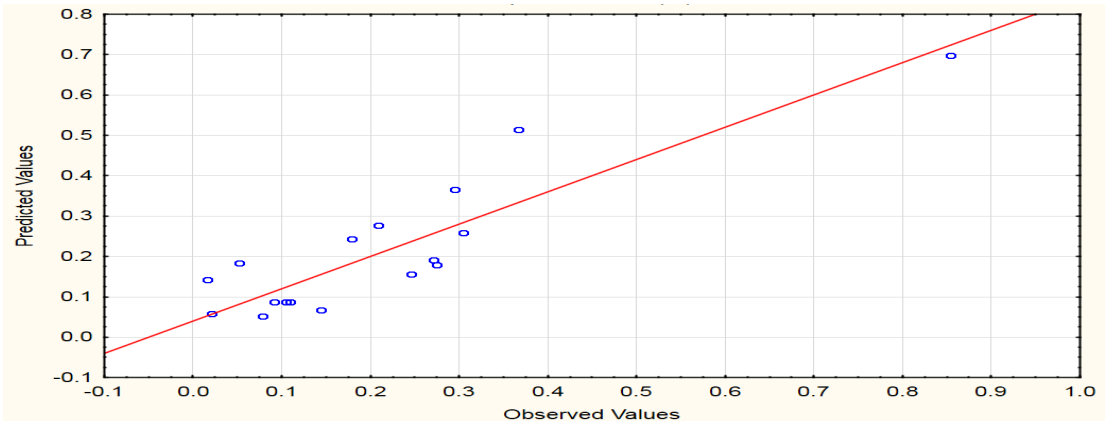

Figure 65. Temperature rise fitted line

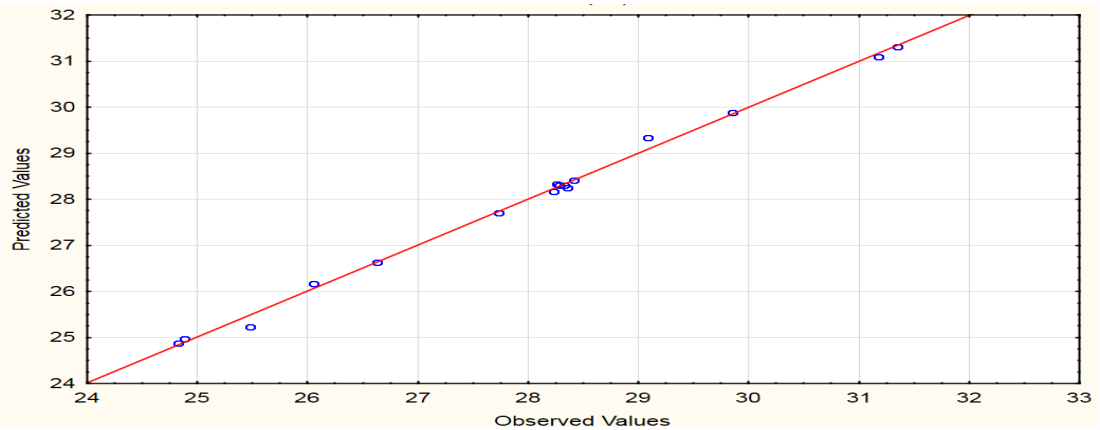

Figure 66. Noise fitted line

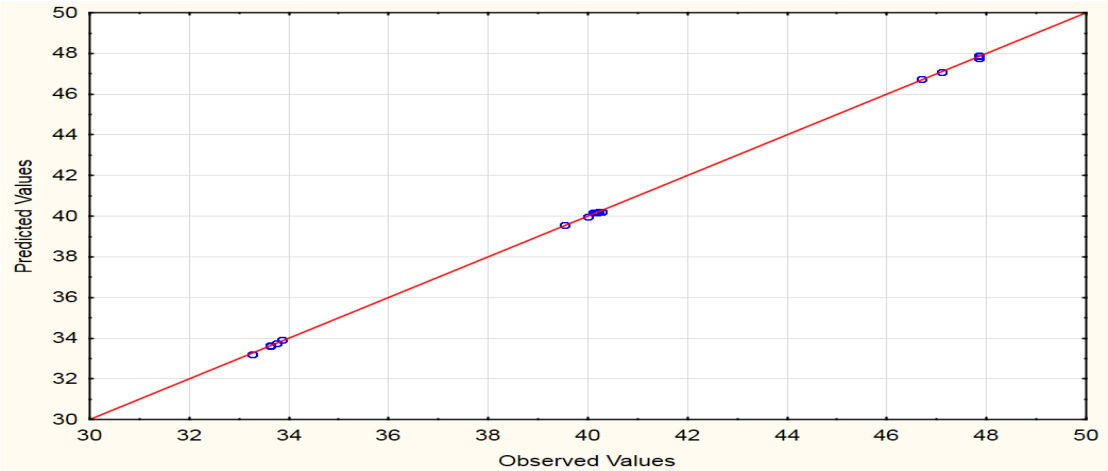

Figure 67. Efficiency fitted line

To further analyze the relationship between factors and responses, surface response plots were created. These 3D surfaces have 3-axis, two are for the factors, and the third one is for the response. In this work, three factors are used. So, it is impossible to plot them all together. Instead, speed and fluid height will be plotted in x-axis and y-axis at every valve angle. To explain, at valve angle 40 degrees, there will be surface plot for the response. At valve angle 60 degrees, there will be another plot, and so on. As a result, for each characteristic variable, there will be three different surface plots.

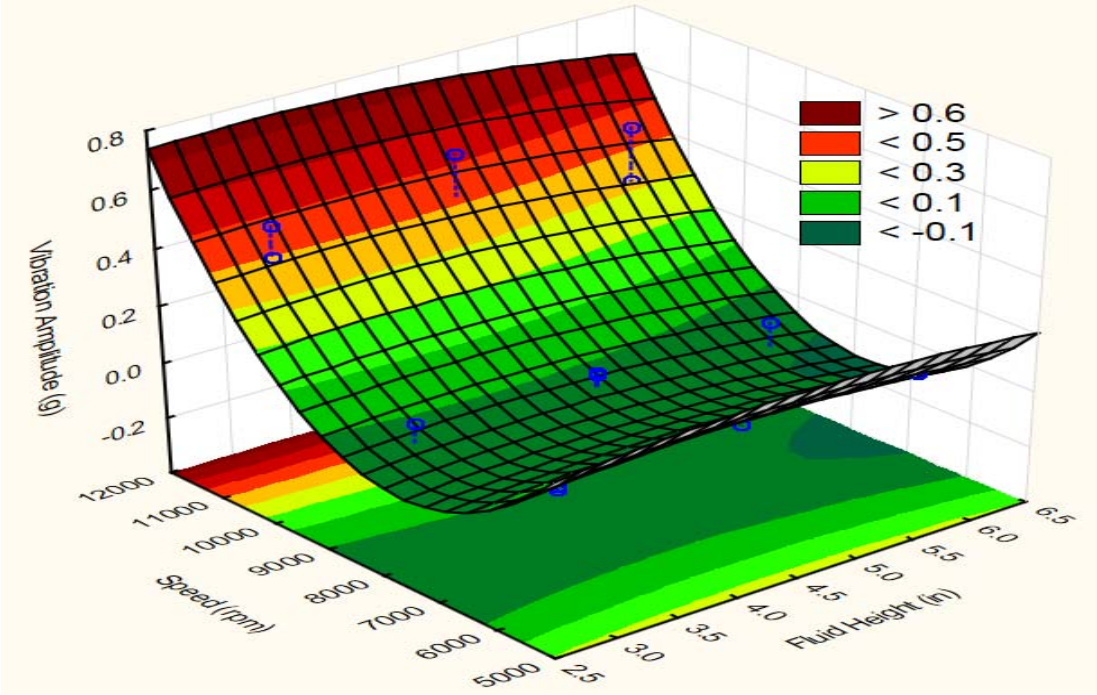

Figure 68. Surface plot for vibration amplitude at valve angle 40 (degrees)

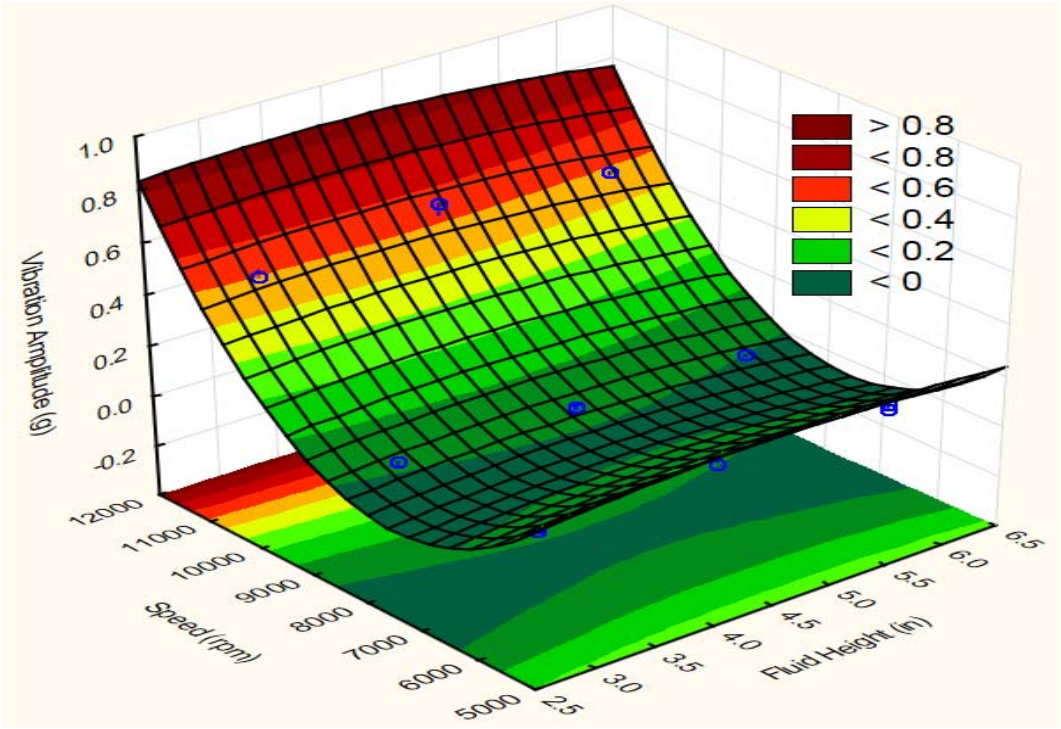

Figure 69. Surface plot for vibration amplitude at valve angle 60 (degrees)

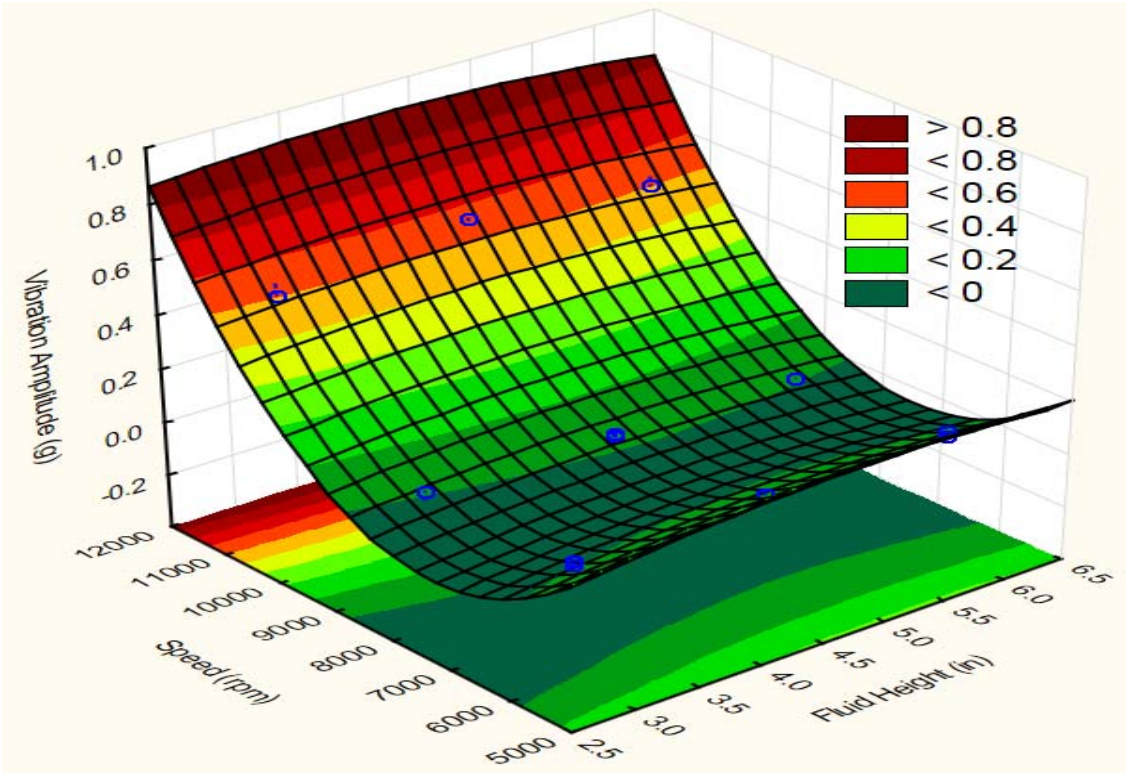

Figure 70. Surface plot for vibration amplitude at valve angle 80 (degrees)

Figure 68Figure 70 show the response surface plots for vibration amplitude. The plots show a quadratic relationship between the vibration amplitude and fluid height and speed. The minimum amplitudes occur between speeds 6000 and 8000 rpm. Changing in fluid height does not affect the amplitudes as much. The figures also show, if the valve angle increases, the amplitudes increase as well.

Figure 71Figure 73 show the response surface plots for the maximum amplitudes frequencies. The plots show that amplitudes increase in their frequencies with increasing speeds, and fluid height is not significant in that. With increasing valve angle, the frequencies of those maximum amplitudes increase also.

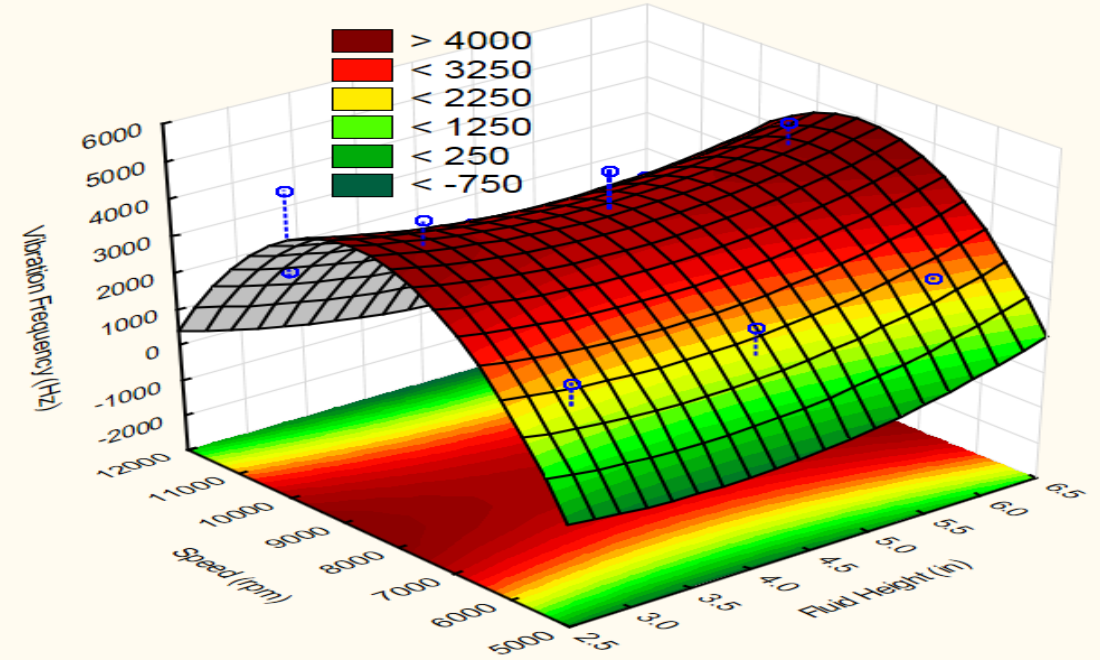

Figure 71. Surface plot for vibration max amplitude's frequencies at valve angle 40 (degrees)

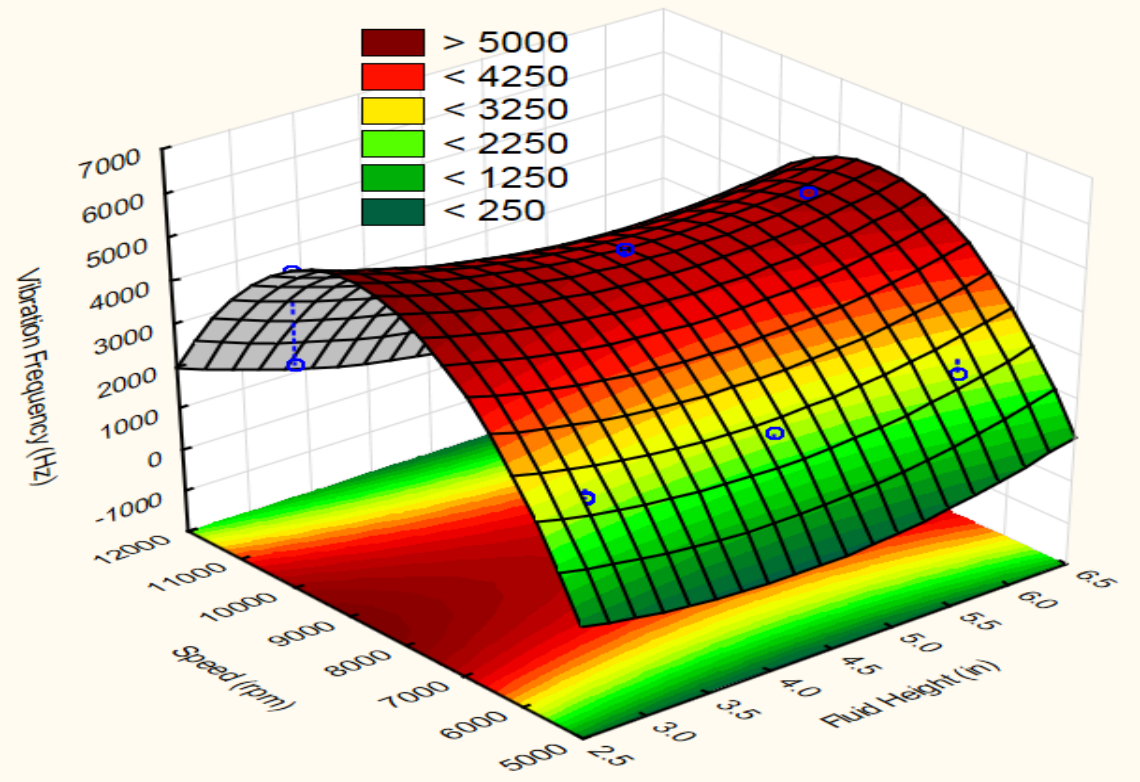

Figure 72. Surface plot for vibration max amplitude's frequencies at valve angle 60 (degrees)

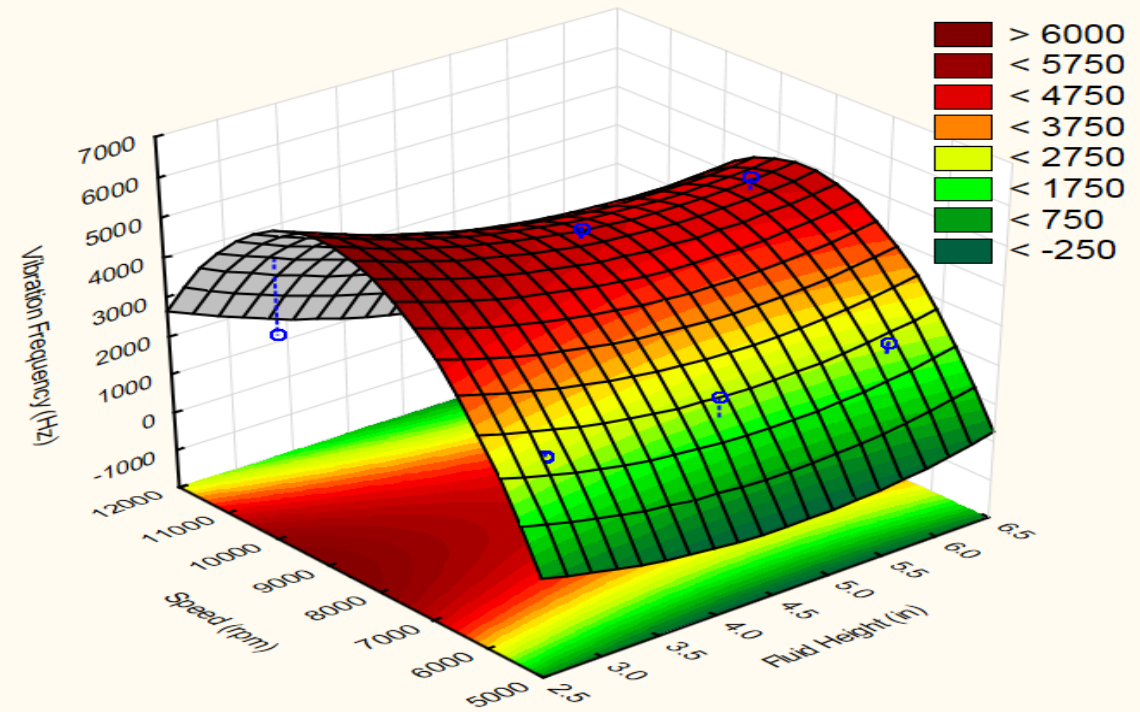

Figure 73.Surface plot for vibration max amplitude's frequencies at valve angle 80 (degrees)

Figure 74-Figure 76 show the response plots for the temperature rise. ANOVA and fit plots showed weak relationship between the model and the actual values. Therefore, these results might not be fully accurate. But generally, the plots show that at low speed and low height, the temperature increases. Also, the temperature increases as the valve angle increases.

Figure 77Figure 79 show the response plot for the pump's noise. As shown, the noise increases as the speed of the pump increases, and the fluid height has very small effect. The noise also reduces as the valve angle increases.

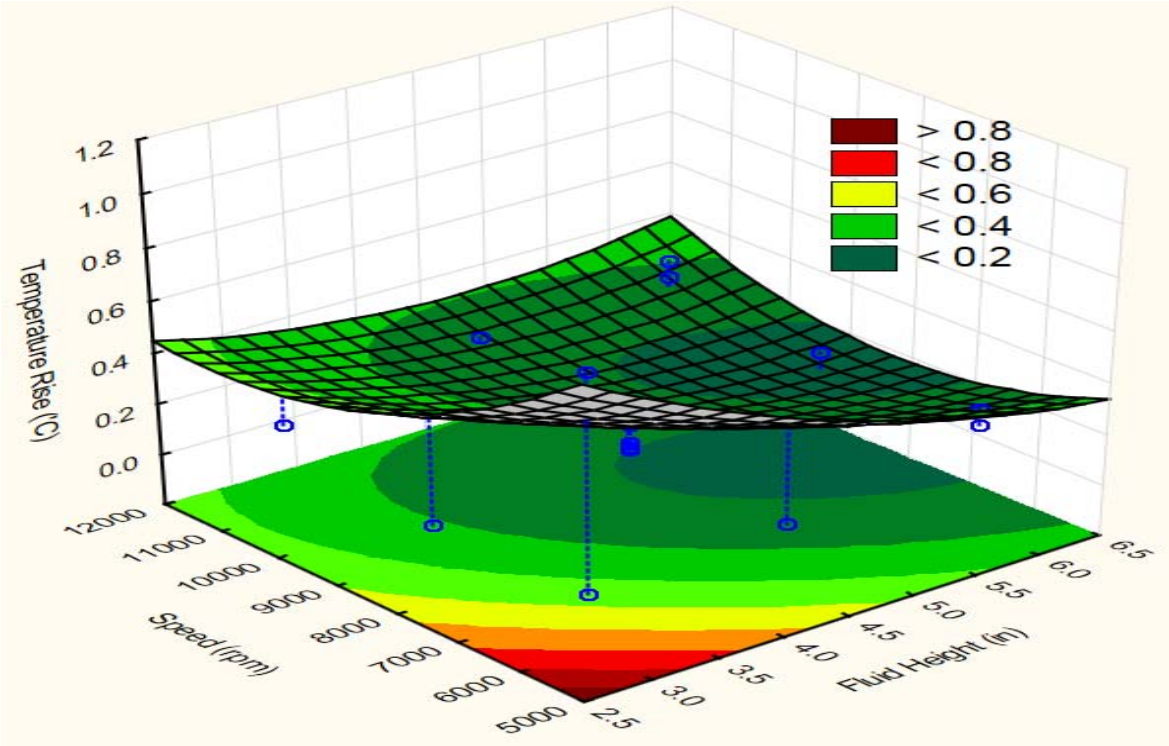

Figure 74.Surface plot for temperature rise at valve angle 40 (degrees)

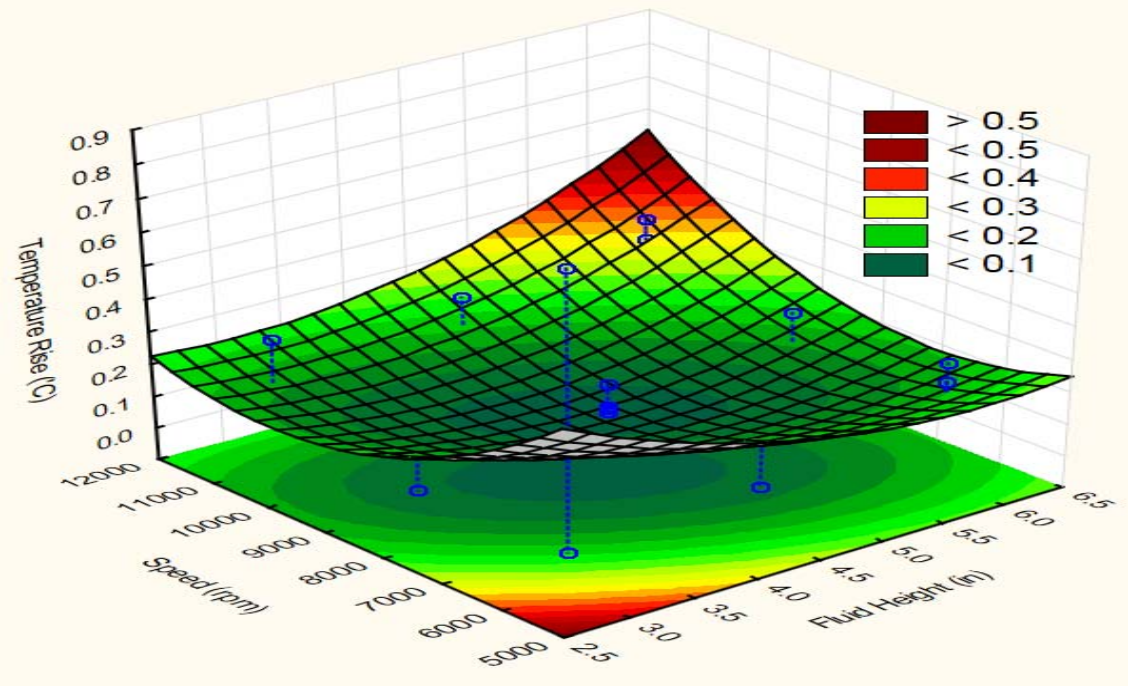

Figure 75.Surface plot for temperature rise at valve angle 60 (degrees)

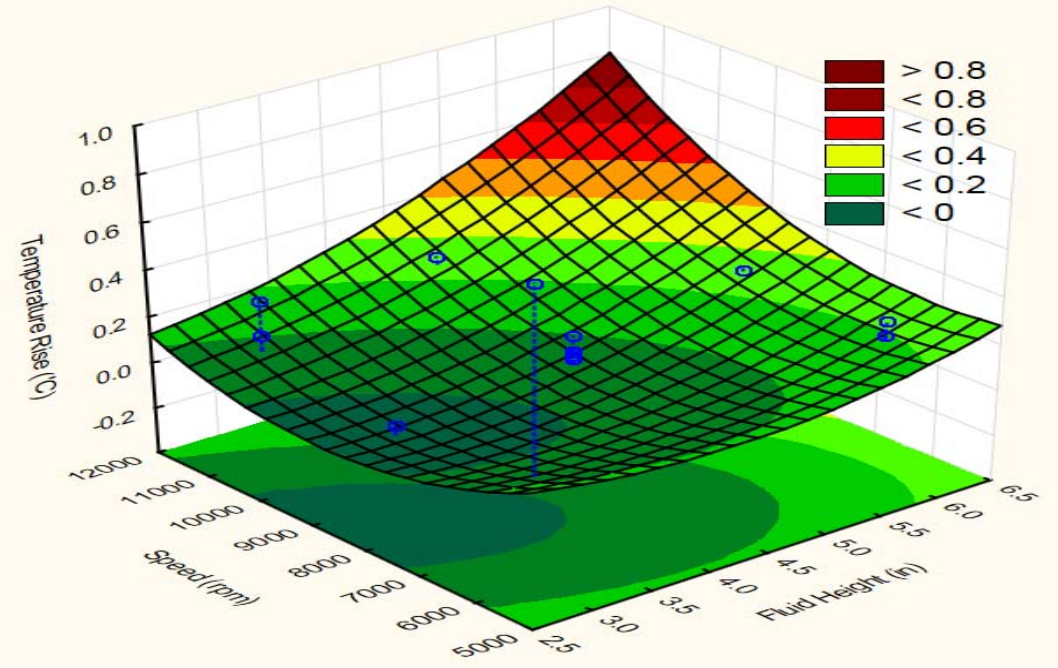

Figure 76.Surface plot for temperature rise at valve angle 80 (degrees)

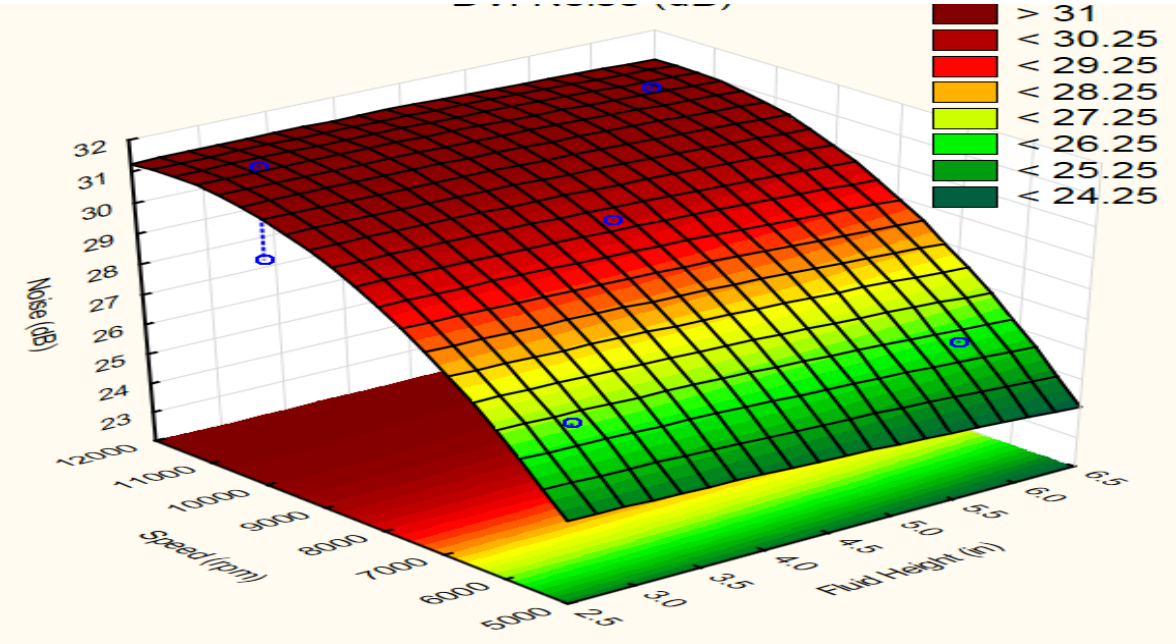

Figure 77.Surface plot for noise at valve angle 40 (degrees)

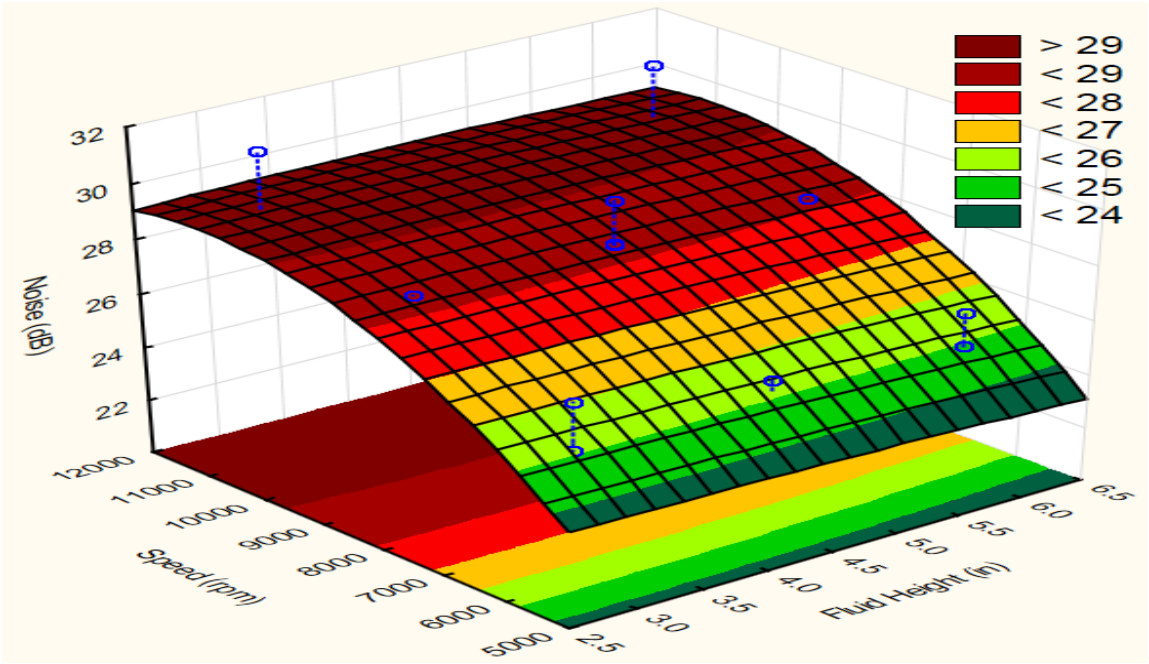

Figure 78.Surface plot for noise at valve angle 60 (degrees)

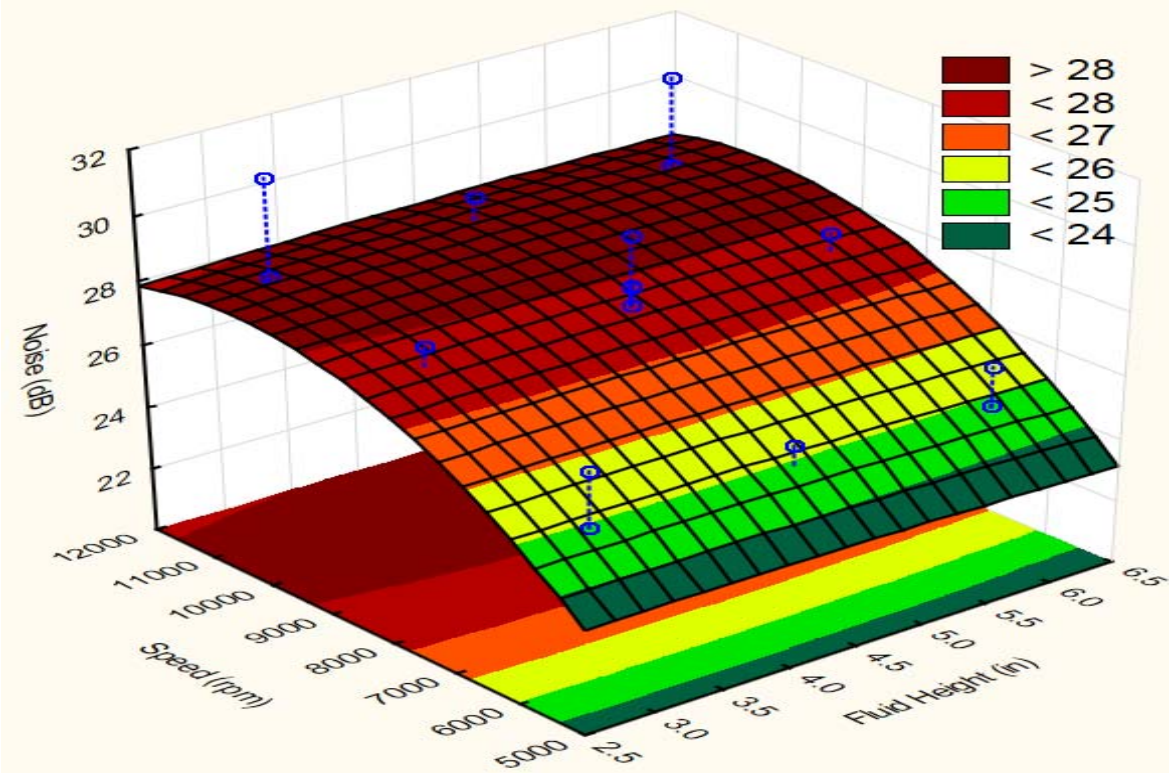

Figure 79.Surface plot for noise at valve angle 80 (degrees)

Figure 80Figure 82 show the response surface plots for the pump's efficiency. As shown, the efficiency increases with increasing the speed, and fluid height has higher effect on this response than any of the earlier ones. Efficiency is higher at 40 degrees than it is at 60 or 80 degrees.

To further analyze the relationships, valve angle was included with the speed for the characteristic variables, while keeping the fluid height at 4.5 inches. So, one response surface plot for each response is done.

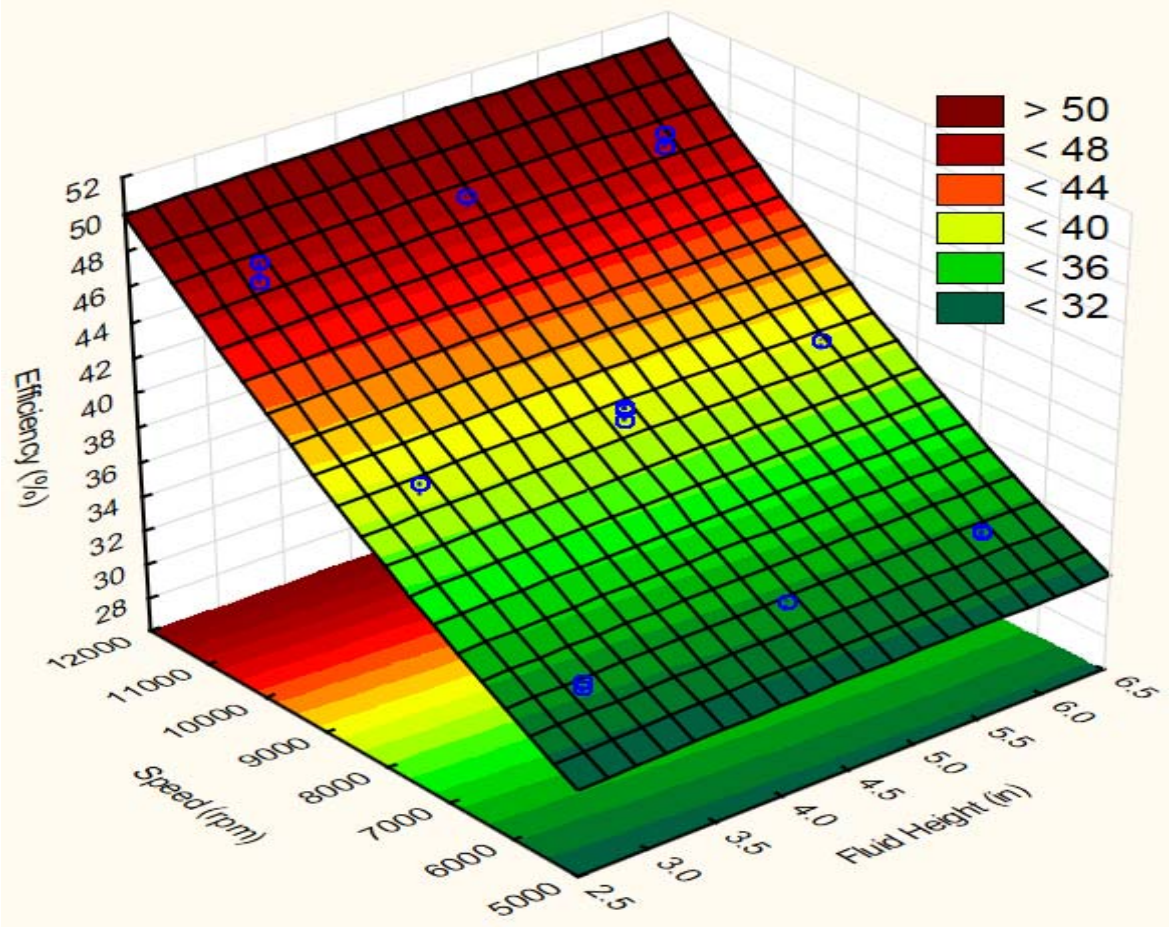

Figure 80.Surface plot for efficiency at valve angle 40 (degrees)

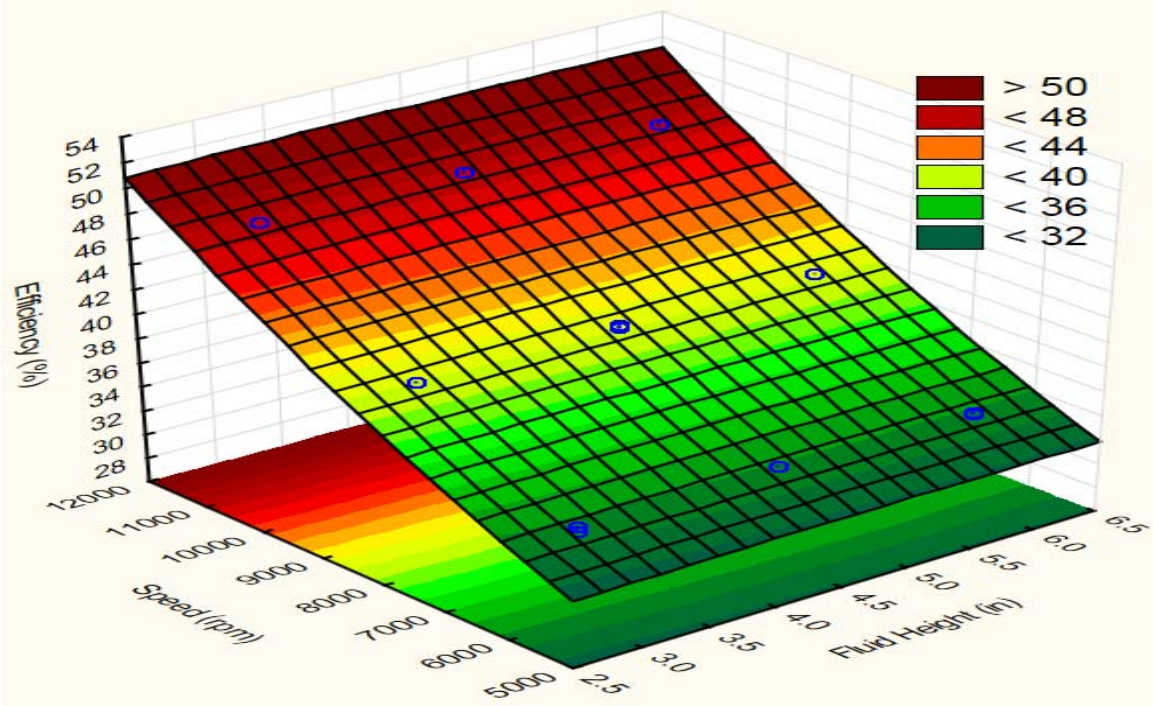

Figure 81.Surface plot for efficiency at valve angle 60 (degrees)

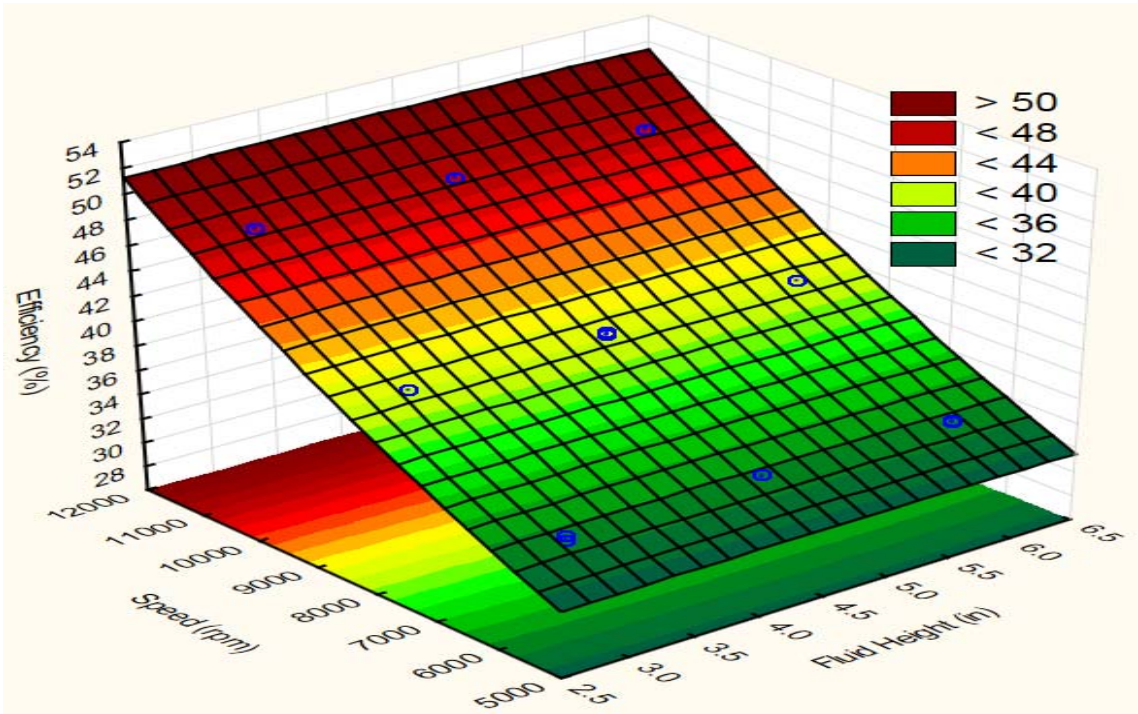

Figure 82.Surface plot for efficiency at valve angle 80 (degrees)

Figure 83Figure 87 show the response surface plots for the characteristic variables. The x-axis and y-axis are for pump speed and valve angle respectively. These surfaces are created by keeping the fluid height at a constant value, 4.5 inches. Figure 83 shows the vibration amplitude. The figure shows a quadratic relationship, and the amplitude is higher at valve angle 80 degrees and speed higher than 11000 rpm. Figure 84 shows the maximum vibration amplitude's frequencies. The figure shows that the maximum frequencies occur between speeds 6000 and 8000 rpm. Figure 86 shows the response surface plot of the pump's noise. The figure shows that at lower valve angles and higher speeds, the pump noise is the highest. The larger the valve angle is the lower the pump noise. Figure 87 shows the response surface plot for the pump's efficiency. The plot shows that the higher the speeds, the higher the efficiency. Valve angle affect is not really as important as shown, but it has an effect as discussed earlier in the ANOVA tables.

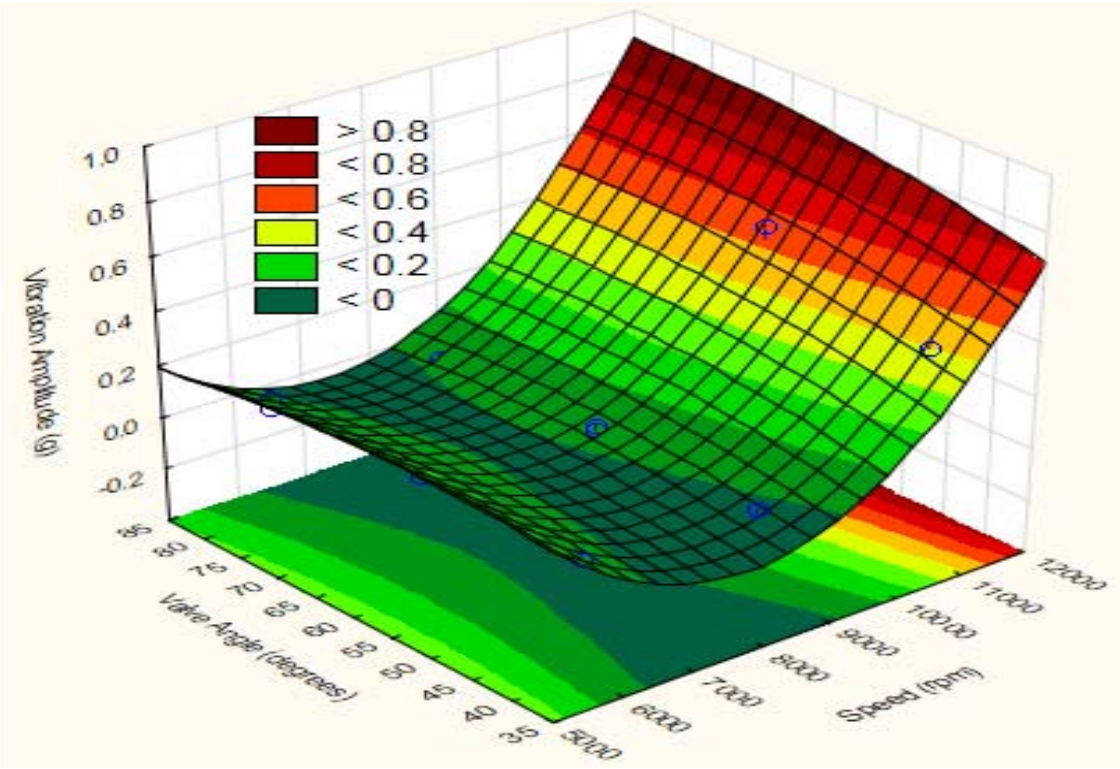

Figure 83. Vibration amplitude at 4.5 inches

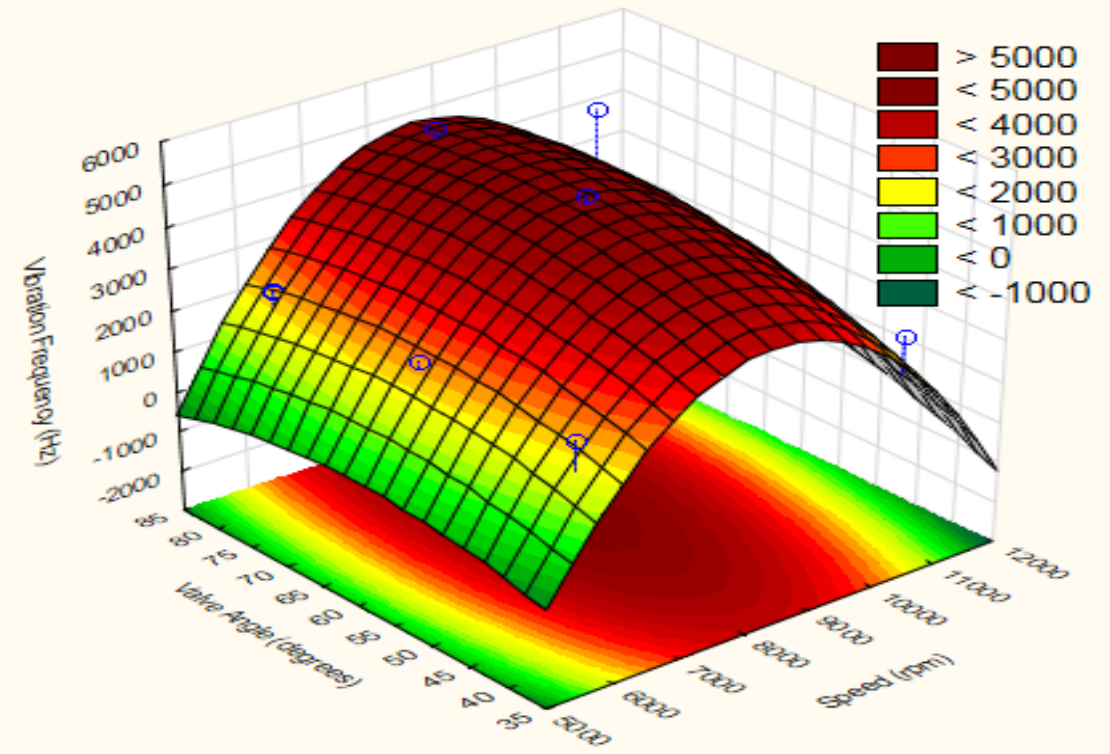

Figure 84.Vibration maximum amplitude's frequencies at 4.5 inches

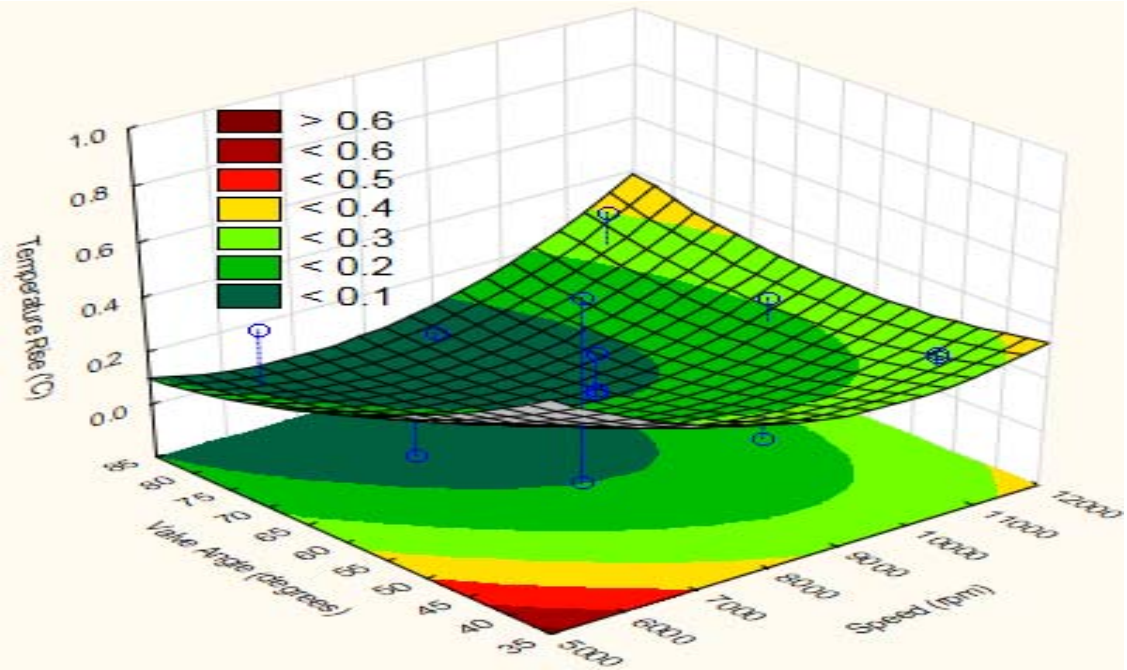

Figure 85. Temperature rise at 4.5 inches

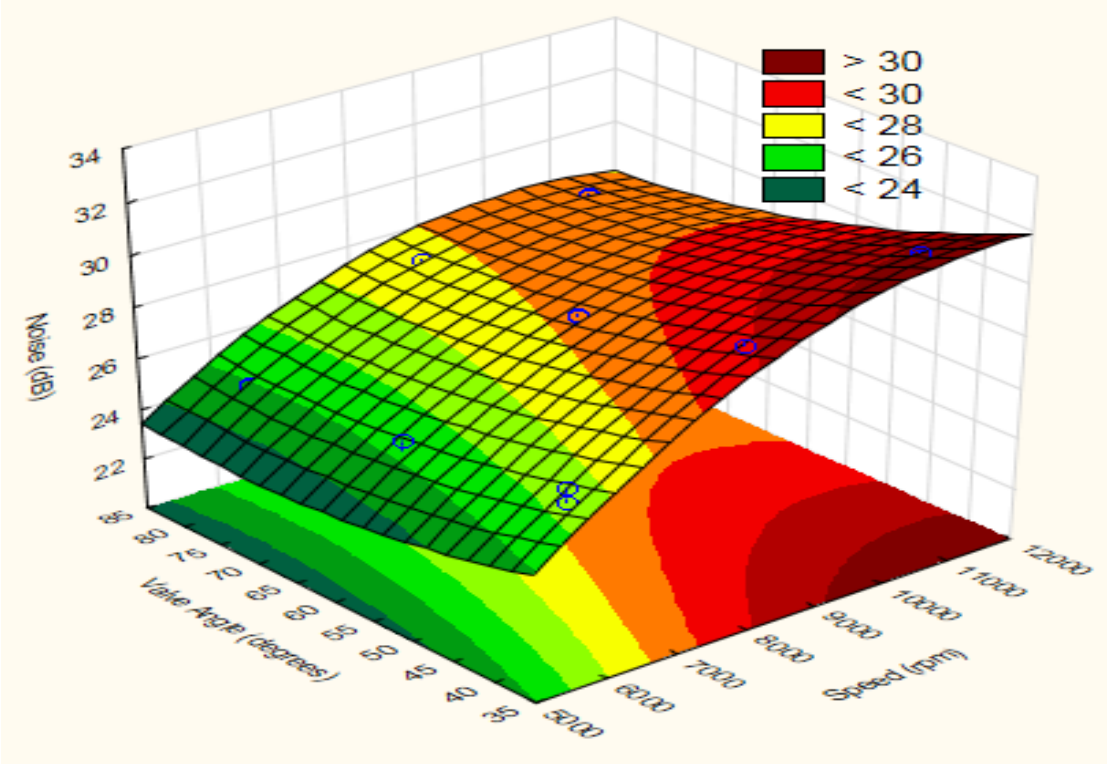

Figure 86. Noise of the pump at 4.5 inches

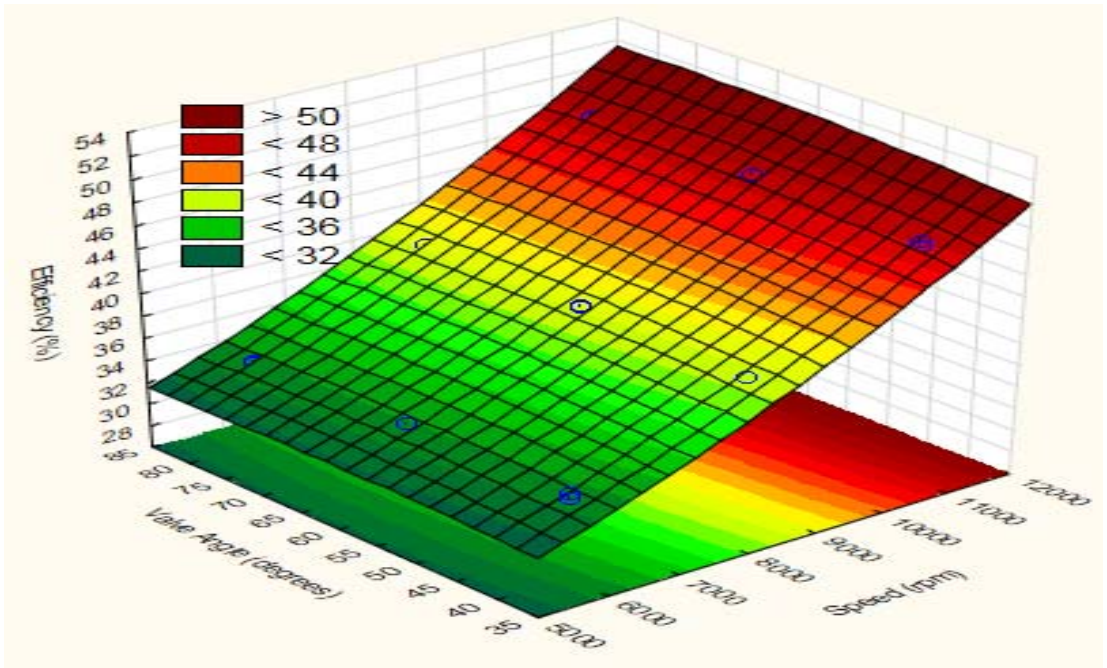

Figure 87. Efficiency of the pump at 4.5 inches

4.1.4 FMEA Results

Table 28. Common failures and their percent contributions in some phenomena in centrifugal pump [84]

No.	Failure cause	Failure mode			
		External leakage (%)	Spurious stop (%)	Vibration (%)	Total relative contribution (%)
1	Blockage/plugged	0.31	0.10	0.05	0.46
2	Breakage	0.05	0.05	0.31	0.41
3	Cavitation	0.15	0.00	0.05	0.20
4	Clearance/misalignment	0.15	0.00	0.97	1.12
5	Control failure	0.00	0.21	0.05	0.26
6	Corrosion	0.41	0.15	0.00	0.56
7	Electrical failure - general	0.00	0.51	0.00	0.51
8	Fatigue	0.15	0.00	0.05	0.20
9	Faulty signal	0.00	0.67	0.15	0.82
10	Instrument failure - general	0.10	1.39	0.10	2.59
11	Leakage	2.72	0.21	0.05	2.98
12	Looseness	0.36	0.05	0.05	0.46
13	Mechanical failure - general	3.59	0.97	0.82	5.38
14	Misc. external influence	0.46	0.10	0.51	1.07
15	Out of adjustment	0.00	0.21	0.10	0.31
16	Over heating	0.05	0.05	0.00	0.10
17	Unknown	0.05	0.15	0.15	0.35
18	Vibration	0.05	0.51	0.46	1.02
19	Wear	0.15	0.05	0.26	0.46
Total		8.75	5.38	4.13	19.26

Table 28 shows the common failures and their percent contributions in some phenomena in centrifugal pumps. These data are collected from experimental testing. The table shows that breakage, clearance/misalignment, mechanical failure (general), and wear are the most common failures that relate to vibration increase in the system.

Table 29 shows the FMEA for the system used in this work. The table gives clear idea of the failures associated with the system used in this work. This can serve as a correction method before problems occur.

Table 29. Failure mode effects analysis for this system

Function or Equipment Identification	Functional or Equipment Purpose	Failure Modes	Failure Mechanism	Failure Detection	Failure Compensation	Failure Effects	Severity	Frequency	Risk Level	Preventative Measures
Flow Valve Angle	Controls the valve angle in which fluid flows past	Flow valve fails to allow enough fluid to pass	Stallout of the pump	Back pressure, turbulent flow of fluid	Detection likely, operator shuts off system	Potential breakage of valve and pump	7	3	21	Double check input of valve angle selection before starting system; Set shut off ranges for available valve angles
		Flow valve allows too much fluid to pass	No cavitation occurs	Ideal testing results; no cavitation occurs	None	Bad testing data; no severe damage to system	1	3	3	
Fluid Level	Determines amount of fluid passing through pump	Fluid level is too high for desired testing criteria	Long wait period for cavitation to occur	Inspection of tank	Open resevoir valve; lower fluid level	Bad testing data; no severe damage to system	1	6	6	Set a timer for re-filling the tank before testing; use gage on tank to measure fluid height
		Fluid level fails to provide an adequate height for feasible testing	Cavitation occurs when pump is initially turned on	Auditory inspection	Detection likely, operator shuts off system	"Dry cavitation", potential harm to pump; overheating	7	4	28	
Power Contoller	Controls the speed of pump	Power controller is set too high	Overload of pump	Inspection and smoke detection	Detection likely, operator shuts off system	Potential breakage of pump; possible fire and overheating	8	4	32	Double check input of power selection before starting system; Set shut off ranges for available power levels
		Power contoller is set too low	Fluid unable to properly flow	Inspection	Increase power input	Potential breakage of pump; no immediate harm	3	2	6	

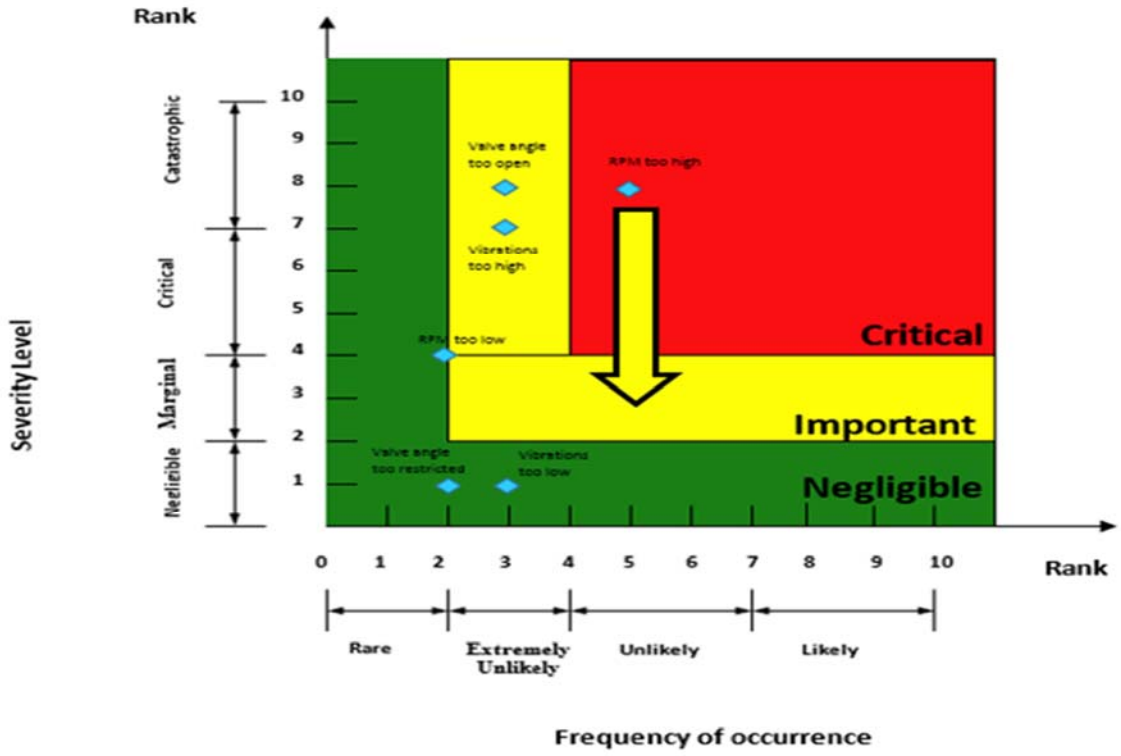

Figure 88. FMEA graph

Figure 88 shows the FMEA graph for the pump operation system. This figure was constructed based on the FMEA table shown earlier. As shown, the red area is critical, where the failure is catastrophic and frequent. It is very important for all point to be at least in the yellow or green zones, where the failures are less frequent and catastrophic. As shown, one point is in the red zone, this is point is higher speed. Higher speed causes multiple issues with the pump and the system as all. These issues will be shown as high vibrations, cavitation and mechanical failures. To avoid this issue, the pump can be used without reaching the failure speeds, that causes high intensity failures.

4.3 Vibration Analysis Results

Vibrations as mentioned earlier, can be used as a monitoring tool. In this work, two types of vibration analysis have been done; normal and failure conditions. In the normal stage, the pump and the system ran at the proper fluid height (NPSHa>NPSHr), safety speed limits, and safety valve angles. The goal of this analysis was to monitor the mechanical failures associated with the pump. These failures can be in form of, misalignment, unbalance, and looseness. These failures might occur in the bearings, base, or even in the casing of the pump.

Figure 89 shows the spectra diagram of vibration signals of four states used by Yunlong [85]. In his work, Yunlong used the vibration signals to detect mechanical failures in a centrifugal pump. He simulated those failures by disassembling a coupler connected to the motor, loosening of some bolts, and mass unbalance by bolting the disk connected to the coupler. The figure, shows multiple vibrations signals and how they are related to the failure mode. Figure 90 shows a spectrum of misalignment done by Xue [86]. Xue used time domain and spectral data of vibration to detect misalignment in the centrifugal pump. Those two figures, will be the guideline for the vibration analysis constructed in this work.

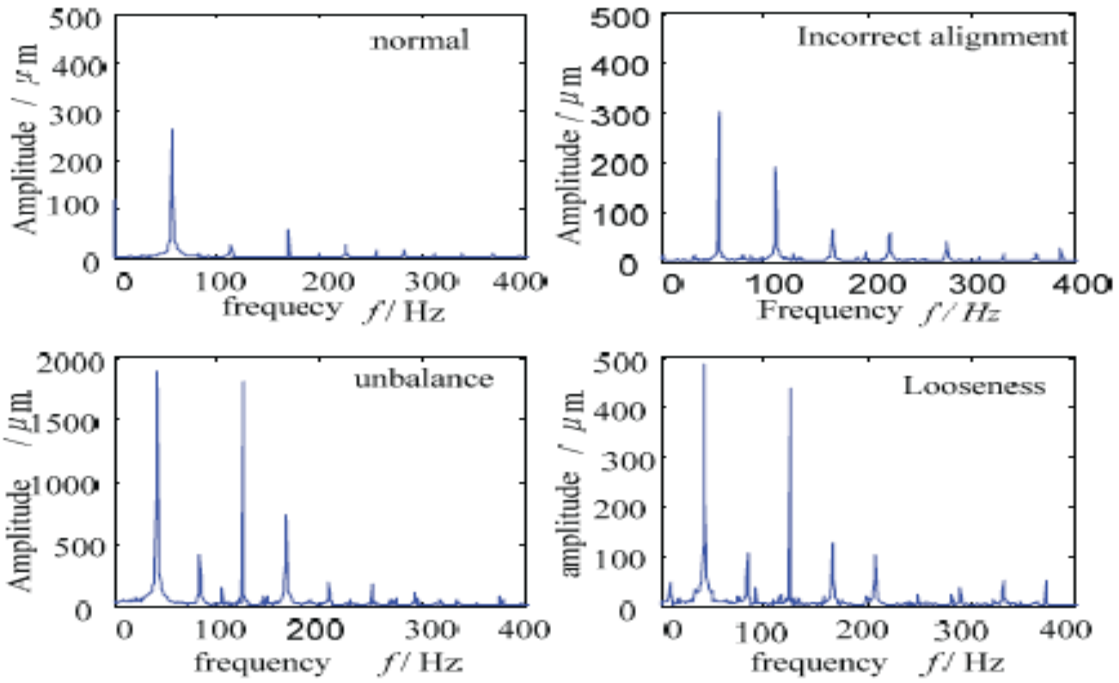

Figure 89. Spectral diagram of vibration signals [85]

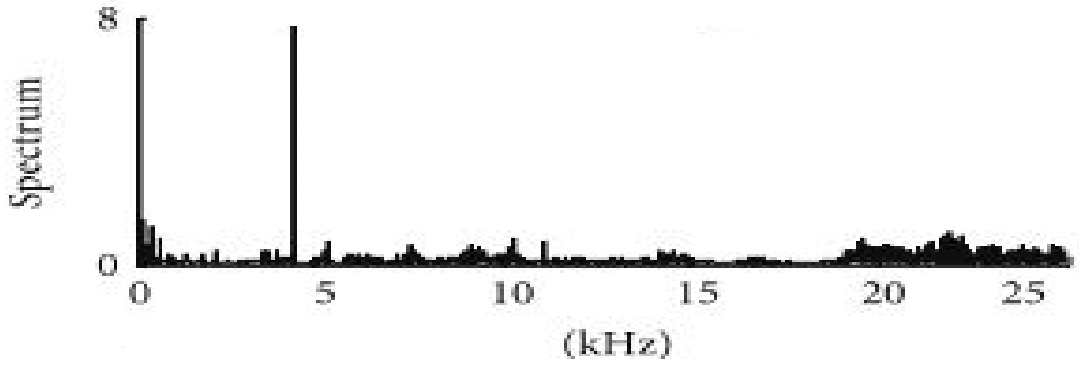

Figure 90. Spectrum of vibration data of misalignment [86]

Figure 91Figure 99 show the spectrum results for the Taguchi experiments. As shown below, as the speed increases, the vibration intensity increases and changes in modes. At 6000 rpm, the spectrum behaves normally as shown in Figure 89. But, at 8000 rpm pump speed, the vibration tends to behave as there is unbalance in the system. At 11,000 rpm, the vibrations take the mode of misalignment. Valve angle and fluid height seem to have negligible effects on the vibration.

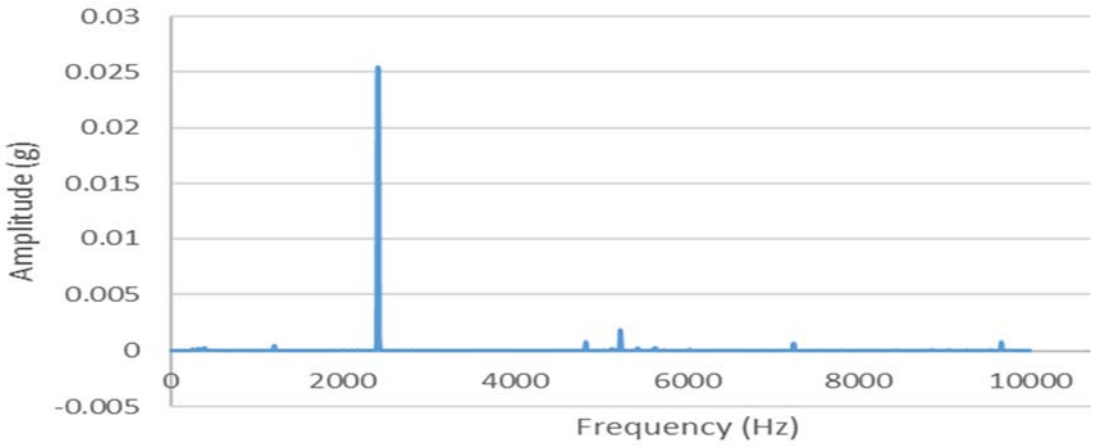

Figure 91. Taguchi experiment 1 spectrum results

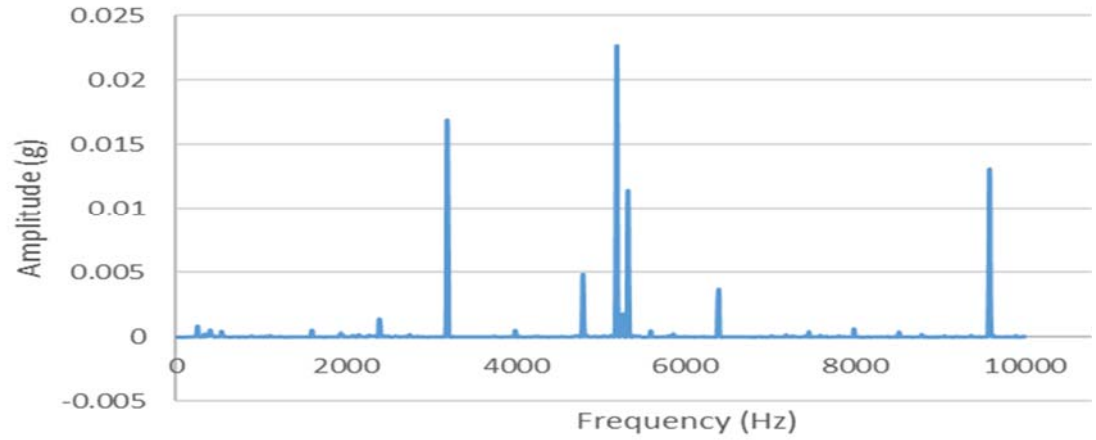

Figure 92. Taguchi experiment 2 spectrum results

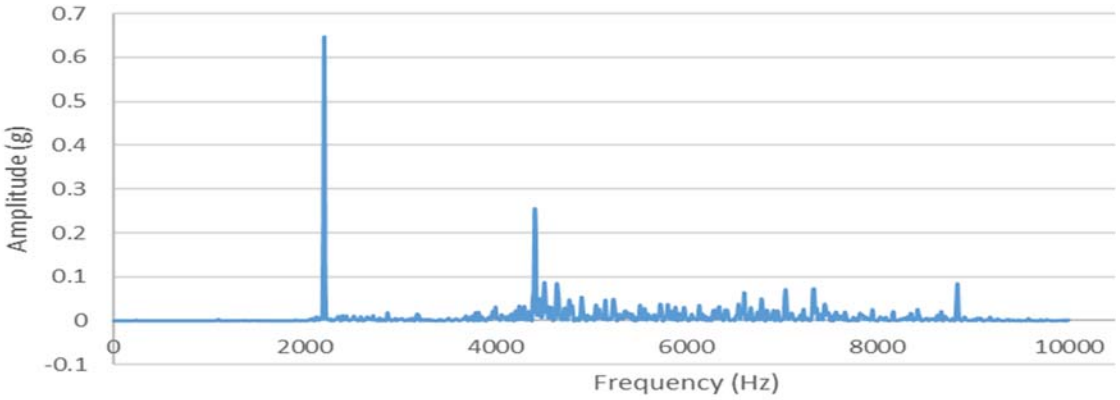

Figure 93. Taguchi experiment 3 spectrum results

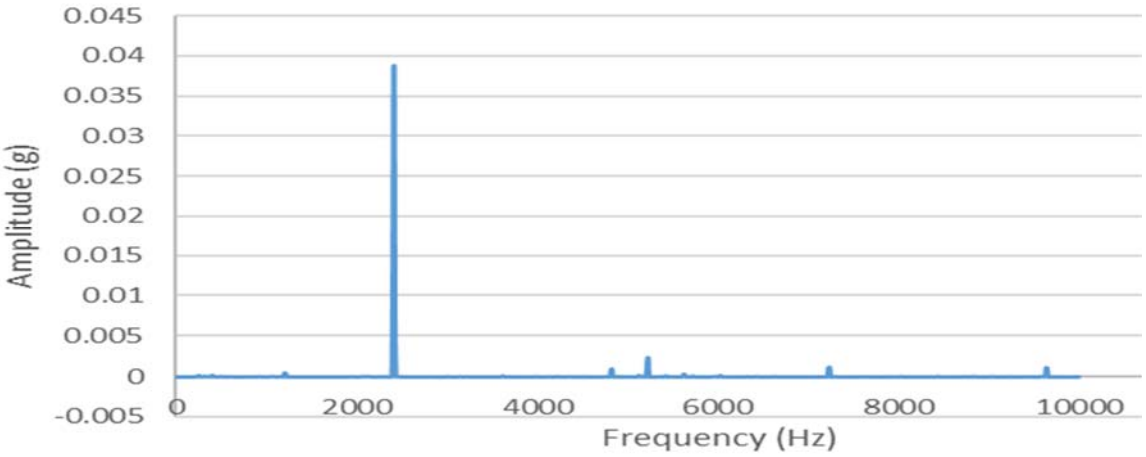

Figure 94. Taguchi experiment 4 spectrum results

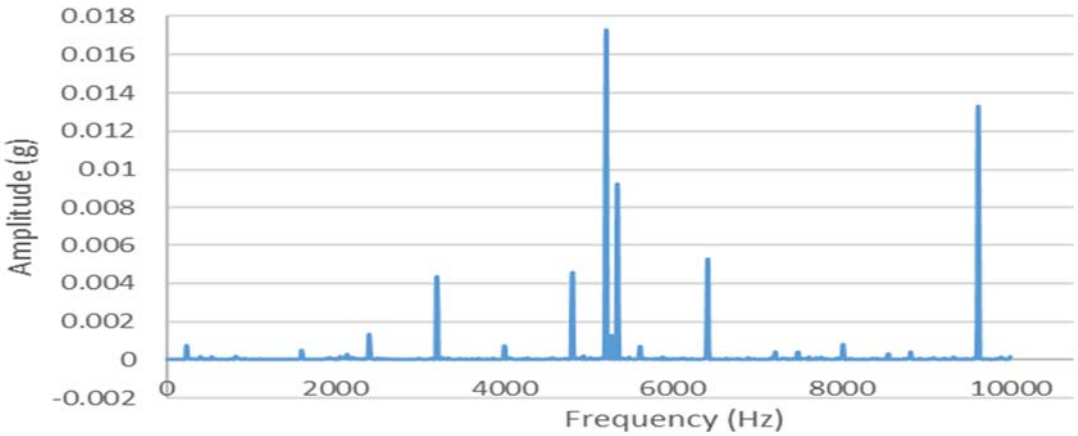

Figure 95. Taguchi experiment 5 spectrum results

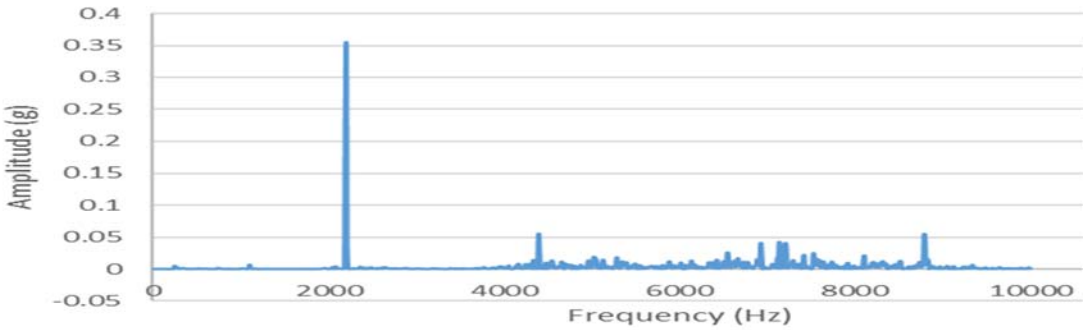

Figure 96. Taguchi experiment 6 spectrum results

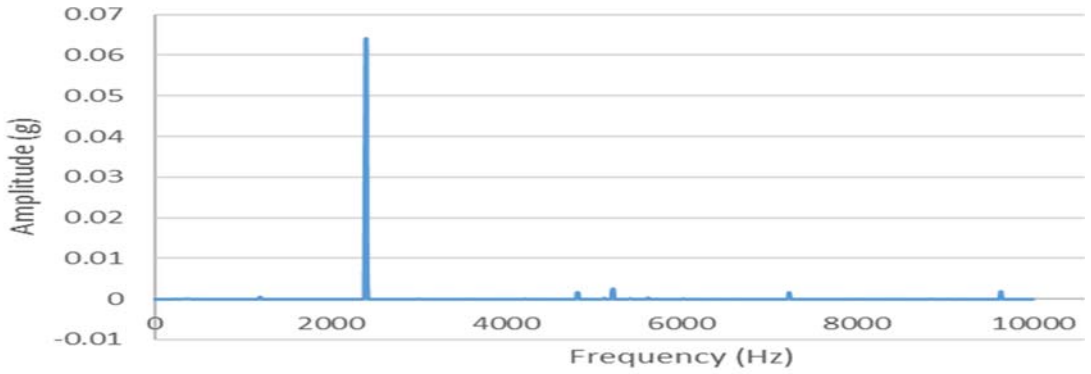

Figure 97. Taguchi experiment 7 spectrum results

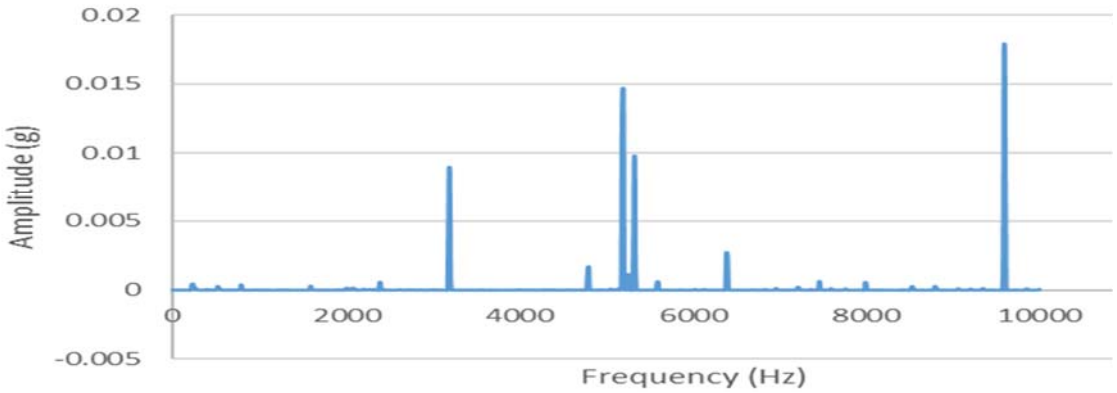

Figure 98. Taguchi experiment 8 spectrum results

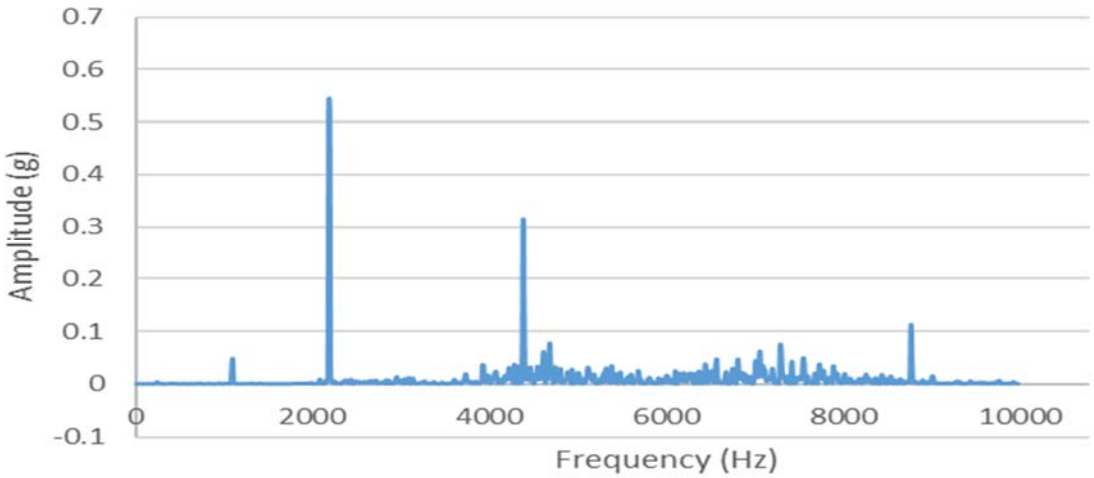

Figure 99. Taguchi experiment 9 spectrum results

The second type of vibration experiments conducted was the failure stage. At this stage, the pump speed, valve angle, and fluid height were exceeding the safety limits. For speed, the pump was running at speeds higher than 11,000 rpm, valve angles values were below 30 degrees, and fluid height was below the NPSHr.

Figure 100 shows vibration spectrum at pump speed of 12000 rpm. This speed is higher than the recommended speed limit of 11000 rpm. The valve was fully open (90 degrees) and the fluid height was 6 inches. The results showed same trend as 11000 rpm; the looseness is occurring and some unbalance is also happening. Also, amplitudes of the vibration doubles.

Figure 101 shows the vibration spectrum at valve angle of 10 degrees. The recommended minimum limit for the valve opening was 30 degrees. Pump speed and fluid height were kept at a safety limit of 6000 rpm and 6 inches respectively. Unbalance in the system starts to occur when the valve angle is that low. Even if the speed and fluid height were safe.

Figure 102 shows the vibration spectrum at low fluid height; when NPSHa<NPSHr. At this stage, air is introduced to the system. Speed is kept at 6000 rpm, and valve angle at 45 degrees. The results showed low amplitude frequencies. The failure more introduced consisted of looseness and misalignment.

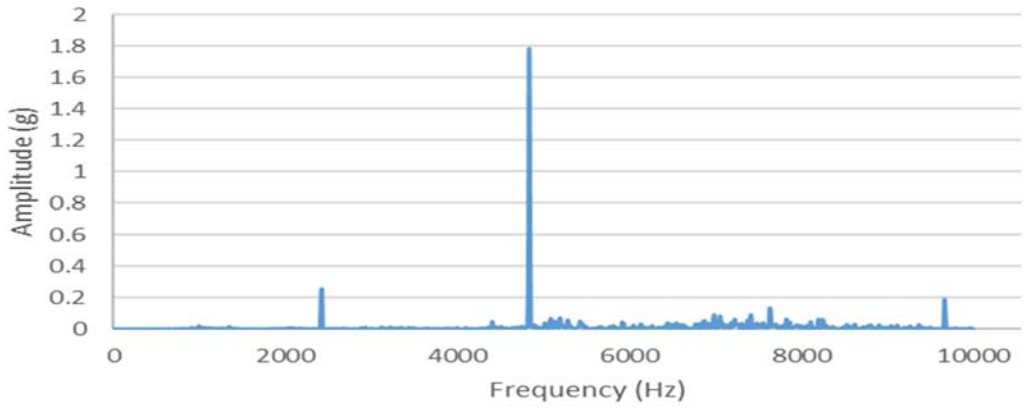

Figure 100. Vibration spectrum at 12000 rpm

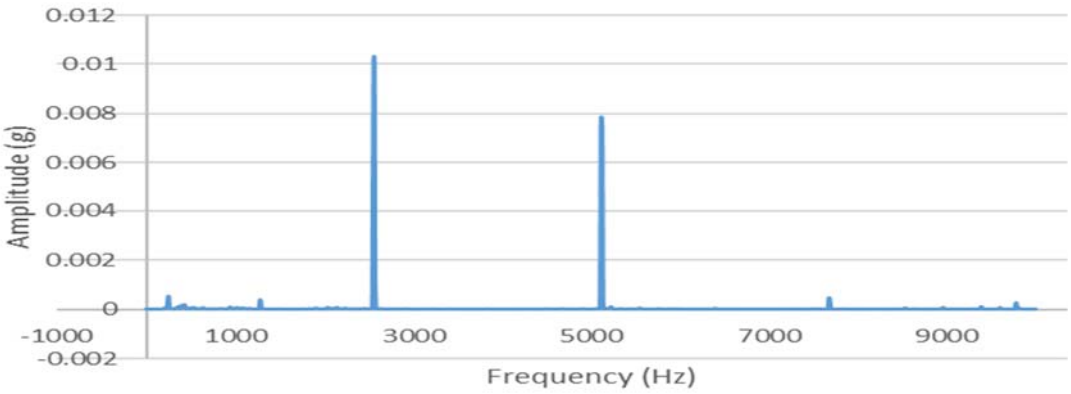

Figure 101. Vibration spectrum at 10 degrees' valve angle

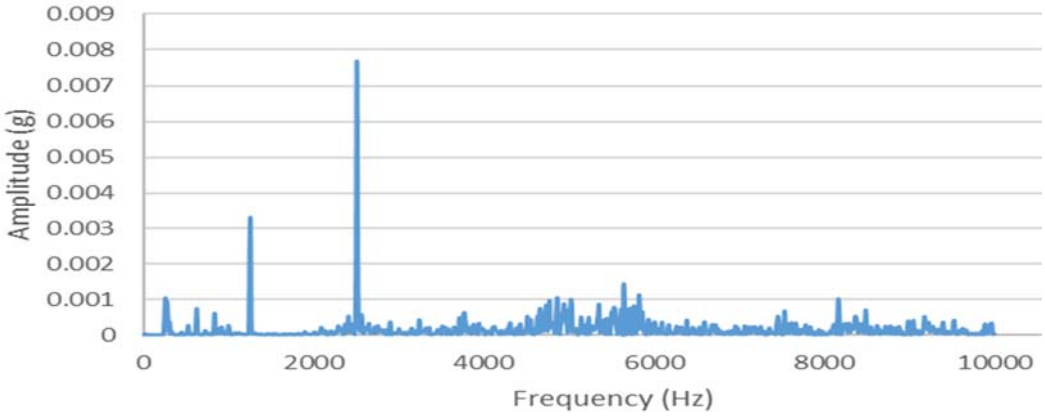

Figure 102. Vibration spectrum when NPSHa<NPSHr

4.3 Control Results

4.3.1 Systems Modeling Results

The results from analyzing the system and understanding the relationship between factors and responses can be used to program the controls. As mentioned earlier, two control systems of a concern in this work, speed and valve angle. Those two controls are affecting the system's responses as shown earlier in the experimental results. The main goal of these controls is to maintain the highest efficiency and lowest risk of the centrifugal pump.

Before the control design step, modeling the systems are needed. Therefore, transient analysis was done using identification MATLAB toolbox to create transfer functions for the two controls. These transfer functions are relating the inputs from speed and valve angle to the output flowrate as discussed in chapter four.

Figure 103 shows the experimental data used in creating the transfer function. Two variables used in training; input (u1) which is the voltage supplied to the motor to create the desired speed, output (y1) which is the output flowrate reading in voltage. 0.1 sample size was used to collect the experimental data. Because of the sampling rate, the transfer function created was discrete and is shown in Eqn. 19. To create a continuous transfer function from the discrete transfer function, Tustin's approximation method is used [87]. Equation 20 shows the continuous transfer function. This transfer function has two poles and one zero.

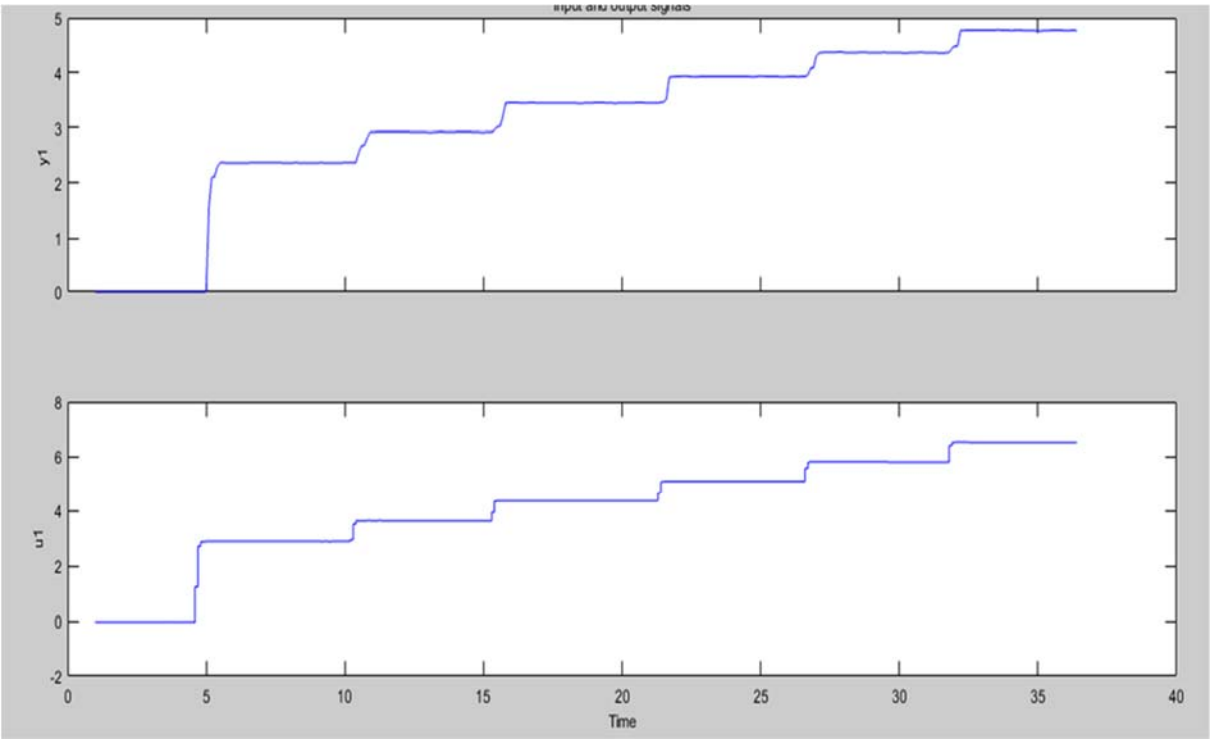

Figure 103. Experimental data for input (u1) speed and output (y1) flowrate

$$G(z) = \frac{0.07186\, z^{-1}}{1 - 1.574\, z^{-1} + 0.6675\, z^{-2}} \qquad \text{Equation 19}$$

$$G(s) = \frac{0.4152\, s + 8.82}{s^2 + 4.042\, s + 11.48} \qquad \text{Equation 20}$$

Figure 104 shows a step response for the speed transfer function. The figure shows that this open loop transfer function has a settling time of 1.7 seconds, rise time of 0.54 seconds, peak time 1.1 seconds, and overshoot of 9.84 %. Light background blue color shows the confident interval for each value.

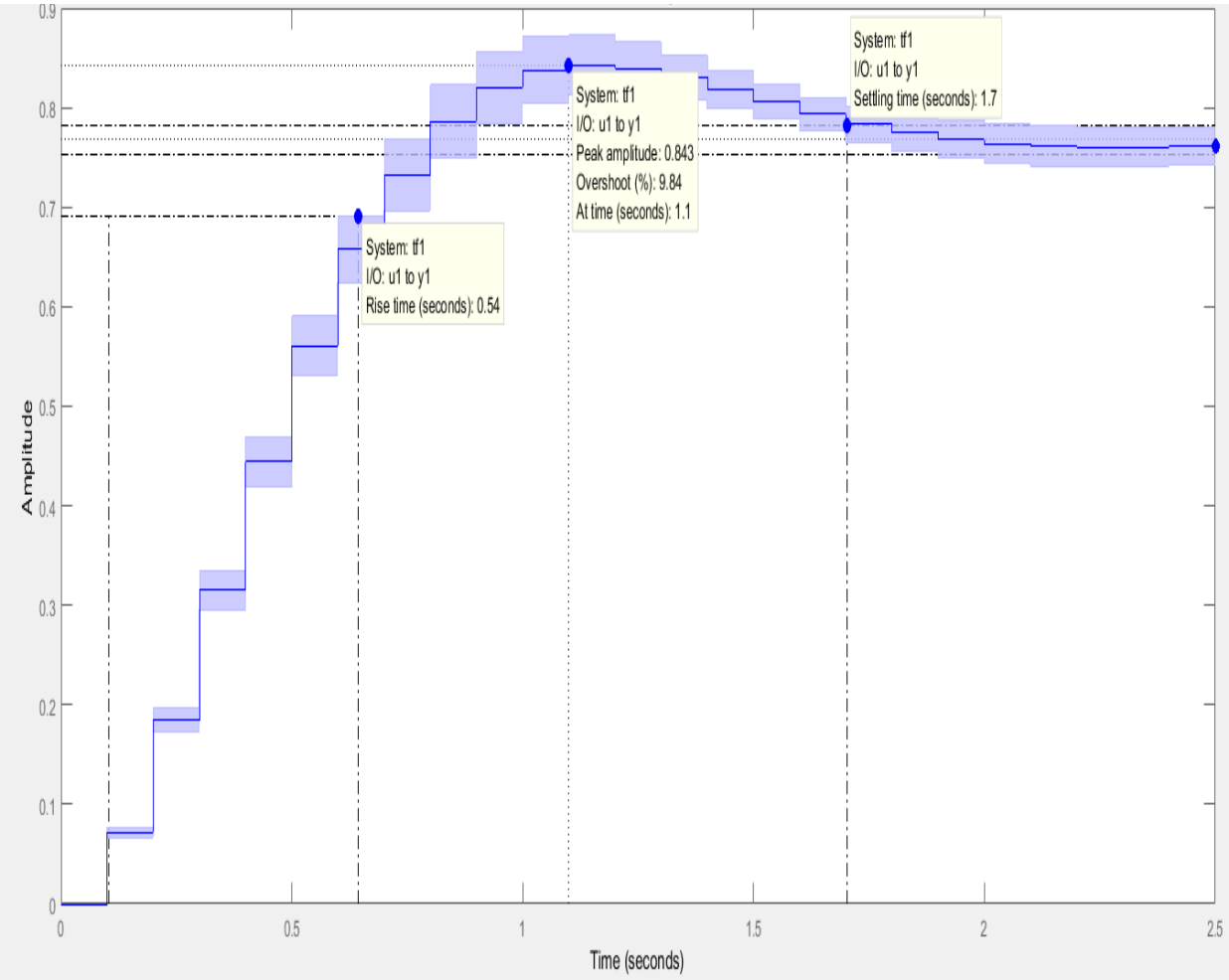

Figure 104. Step response of speed transfer function

Figure 105 shows the bode plot for the speed-flowrate transfer function. It is shown that this transfer function has a gain peak at -1.9 dB at frequency of 1.73 rad/s, gain margin of 33.1 dB at frequency of 31.4 rad/s, and phase change at -45 degrees. Figure 106 shows the modeled versus the experimental data. The dashed lines show a 95% confidence interval, blue solid line shows the model data, and black shows the experimental data. The model is within the confidence interval after the input exceeds 3, which is in the range of this work. The R-squares value is 89.9%, which is acceptable for this work. Therefore, this transfer function is a good approximation for speed-flowrate system.

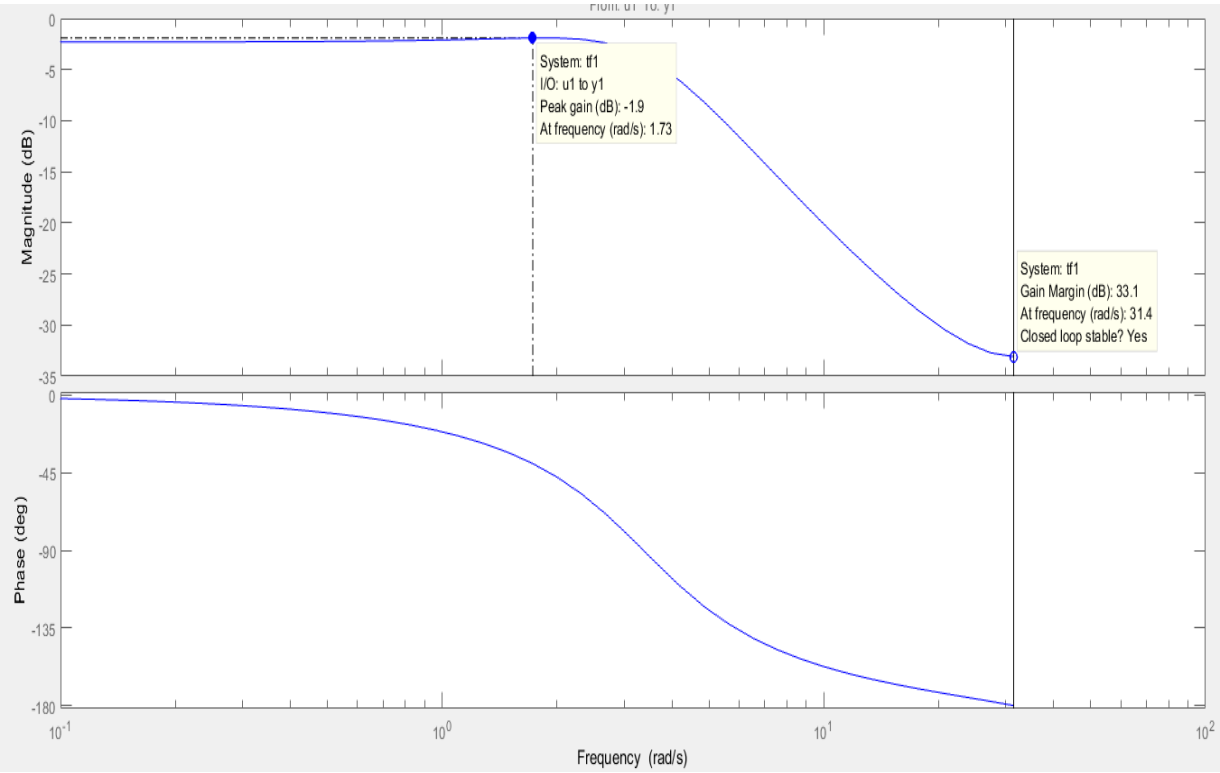

Figure 105. Bode plot for speed transfer function

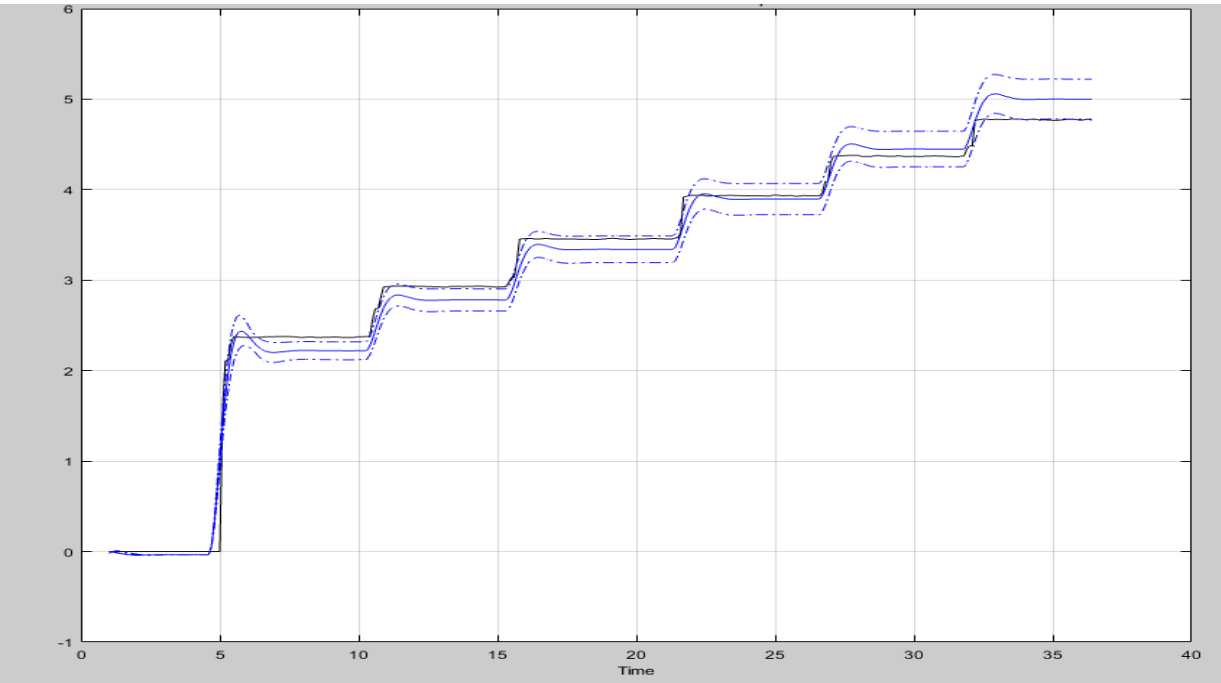

Figure 106. Model versus Experimental data output

4.3.2 Control Methods Results

After obtaining a suitable model for speed and valve angle, it is now feasible to create control systems for both. There are two methods used in creating the controls; single and dual control. Single control focuses on creating a separate controller for speed and valve angle. Dual control means creating a controller that controls both signals in the same time. For single controller, each of the control methods described in chapter four are used.

Figure 107Figure 111 show the training data and validation for Narma-L2 NN. To recall, the NN setup process takes two stages; modeling and control. In the modeling step, the training data is divided into three groups; training, validation, and testing. In the training group, 70% of the data used for training is going to train the network output to match the experimental output. In the validation group, 20% of the incoming data is going to minimizing the fitting process. In the testing group, 10% of the incoming data is going to test the model of the neural network. As shown from the figures, the mean square error is minimized at all the three groups, and the fitting data have R-square value of 1.0 [88].

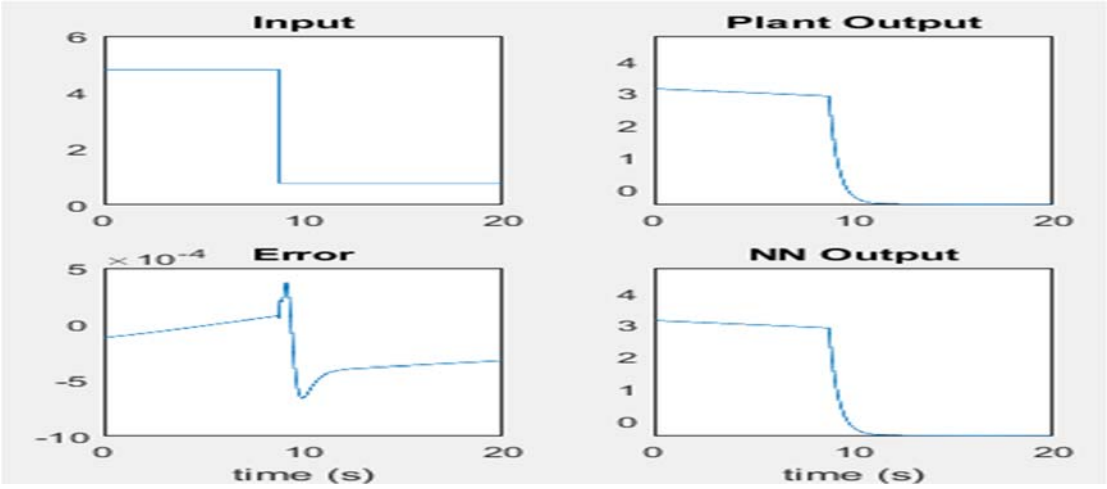

Figure 107. Training data results

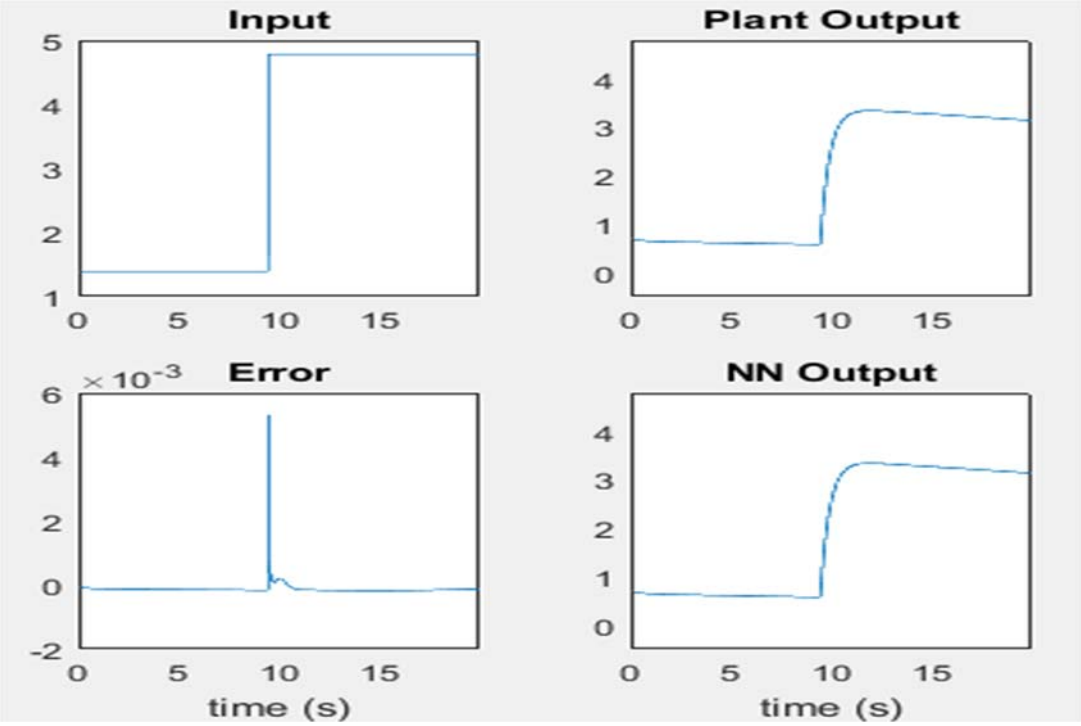

Figure 108. Validation data results

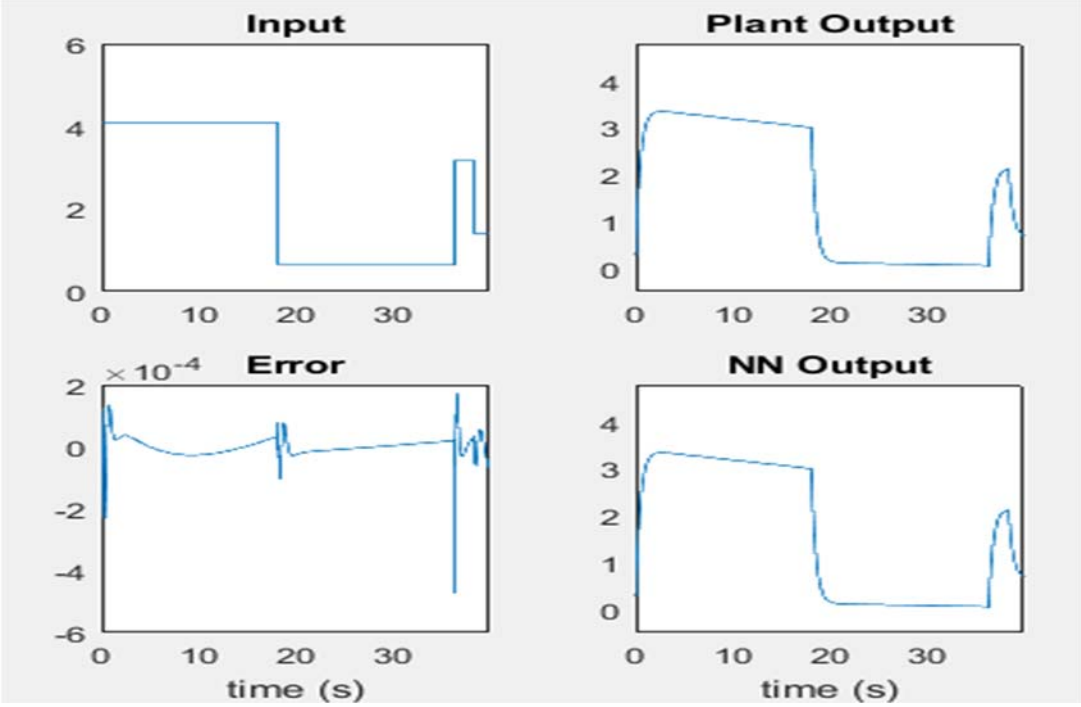

Figure 109. Testing data results

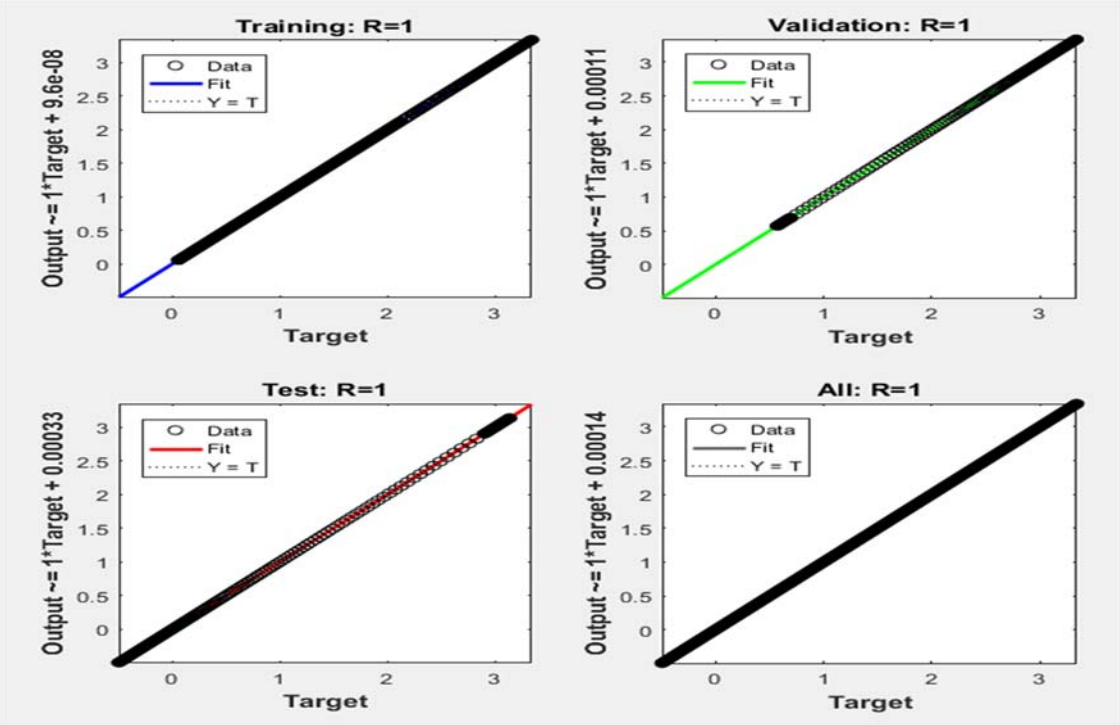

Figure 110. Model fit data for Narma-L2

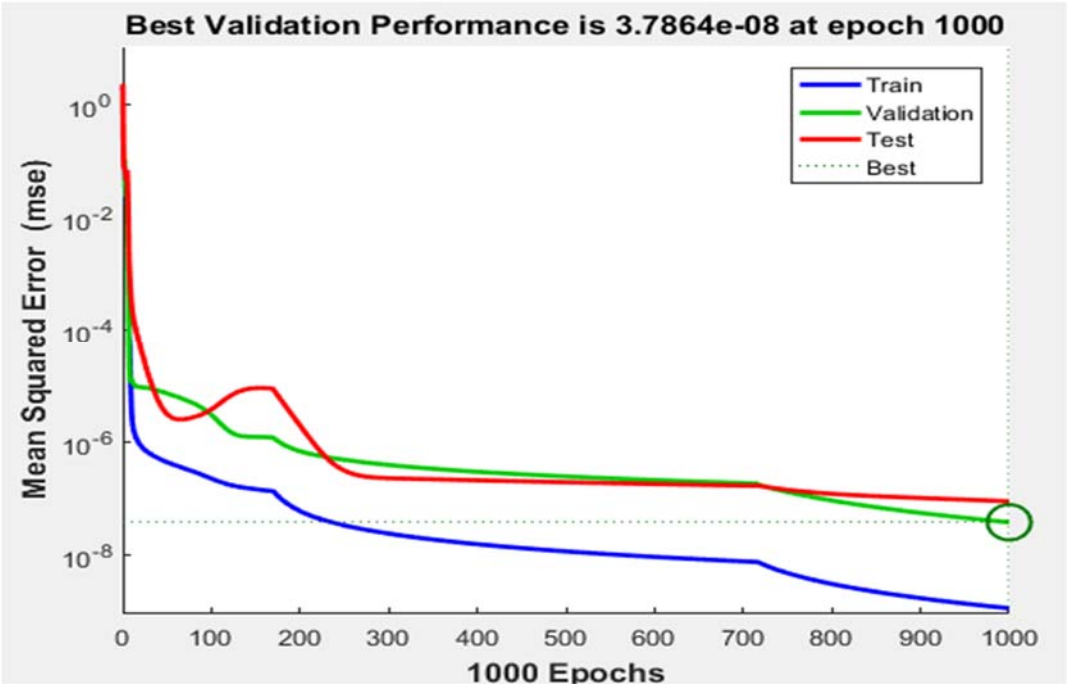

Figure 111. Validation performance curves

Figure 112-Figure 113 show the responses of the speed controller methods used. As shown in the figures, for two step inputs 5 and 10, the PID controller does the best job when the input starts from zero. But, when the second step input is applied, the Narma-L2 does the best. In general, users do not apply the reference input needed when starting the machine. There will be initial input to warmup the machine, then the operation will start. Therefore, for this work, Narma-L2 NN is recommended to use in a single speed controller. Narma-L2 has the fastest peak and settling times with very small overshoot at the second step input. Predictive NN performs the worst with high overshoot values and longest settling time.

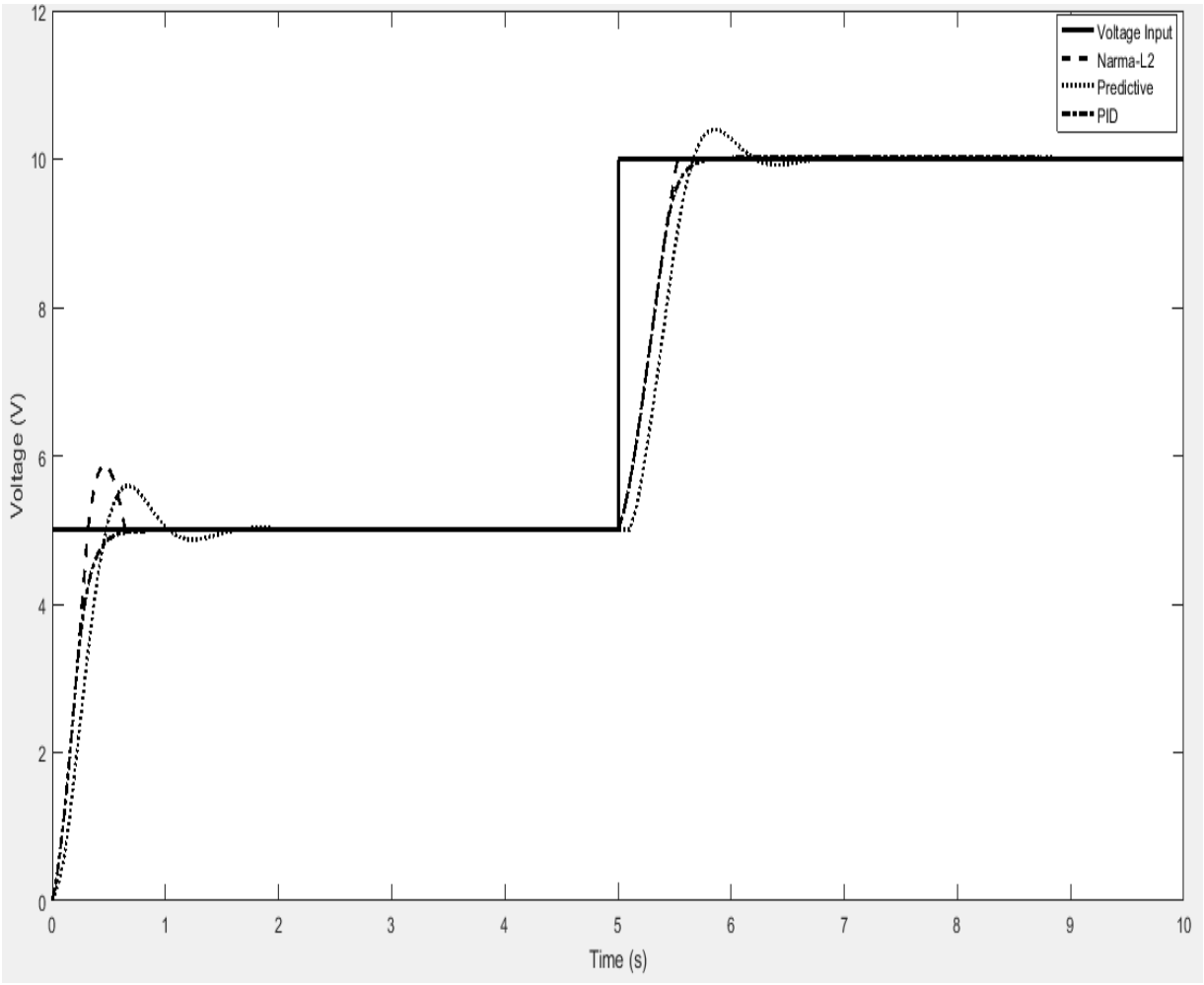

Figure 112. Speed controller results.

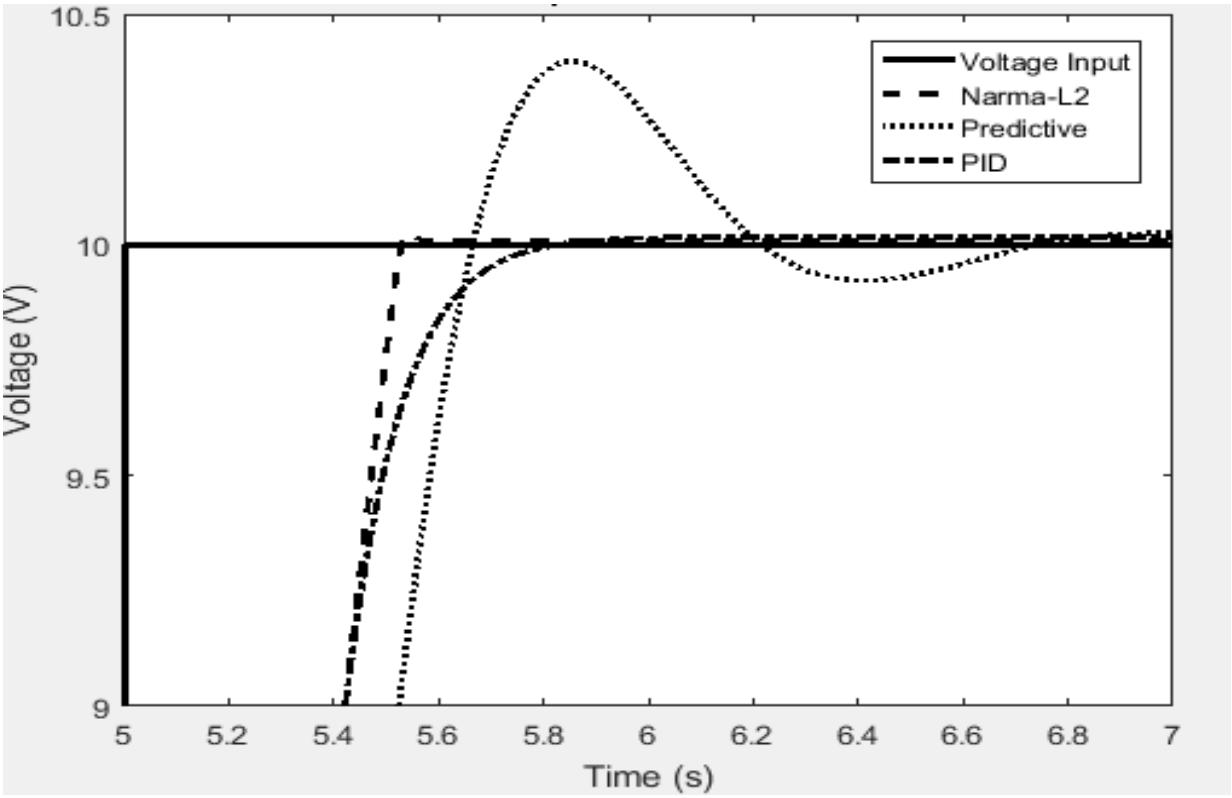

Figure 113. Speed controller results

Figure 114Figure 115 show the responses of the valve angle controller methods used. The figures show that Narma-L2 NN performs the best in both step inputs. Narma-L2 has the fastest peak and settling times and lowest overshoot. Both, PID and Predictive NN have long settling and peak times and high overshoots. Therefore, Narma-L2 will be used as the valve angle controller.

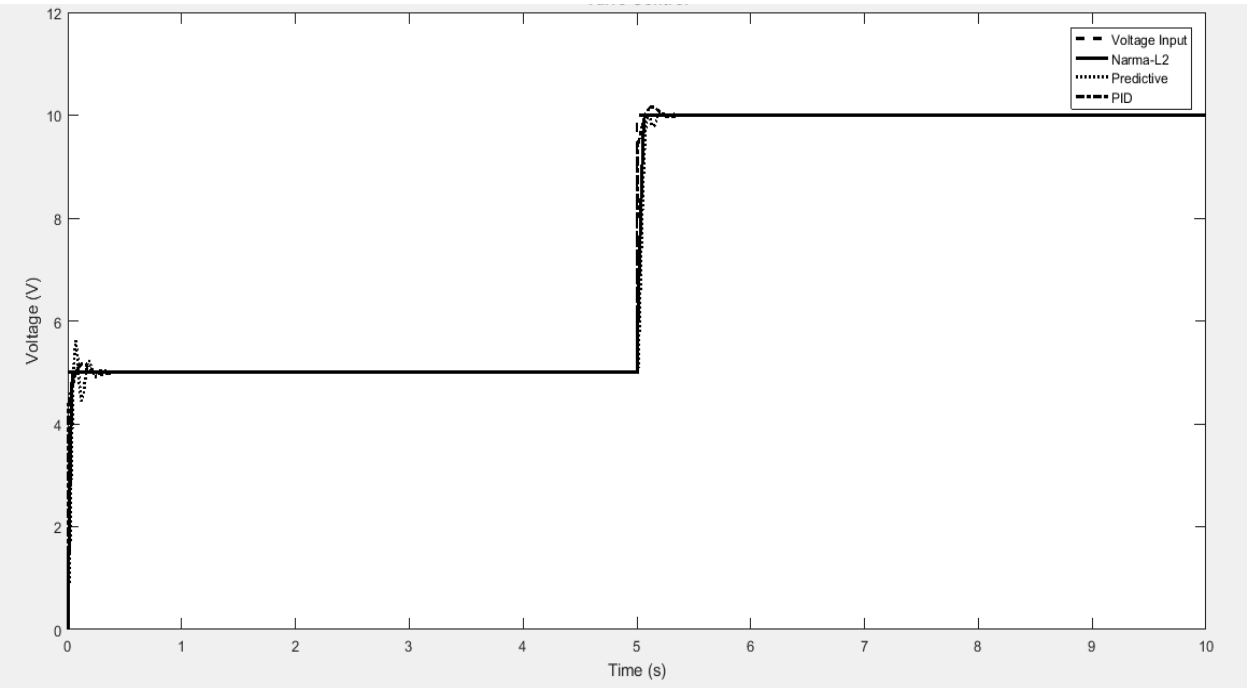

Figure 114. Valve angle controller results

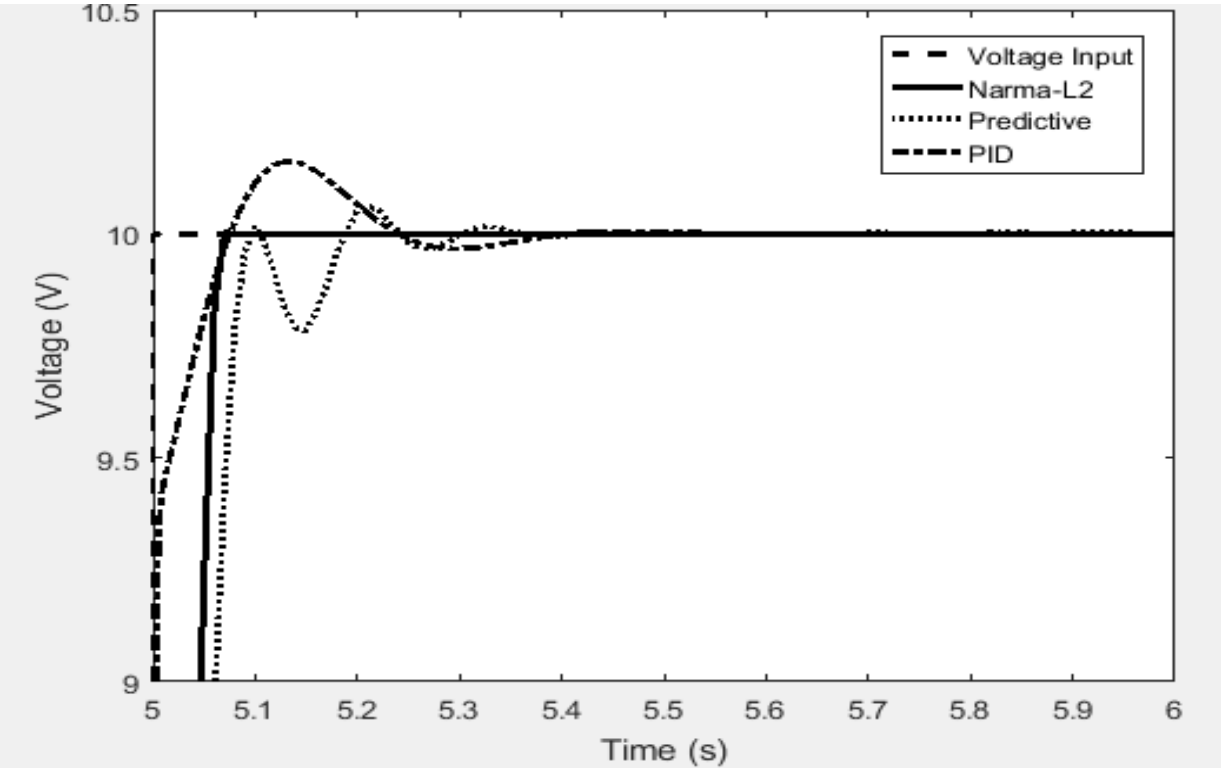

Figure 115. Valve angle controller results

The second type of control method used was dual control. In this controller, speed and valve angle are working together to achieve the reference flowrate. The data used to train this network is the safes, lowest risk data. This data was collected from the safest setting acquired from the design of experiments explained earlier. Low risk means, lower vibration amplitudes and frequencies, less noise, highest efficiency, and lowest temperature rise.

Figure 116 shows the fuzzy-neuro controller response. The input for the controller is created as dynamic input, which means it is changing with time to simulate the different demands of pumping powers. The results are very satisfying; it shows that the controller follows the demand function with a maximum error of 0.25% as shown in Figure 117.

In summary, this work gives the user the ability of choosing which control method works best to keep the system safe. For most of the controllers in the market, single control is used. Therefore, Narma-L2 is recommended. But, for optimal control and variable speeds and valves situations, fuzzy-neuro controller is recommended. Fuzzy-neuro controller does not require any system modeling. This feature allows for wide variety of situations, as most of the centrifugal pump systems are very complicated dynamic systems. Therefore, obtaining a model will be a very difficult job. In fuzzy-neuro method, the only requirements are input and output data.

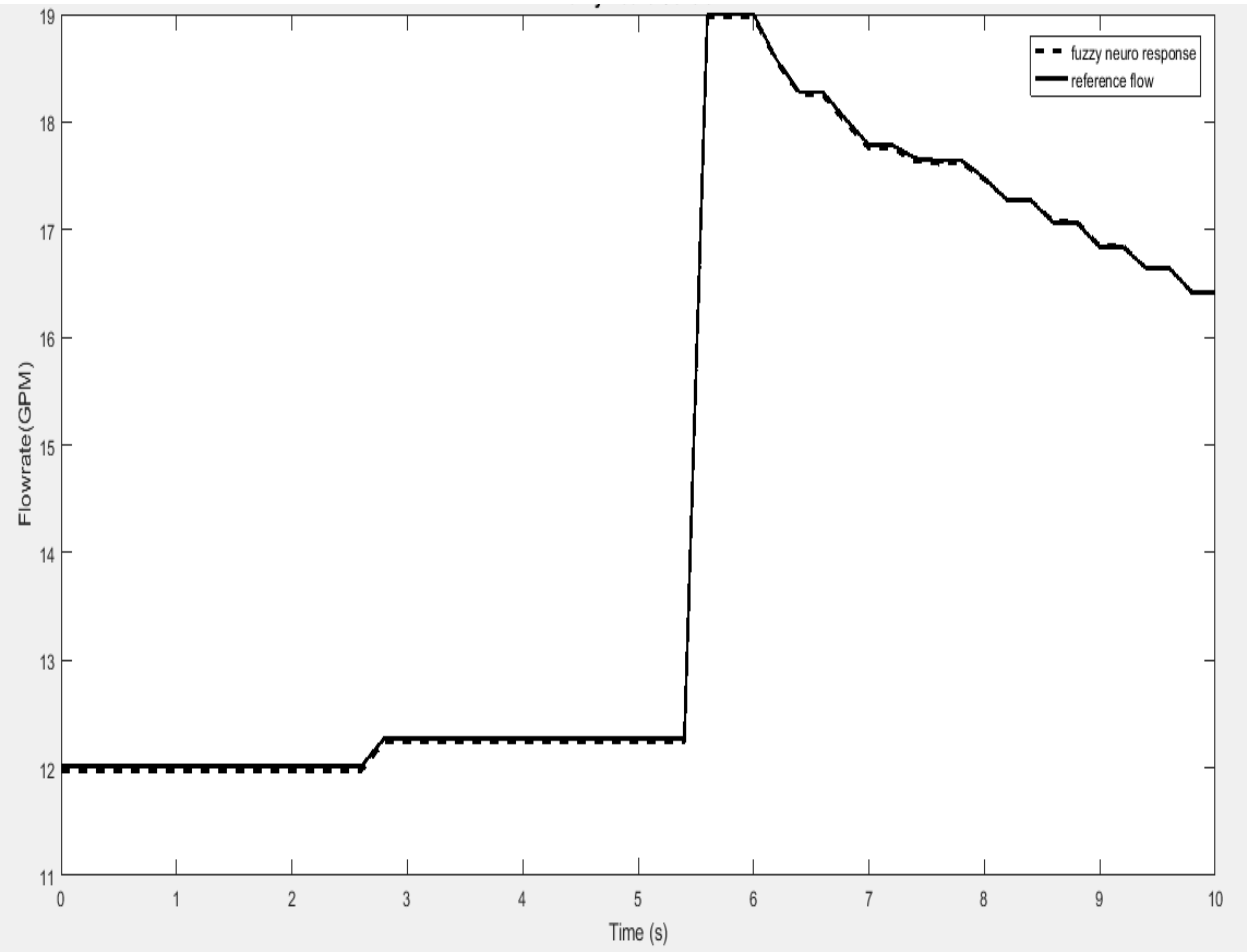

Figure 116. Fuzzy-Neuro controller response

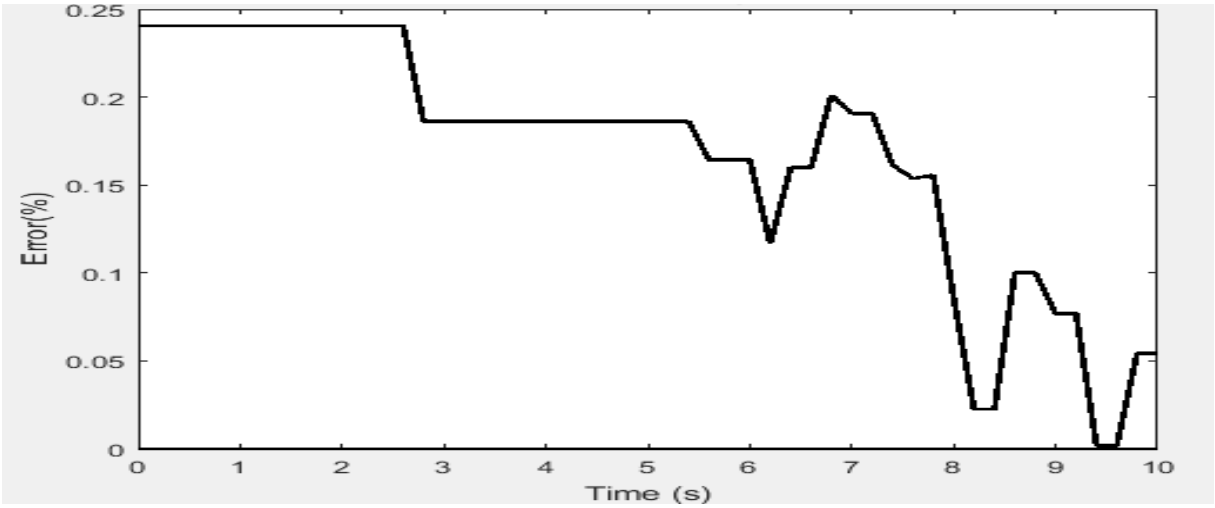

Figure 117. Error in the Fuzzy-Neuro controller

5. Conclusion

To conclude, this work presented a system for health monitoring of rotary pumps in general and especially centrifugal pumps. The system could use intelligent methods such as neural network and fuzzy logic to predict failures before occurring. The setup tools to establish those intelligent systems are commonly used in the literature. MATLAB was used to implement the artificial intelligent methods. This meant, an ease to program and execute of the networks.

The other objective of this work was to provide a systematic method to create a monitoring system. This work presented a step by step procedure to characterize, plan, and control a centrifugal pump's operation. This work allows an engineer to follow this work and implement it in a different setup to achieve the same conclusions.

6. Future Recommendations

This work was mainly done using two neural network techniques. Some suggestions would be to explore more methods and compare the results. Also, extra tuning might result in higher accuracy results. Tuning could be done by increasing the number of training samples, training epochs, and increasing the number of layers used.

The modeling and testing of this work was done using Simulink in MATLAB's environment. So, the next step could be done by installing this network on a neural network chip and implementing it in the physical system. Then, a comparison between the analytical and experimental results could be achieved.

References

1. 2016, U.S.E.I.A.I.e.o., *World energy demand and economic outlook.* International energy outlook 2016, 2016.
2. WaIde, P. and C.U. Brunner, *Energy-efficiency policy opportunities for electric motor-driven systems.* 2011.
3. ETSU, A.P., (United Kingdom), *STUDY ON IMPROVING THE ENERGY EFFICIENCY OF PUMPS.* European Commission, 2001.
4. Pearson, C., *Centrifugal pumps.* Construction | Mechanical Engineering | Automotive News Tips, 2010.
5. Ogochukwu, O.C., *Basic Concepts of Operation, Maintenance, and Troubleshooting of Centrifugal Pumps.* static & Rotating Equipment: Compressors, Centrifugal Pumps and GRE/GRP/FRP Piping, 2015.
6. Girdhar, P. and O. Moniz, *Practical centrifugal pumps*. 2011: Elsevier.
7. Shankar, V.K.A., et al., *A comprehensive review on energy efficiency enhancement initiatives in centrifugal pumping system.* Applied Energy, 2016. **181**: p. 495-513.
8. Viholainen, J., *Energy-efficient control strategies for variable speed driven parallel pumping systems based on pump operation point monitoring with frequency converters.* Acta Universitatis Lappeenrantaensis, 2014.
9. Sahoo, T. and A. Guharoy, *Energy cost savings with centrifugal pumps.* World Pumps, 2009. **2009**(510): p. 35-37.
10. Energy, U.S.D.o., *Improving Motor and Drive System Performance.* Advanced Manufacturing Office, 2014.
11. Inc., V.P., *Efficiency and Life-Cycle-Cost Calculation.* 2007.
12. McKee, K.K., et al. *A review of major centrifugal pump failure modes with application to the water supply and sewerage industries*. in *ICOMS asset management conference*. 2011.
13. Shiels, S., *How centrifugal pump hydraulics affect rolling element bearing life.* World pumps, 1998. **1998**(387): p. 32-35.
14. Shiels, S., *Optimizing centrifugal pump operation.* World Pumps, 2001. **2001**(412): p. 35-39.
15. Shiels, S., *Centrifugal Pump Academy: Causes of intermittent and chronic cavitation.* World pumps, 1998. **1998**(380): p. 57-60.
16. Turton, R.K. and R. Baker, *An introductory guide to pumps and pumping systems*. 1993: Mechanical Engineering Publications.
17. Rayner, R., *Pump users handbook*. 1995: Elsevier.
18. Karassik, I.J., et al., *Pump handbook*. Vol. 3. 1976: McGraw-Hill.
19. Palgrave, R., *Diagnosing pump problems from their noise emissions signature*, in *Pump Technology*. 1989, Springer. p. 9-28.
20. Hicks, T.G. and T.W. Edwards, *Pump Application Engineering*. 1971: McGraw-Hill Companies.
21. Stepanoff, A., *Centrifugal and Axial Flow Pumps. Theory, Design, and Application, 1957*. John Wiley, New York.
22. Sahoo, T., *Making centrifugal pumps more reliable.* World pumps, 2009. **2009**(513): p. 32-36.
23. Karassik, I. and J.T. McGuire, *Centrifugal pumps*. 2012: Springer Science & Business Media.
24. Shiels, S., *Successful centrifugal pump commissioning and start-up.* World pumps, 2000. **2000**(411): p. 24-26.
25. Mc Nally, W., *Troubleshooting the ball bearings in a centrifugal pump.* World pumps, 2004. **2004**(454): p. 28-29.

26. Pace, S.E., S. Florjancic, and U. Bolleter. *Rotordynamic developments for high speed multistage pumps*. in *Proceedings of the Third International Pump Symposium, Turbomachinery Laboratory, Texas A&M University, College Station, Texas*. 1986.
27. Beebe, R.S., *Predictive maintenance of pumps using condition monitoring*. 2004: Elsevier.
28. Shiels, S., *Centrifugal pump academy: Motor trip! Predicting the unforeseen disaster.* World Pumps, 1999. **1999**(394): p. 29-31.
29. Holland, F.A. and F. Chapman, *Pumping of liquids*. 1966: Reinhold Pub. Corp.
30. Heng, A., et al., *Rotating machinery prognostics: State of the art, challenges and opportunities.* Mechanical systems and signal processing, 2009. **23**(3): p. 724-739.
31. Bazovsky, I., *Reliability theory and practice*. 2004: Courier Corporation.
32. Jardine, A.K. and A.H. Tsang, *Maintenance, replacement, and reliability: theory and applications*. 2013: CRC press.
33. Vachtsevanos, G., et al., *Intelligent fault diagnosis and prognosis for engineering systems. 2006, Hoboken*. New Jersey, USA: John Wiley & Sons, Inc.
34. Pusey, H.C. *An assessment of turbomachinery condition monitoring and failure prognosis technology*. in *SPIE proceedings series*. 1999. Society of Photo-Optical Instrumentation Engineers.
35. Jardine, A.K., D. Lin, and D. Banjevic, *A review on machinery diagnostics and prognostics implementing condition-based maintenance.* Mechanical systems and signal processing, 2006. **20**(7): p. 1483-1510.
36. Li, C.J. and H. Lee, *Gear fatigue crack prognosis using embedded model, gear dynamic model and fracture mechanics.* Mechanical systems and signal processing, 2005. **19**(4): p. 836-846.
37. Oppenheimer, C.H. and K.A. Loparo. *Physically based diagnosis and prognosis of cracked rotor shafts*. in *AeroSense 2002*. 2002. International Society for Optics and Photonics.
38. Marble, S. and B.P. Morton. *Predicting the remaining life of propulsion system bearings*. in *2006 IEEE Aerospace Conference*. 2006. IEEE.
39. Qiu, J., et al., *Damage mechanics approach for bearing lifetime prognostics.* Mechanical systems and signal processing, 2002. **16**(5): p. 817-829.
40. Kazmierczak, K. *Application of autoregressive prognostic techniques in diagnostics*. in *Proceedings of the Vehicle Diagnostics Conference, Tuczno, Poland*. 1983.
41. Cempel, C., *Simple condition forecasting techniques in vibroacoustical diagnostics.* Mechanical Systems and Signal Processing, 1987. **1**(1): p. 75-82.
42. Lee, J. *A systematic approach for developing and deploying advanced prognostics technologies and tools: methodology and applications*. in *Proceedings of the Second World Congress on Engineering Asset Management, Harrogate, UK*. 2007.
43. Tse, P. and D. Atherton, *Prediction of machine deterioration using vibration based fault trends and recurrent neural networks.* Journal of vibration and acoustics, 1999. **121**(3): p. 355-362.
44. Joshi, R. and C. Reeves. *Beyond the Cox model: artificial neural networks for survival analysis part II*. in *Proceedings of the eighteenth international conference on systems engineering*. 2006.
45. Negnevitsky, M., *Artificial intelligence: a guide to intelligent systems*. 2005: Pearson Education.
46. Yam, R., et al., *Intelligent predictive decision support system for condition-based maintenance.* The International Journal of Advanced Manufacturing Technology, 2001. **17**(5): p. 383-391.
47. Wang, P. and G. Vachtsevanos, *Fault prognostics using dynamic wavelet neural networks.* AI EDAM, 2001. **15**(04): p. 349-365.
48. Shao, Y. and K. Nezu, *Prognosis of remaining bearing life using neural networks.* Proceedings of the Institution of Mechanical Engineers, Part I: Journal of Systems and Control Engineering, 2000. **214**(3): p. 217-230.
49. Gebraeel, N., et al., *Residual life predictions from vibration-based degradation signals: a neural network approach.* IEEE Transactions on industrial electronics, 2004. **51**(3): p. 694-700.

50. Goode, K., J. Moore, and B. Roylance, *Plant machinery working life prediction method utilizing reliability and condition-monitoring data.* Proceedings of the Institution of Mechanical Engineers, Part E: Journal of Process Mechanical Engineering, 2000. **214**(2): p. 109-122.
51. Jardine, A., P. Anderson, and D. Mann, *Application of the Weibull proportional hazards model to aircraft and marine engine failure data.* Quality and reliability engineering international, 1987. **3**(2): p. 77-82.
52. Sun, Y., et al., *Mechanical systems hazard estimation using condition monitoring.* Mechanical systems and signal processing, 2006. **20**(5): p. 1189-1201.
53. Wang, W., *A model to predict the residual life of rolling element bearings given monitored condition information to date.* IMA Journal of Management Mathematics, 2002. **13**(1): p. 3-16.
54. Cempel, C., H. Natke, and J. Yao, *Symptom reliability and hazard for systems condition monitoring.* Mechanical Systems and Signal Processing, 2000. **14**(3): p. 495-505.
55. Gowid, S., R. Dixon, and S. Ghani, *A novel robust automated FFT-based segmentation and features selection algorithm for acoustic emission condition based monitoring systems.* Applied Acoustics, 2015. **88**: p. 66-74.
56. Dalvand, F., A. Kalantar, and M.S. Safizadeh, *A Novel Bearing Condition Monitoring Method in Induction Motors Based on Instantaneous Frequency of Motor Voltage.* IEEE Transactions on Industrial Electronics, 2016. **63**(1): p. 364-376.
57. Nourmohammadzadeh, A. and S. Hartmann. *Fault Classification of a Centrifugal Pump in Normal and Noisy Environment with Artificial Neural Network and Support Vector Machine Enhanced by a Genetic Algorithm*. in *International Conference on Theory and Practice of Natural Computing*. 2015. Springer.
58. McKee, K.K., et al., *A vibration cavitation sensitivity parameter based on spectral and statistical methods.* Expert Systems with Applications, 2015. **42**(1): p. 67-78.
59. Senthilkumar, M., M. Yuvaraja, and M. Kok. *Fault Diagnosis of Centrifugal Pump and Vibration Control Using Shape Memory Alloy Based ATDVA*. in *Applied Mechanics and Materials*. 2015. Trans Tech Publ.
60. Kostyukov, V., A. Kostyukov, and C. Boychenko, *Intelligent Machinery Condition Monitoring based on Adaptive Measurements.* Procedia Engineering, 2016. **152**: p. 527-530.
61. Luo, Y., et al., *Research on the induction motor current signature for centrifugal pump at cavitation condition.* Advances in Mechanical Engineering, 2015. **7**(11): p. 1687814015617134.
62. Shane Corlman, S.E.-G., *REDUCING ENERGY WASTE IN CENTRIFUGAL PUMP SYSTEMS THROUGH THE IMPLEMENTATION OF BEP OPTIMIZED PRESSURE AND FLOW CONTROL.* 2015.
63. Manual, L.U., *National Instruments.* Austin, TX, 1998.
64. Brigham, E.O. and E.O. Brigham, *The fast Fourier transform*. Vol. 7. 1974: Prentice-Hall Englewood Cliffs, NJ.
65. Anderson, M.J. and P.J. Whitcomb, *Design of experiments*. 2000: Wiley Online Library.
66. Wu, Y. and A. Wu, *Taguchi methods for robust design*. 2000: American Society of Mechanical Engineers.
67. Myers, R.H., D.C. Montgomery, and C.M. Anderson-Cook, *Response surface methodology: process and product optimization using designed experiments*. 2016: John Wiley & Sons.
68. Taguchi, G. and S. Konishi, *Taguchi Methods: Orthogonal Arrays and Linear Graphs-Tools for Quality Engineering*. 1987: American Supplier Institute, Center for Taguchi Methods.
69. Taguchi, G. and V. Cariapa, *Taguchi on robust technology development*. 1993, American Society of Mechanical Engineers.
70. Ryan, T.P. and J. Morgan, *Modern experimental design.* Journal of Statistical Theory and Practice, 2007. **1**(3-4): p. 501-506.

71. Khuri, A.I. and S. Mukhopadhyay, *Response surface methodology.* Wiley Interdisciplinary Reviews: Computational Statistics, 2010. **2**(2): p. 128-149.
72. Stamatis, D.H., *Failure mode and effect analysis: FMEA from theory to execution*. 2003: ASQ Quality Press.
73. Huang, G.Q. and K. Mak, *Failure mode and effect analysis (FMEA) over the WWW*, in *Internet Applications in Product Design and Manufacturing*. 2003, Springer. p. 135-146.
74. Den Hartog, J.P., *Mechanical vibrations*. 1985: Courier Corporation.
75. Bracewell, R., *The fourier transform and iis applications.* New York, 1965. **5**.
76. Ljung, L. and T. Glad, *Modeling of dynamic systems Prentice Hall.* Englewood Cliffs, New Jersey, USA, 1994.
77. Ljung, L., *System Identification: Theory for the User, PTR Prentice Hall Information and System Sciences Series*. 1999, Prentice Hall, New Jersey.
78. Demuth, H. and M. Beale, *Neural Networks Toolbox for Use with MATLAB: User's Guide*. 1992: Math Works.
79. Demuth, H. and M. Beale, *Neural network toolbox for use with MATLAB.* 1993.
80. Documentation, M., *The MathWorks Inc*. 2005.
81. Sivanandam, S., S. Sumathi, and S. Deepa, *Introduction to fuzzy logic using MATLAB*. Vol. 1. 2007: Springer.
82. Turban, E. and L.E. Frenzel, *Expert systems and applied artificial intelligence*. 1992: Prentice Hall Professional Technical Reference.
83. Michael Scheller, S.E.-G., *Characterization and Nondimensional Analysis of a Variable Speed Centrifugal Pump.* 2014.
84. Azadeh, A., V. Ebrahimipour, and P. Bavar, *A fuzzy inference system for pump failure diagnosis to improve maintenance process: The case of a petrochemical industry.* Expert Systems with Applications, 2010. **37**(1): p. 627-639.
85. Yunlong, Z. and Z. Peng, *Vibration fault diagnosis method of centrifugal pump based on emd complexity feature and least square support vector machine.* Energy Procedia, 2012. **17**: p. 939-945.
86. Xue, H., et al., *Intelligent diagnosis method for centrifugal pump system using vibration signal and support vector machine.* Shock and Vibration, 2014. **2014**.
87. Franklin, G.F., et al., *Feedback control of dynamic systems*. Vol. 2. 1994: Addison-Wesley Reading.
88. Hagan, M.T., et al., *Neural network design*. Vol. 20. 1996: PWS publishing company Boston.

Appendix

1- Pressure Sensors (PX309):

- Excitation: 9 to 30 Vdc (<10mA)
- Output: 0 to 5 Vdc
- Accuracy: ±0.25% FS BSL at 25ºC; includes linearity, hysteresis and repeatability
- Zero Offset: ±2% FSO; ±4% for 1 and 2 psi ranges
- Total Error Band: ±2% FSO, includes linearity, hysteresis, repeatability, thermal hysteresis and thermal errors (except 1 psi = ±4.5% and 2 psi = ±3%)
- Operating Temperature: -40 to 85°C (-40 to 185°F). [7]

2- Vibration Sensor - Model 8042-01 Accelerometer

- Submersible IEPE Accelerometer
- 16kHz Bandwidth
- ±10g, ±80g & ±500g Dynamic Ranges
- IP68 Protection, >100 meters
- Welded Titanium Housing
- Case Isolated, Internally Shielded
- -20° to +80°C Operating Range
- Annular Shear Mode Crystal

3- Temperature Sensor (5B34):

- Output Range (RL > 50 kΩ): 0 V to +5 V
- Input Offset vs. Temperature: ±0.02°C/°C
- Output Offset vs. Temperature: ±20 µV/°C
- Accuracy: ±0.05% Span
- Conformity Error: ±0.05% Span. [8]

4- Flow Meters Sensor (FTB-1425):

- Accuracy: ±1% of reading for 1" and larger, ±1% of reading over the upper 70% of the measuring range for 1⁄2" meters
- Calibration: Water (NIST traceable calibration)
- Pressure Rating: 5000 psi (maximum)
- Turbine Temperature: -101 to 177°C (-150 to 350°F); -101 to 232°C (-150 to 450°F) (with "-HT" option).[9]

5- Electric Actuator Valve:

- Max working pressure: 1.0MPa
- Rated voltage: DC5V, DC12V, DC24V, AC/DC9-35V (Optional)
- Working current: ≤500MA
- Actuator rotation: 90°
- Max. torque force: 2 N.M
- Environment temperature: -15℃～50℃

Matlab Codes used:

```
function [eta temprise]=make_plots1


cal_d_p_m = 5.9994;
cal_d_p_a = -0.0385;
cal_m_p_m = 6.0018;
cal_m_p_a = -0.0425;
cal_p_p_m = 9.987;
cal_p_p_a = -0.089;
cal_a_p_m = 6.0072;
cal_a_p_a = -0.024;
cal_f_m = 6.4076;
cal_f_a = -1.2904;
cal_v_m = 4.981469;
cal_v_a = 0;
cal_c_m = 5.9427;
cal_c_a = 0.0432;
cal_i_t_m = 20.35;
cal_i_t_a = -1.249;
```

```
cal_o_t_m = 20.401;
cal_o_t_a = -1.347;

rpm = [1,2,3,4,5,6,7,8,9];
for ii = 1:9
    skipcount = 0;
    for jj = 1:9

        filename = ['trial',num2str(rpm(ii))];
        filename2 = ['vibration',num2str(rpm(ii)),'.xlsx'];
        if exist(filename,'file')==0
            skipcount = skipcount + 1;
            continue
        end
        ic = jj-skipcount;
        output = tdfread(filename);
        mtp(ii) = mean(output.Inlet_Pressure)*cal_m_p_m+cal_m_p_a;
        pp(ii) = mean(output.Discharge_Pressure)*cal_p_p_m+cal_p_p_a;
        fr(ii) = mean(output.Flowrate)*cal_f_m+cal_f_a;
        v(ii) = mean(output.Voltage)*cal_v_m+cal_v_a;
        c(ii) = mean(output.Current)*cal_c_m+cal_c_a;
        eta(ii) = fr(ii)*(pp(ii)-mtp(ii))/v(ii)/c(ii)*0.435;
        to(ii) = mean(output.Temp_Out)*cal_o_t_m+cal_o_t_a;
        ti(ii) = mean(output.Temp_In)*cal_i_t_m+cal_i_t_a;
        trise(ii) = to(ii)-ti(ii);
        temprise(ii)=abs(max((output.Temp_Out)*cal_o_t_m+cal_o_t_a)-
min((output.Temp_In)*cal_i_t_m+cal_i_t_a));

      %%
         if exist(filename2,'file')==0
            skipcount = skipcount + 1;
            continue
        end


    end
end

function [amplmax freqmax]=makevibration


rpm = [1,2,3,4,5,6,7,8,9];

for ii = 1:length(rpm);
    skipcount = 0;

     filename2 = ['vibration',num2str(rpm(ii)),'.xlsx'];

      %%
         if exist(filename2,'file')==0
            skipcount = skipcount + 1;
            continue
        end

        output2 = xlsread(filename2);
```

```
        ampl=output2(:,2);
        freq=output2(:,1);


      [amplmax(ii) index(ii)]=max(ampl);
      freqmax(ii)=freq(index(ii));

end


end

%
clear all;
clc,
tic
%% running the simulink models:
sim('allspeed')
sim('allvalve')

%% Getting the results:
%% Speed Control:
input1=speed(:,1);
narma1=speed(:,2);
predictive1=speed(:,3);
pid1=speed(:,4);

%% Valve Control:
input2=valve(:,1);
narma2=valve(:,2);
predictive2=valve(:,3);
pid2=valve(:,4);

%% plotting the results:

% plotting speed over time
figure
plot(time,input1,'-g','LineWidth',2);hold on;
plot(time,narma1,'-b','LineWidth',2)
plot(time,predictive1,'-r','LineWidth',2)
plot(time,pid1,'-m','LineWidth',2)
set(gca,'Color',[0.8 0.8 0.8]);
legend('Voltage Input','Narma-L2','Predictive','PID')
title('Speed Control','LineWidth',5)
xlabel('Time (s)')
ylabel('Voltage (V)')


% plotting the response only

figure
plot(time,input1,'-g','LineWidth',2);hold on;
plot(time,narma1,'-b','LineWidth',2)
plot(time,predictive1,'-r','LineWidth',2)
```

```
plot(time,pid1,'-m','LineWidth',2)
set(gca,'Color',[0.8 0.8 0.8]);
legend('Voltage Input','Narma-L2','Predictive','PID')
title('Speed Control','LineWidth',5)
xlabel('Time (s)')
ylabel('Voltage (V)')
axis([5 7 9 10.5])

xlabel('Time (s)')
ylabel('Voltage (V)')



%% Valve Control
% plotting speed over time
figure
plot(time2,input2,'-g','LineWidth',2);hold on;
plot(time2,narma2,'-b','LineWidth',2)
plot(time2,predictive2,'-r','LineWidth',2)
plot(time2,pid2,'-m','LineWidth',2)
set(gca,'Color',[0.8 0.8 0.8]);
legend('Voltage Input','Narma-L2','Predictive','PID')
title('Valve Control','LineWidth',5)
xlabel('Time (s)')
ylabel('Voltage (V)')

% plotting the response only
shorttime=linspace(time2(992),time2(1356));
input2short=linspace(input2(992),input2(1356));
narma2short=linspace(narma2(992),narma2(1356));
predictive2short=linspace(predictive2(992),predictive2(1356));
pid2short=linspace(pid2(992),pid2(1356));

figure
plot(time2,input2,'-g','LineWidth',2);hold on;
plot(time2,narma2,'-b','LineWidth',2)
plot(time2,predictive2,'-r','LineWidth',2)
plot(time2,pid2,'-m','LineWidth',2)
set(gca,'Color',[0.8 0.8 0.8]);
legend('Voltage Input','Narma-L2','Predictive','PID')
title('Valve Control','LineWidth',5)
xlabel('Time (s)')
ylabel('Voltage (V)')
axis([5 6 9 10.5])


toc
```